^{40}Ar-^{39}Ar THERMOCHRONOLOGICAL STUDY OF THE TRANS HIMALAYA IN LADAKH SECTOR, INDIA

by

Rajneesh Bhutani

Thesis submitted to

the Maharaja Sayajirao University of Baroda

for the degree of

Doctor of Philosophy in Geology

September, 2001

Physical Research Laboratory

Ahmedabad – 380 009, India

CERTIFICATE

I hereby declare that the work presented in this thesis is original and has not formed the basis for the award of any degree or diploma by any university or institution.

Rajneesh Bhutani
(Author)

Prof. R.Ramesh
(Guide)
Physical Research Laboratory,
Navrangpura, Ahmedabad 380 009
India

Prof. Nikhil Desai
(Co-Guide)
M.S. University of Baroda
Baroda 390 002
India

Head, Department of Geology
M.S.University of Baroda
Baroda 390 002
India

Contents

Acknowledgements

Life is under no obligation to give us what we want. I acknowledge and thank life to provide me this opportunity to express my thanks in words to all my well-wishers.

I thank Dr. Kanchan Pande, for always encouraging me and giving me full freedom in thinking, acting, and pursuing things in my own way. His friendly nature and optimistic philosophy towards life has always kept me going. I owe a great debt to Prof. Ramesh who has always been very kind to me. I am proud of being associated with scientist of such a high caliber. I learned so many things from him. I learned the quality of being inquisitive and rational. I learned to enjoy learning from him. I am thankful to Prof. T. R .Venkatesan for teaching me and familiarizing me with the Ar-Ar mass spectrometry. Whatever I know about Ar-Ar is due to his painstaking efforts. His exemplary devotion and dedication to work inspired me to keep trying during the difficult times with machine.

I am indebted to Prof. K .K. Sharma who provided six samples (LG series) for the present study and his useful suggestions from time to time. I appreciate the help extended by Dr. O. M. Lovera of UCLA to run the FORTRAN programs of his MDD model.

I have been benefited a lot by encouraging discussions with Prof. Krishnaswami. He encouraged me to pursue my interest in Geodynamics. Lively discussions with prof Somayajulu has always been encouraging. Prof. Murty has patiently listened to my constant cribbing during the rough patch with the instrument. I express my sincere thanks to him for helping me to overcome some of the problems related to the instrument. I got benefited to a great extent by suggestions made by Profs. T. M. Harrison, Mike Searle, C.J. Wilson & Rejean Hebert. I am also thankful to Dr. K.S. Misra & Prof. Viladakar for their useful suggestions. I thank Prof. Nikhil Desai for taking the responsibility of being a co-guide.

I thank Dr. P. N. Shukla, who helped me a lot with REE analyses and taught me various useful things. Dr. M. M. Sarin very generously taught and helped me during my attempt with ICP analyses. He has been very helpful and a great teacher too, during our course work. I owe a great deal to Ravi Bhushan for providing support and painstaking efforts to go through the thesis, He has been a great company throughout.

I am thankful to Prof. Bhandari, Prof. Goswami, Prof. Bhattacharya, Prof. A.K. Singhvi, Dr. J.R.Trivedi, Dr. Srinivasan, Dr. S.K.Gupta and academic committee members for their support and encouragement. I also thank members of GSI, Pune for their support.

I thank Nirjhari Sinha, for helping me in mineral separation, Padia ji for his constant support, M.G. Yadav & Deshpande who helped me whenever I needed, Bhavsar bhai, who never refused any help, and Vaghela bhai.

The work could not have been completed without the help of Pandian ji who promptly responded to the frequent calls from our lab. V.G. Shah, Panchal, Pranav & Rahul. Kurup and Siva are thankfully acknowledged for their prompt help. Workshop, particularly Ubale & Nagewadia, has also been to a great help. Library & Computer center staff is gratefully acknowledged.

The stay and duration at PRL has been memorable mainly due to the lively atmosphere at hostel. Our batch has always been referred to as a single entity ('95 Batch). And I am happy to be a part of such a close-knit group with each and every member (Alam, Alok, Dipu, Jitti, Koushik, Mittu, Rajesh, Sankar, Shukla, Som, Sudhir, Sunish, Vinai) being very different in their own and yet always together whenever needed. I have been lucky to have very good seniors (Gautam Da, Prashant, Tarun, Jyoti, Ratan, Siva, Sunil, Kunu, Nandu, Ghosh, Sanjay) and juniors too. I must also thank Hetu Seth, who has been a great company and discussions with him have been very simulating! My room 058 gang (subrata, Vinai, Prashanto) have been a great company!

Madam Dr. Sheela Kusumgar has been very affectionate to me and I deliciously remember the numerous dinner parties she hosted for us. I never felt away from home during stay in PRL mainly due to affectionate care taken by Deepaji, Shravani, Rashmi & Pauline.

Having said all this I must mention that I could have not done this work but for the kind and loving nature of our friends in Ladakh. Particularly I am indebted to the families of Tahira & Yasin Le in Leh who have provided space for samples and arranged for many other things besides hosting many dinners. We have been fortunate enough to stay with Razak family in Choglamsar for one night. And last but not least I am heavily indebted to Tashi Le, Nonu Le who have guided us through trekking to Spongtang and Viru & Yoru who carried tons of samples and tents on their back without complaining.

Finally I must pay my gratitude to my family which I always took for granted and never cared much. No amount of words would be sufficient to express my gratefulness to them particularly my mother, father and brother. Now little Nikki, Nikka and my bhrajai have added extra charm to life.

List of Figures

List of Tables

Abstract

Collision of Indian continental plate with Asian continental plate caused deformation of a vast region in both the plates resulting in spectacular Himalayan mountain range and Tibetan Plateau. Himalayan-Tibetan orogenic system has been active for last ~ 50 Ma and provided an excellent natural laboratory to understand collision related processes. Trans Himalayan zone consisting of the suture between the two plates also contains pre- syn- and post-collision metamorphic and magmatic rocks. The change in sedimentation from the marine to continental environments also is preserved in various sections of Trans Himalaya.

The Ladakh region of Trans Himalaya, area of the present study, is probably the best sector in the entire 2500 km long collision zone, because it has preserved almost the complete history of Paleozoic Indian passive margin to the post collision molasses. There have been several episodes of volcanism in the Ladakh region represented by the volcanic rocks of varying chemistry. These rocks form linear suites and their inter-relationship as well as their relationship with the plutonic volcanism is not clear. These vary from island-arc type Dras volcanics to baslatic-andesitic Shyok volcanics to the rhyolite of Khardung volcanics. To gain understanding of the temporal relationship between the different volcanics, the cooling history of the plutonic rocks of Ladakh batholith and effect of collision related deformation on the trapped ophiolites are the main objectives of this study. The ^{40}Ar-^{39}Ar technique used in the present study is temperature sensitive and provides clues of tectono-thermal history experienced by different rocks. The results thus obtained help in building a scenario for the tectono-thermal evolution of Trans Himalaya in Ladakh sector in particular and India-Asia collision zone in general.

Samples were collected in five main traverses across Ladakh sector in north west Trans Himalaya, covering Indus Suture ophiolites, Dras volcanics, Ladakh batholith, Khardung volcanics and Shyok Suture volcanics. A total number of thirty samples were analyzed for ^{40}Ar-^{39}Ar isotopic composition including seven serpentinites and one ultramafic rock. Serpentinites and ultramafic rock did not yield useful results due to high amount of trapped gasses masking the signal. Mineral separation was done from the plutonic rocks

of the Ladakh batholith. A biotite and a muscovite, from granodiorite and leucogranite respectively, were also analyzed along with their whole rock samples. The fine-grained rocks from the other volcanic units were analyzed as whole rock samples.

Basalts from Indus Suture ophiolites show post collision resetting of Ar isotopic signatures. These samples show a rapid cooling initially and slower subsequent cooling. This is interpreted to be due to a large-scale tectonic event with an associated temperature increase sufficient to reset the argon clock of these older suture ophiolites. The initial rapid cooling indicates the termination of this event and the subsequent slow cooling could be due to exhumation through erosion if these were subjected to burial by this tectonic event. The ages for this event registered by these two sample were ~38 Ma and ~46 Ma. The difference in ages indicates the protracted nature of this event. However, not all the ophiolites of Indus Suture Zone are affected by subsequent reheating as revealed by a pillow lava which yielded an age of ~ 128 Ma.

Muscovite from Himia leucogranite of the Ladakh batholith yielded good plateau ages of ~ 29 Ma. A biotite of Leh granodiorite yielded a good plateau ages of ~ 44 Ma. The whole rock age spectra of these rocks yield maximum plateau-like ages of ~ 38 Ma & ~ 46 Ma respectively. These cooling ages indicate high post-collision thermal regime in suture zone.

Shyok Suture volcanics, which range from basalt to andesite, show disturbed and complex age spectra. However, all samples from Shyok suture volcanics yielded consistent age spectra. These age spectra indicate strong tectono-thermal events between ~ 25 to 12 Ma, superimposed on older signatures. The rhyolitic Khardung volcanics in juxtaposition with Shyok volcanics in Shyok-Nubra valley did not yield similar patterns in the age spectrum. They yielded plateau ages and plateau-like ages between ~ 52 Ma and ~64 Ma. The contrast in age spectra of the two nearby volcanic units is very significant. A sample taken from the Karakoram fault zone along the Nubra river yielded a good plateau age of ~ 14 Ma. Based on the similarity of Shyok volcanics and its corresponding volcanic units of Kohistan in the west, to island-arc, and Khardung volcanics and other magmatic rocks to the east of it to continental arc, it has been proposed that the two evolved independently along the Asian plate boundary. Other geological evidences have also indicated that continental arc and island arc evolved independently and simultaneously. This requires that pre-collision margin of Asian plate was made up of small portion of oceanic crust at its western end. The juxtaposition of the two type of rocks were facilitated by the Karakoram strike slip fault at ~ 14 Ma.

By synthesizing the thermochronological data from this study and those from other regions of the collision zone, a general scenario of the India-Asia collision zone and a sequence of crustal accommodation is proposed. Deformation has been propagating away from the plate boundaries with time since the initiation of the collision. The corresponding accommodation of crust also has been taking place away from the plate boundaries with time. The major episodes of crustal accommodation and deformation are manifested in the uplift of Tibetan plateau and the formation of large-scale thrusts in Himalayas. Most of the present accommodation of crust seems to be taking place in eastward motion along the large-scale strike slip faults in Tibet and in consequent detachment zone.

Chapter One

Introduction

1.1 Preamble

The collision between continents is a natural consequence of plate-tectonics and results not only in high mountains and vast plateaus but also adds up new continental crust and converts continents to supercontinents thus affecting the global atmospheric, oceanic and biological evolution (Molnar and England, 1990; Ruddiman and Kutzbach, 1991; Krishnaswami et al., 1992; Richter et al., 1992). Most of the mountain belts on the globe are a result of continent-continent collision. The continental part of a lithospheric plate ultimately collides with another continental plate after the intermediate oceanic plate subducts back into the Earth (Fig.1.1). The subducting oceanic plate gives rise to magmatic activity on the overriding plate forming island arc or continental arc, depending on the overriding plate. A few mountain ranges are such continental arcs only. Andes of South America is a typical example of such mountain chains. Though the plate tectonics theory provides a broad framework for understanding mountain building processes, a number of questions related to the genesis of collision related orogenic systems, pre-, syn-, and post-collision magmatism, mechanisms and processes of deformation responsible for uplift of the terrain into high mountain ranges, consequent effects on the atmosphere and ocean and on global climate, remains to be answered. Mountain-building process related to continental collision has been operative throughout the earth's history. Older mountain belts are now exposed as long linear ranges of highly deformed sedimentary and magmatic rocks. Some examples of the continent-continent collision mountain belts in the Phanerozoic are the Appalachian mountain belt of North America and Ural mountains in central Eurasia, which are more than thousands of kilometers along the strike (Fig. 1.2). Still older mountains of the Precambrian are now present in shield areas such as the Indian Peninsula and Grenville in Canada. These ancient mountain building episodes are recognized mainly on the basis of the understanding developed by studying the younger and present mountain belts.

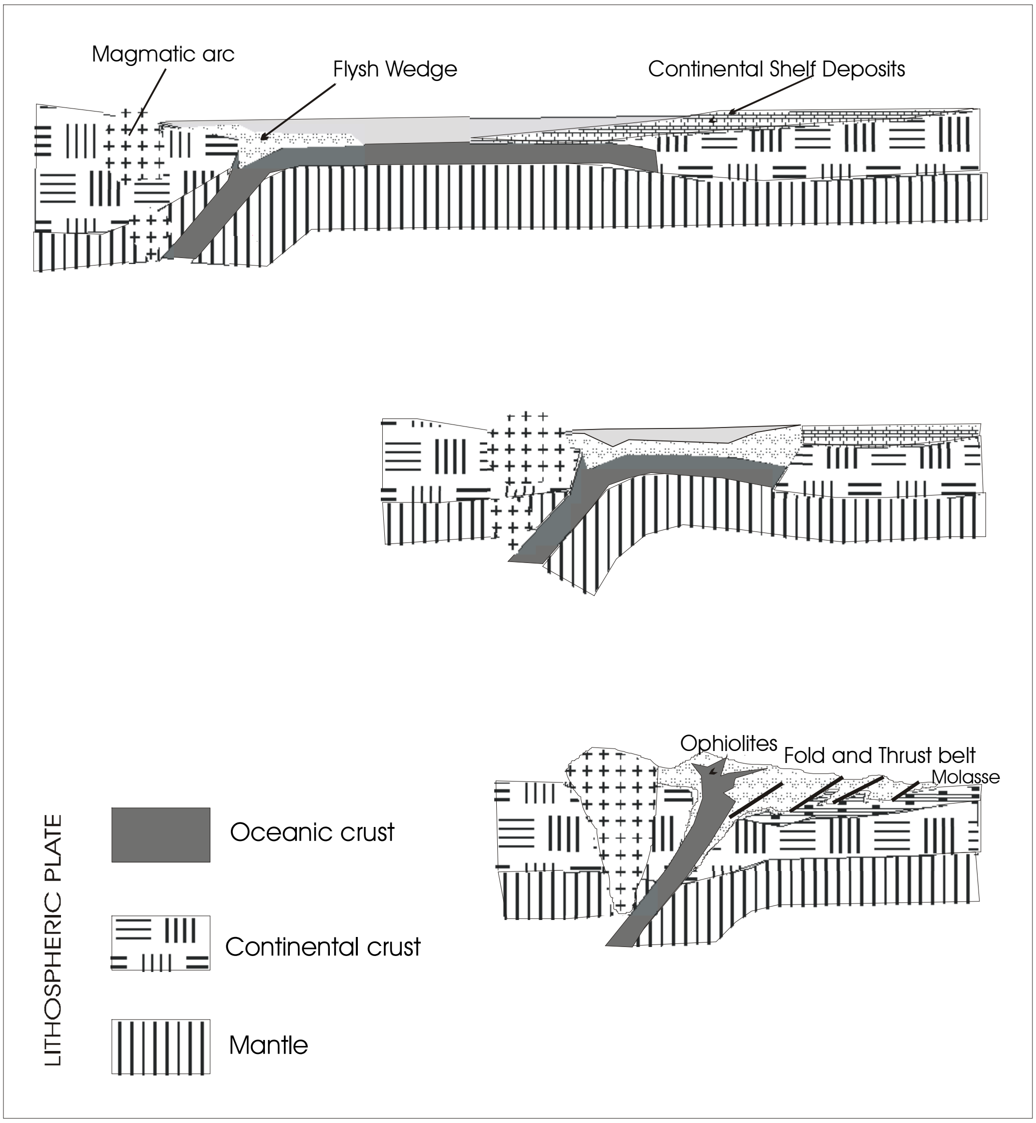

***Fig. 1.1** Diagram showing continent-continent collision. Subducting oceanic plate, beneath the overriding continental plate gives rise to magmatism and continental arc, the sediments on the oceanic floor progressively gets deformed forming flysch wedges along the trench. After the complete subduction of the intermediate oceanic crust some part of it gets trapped/obducted onto the continents. The collision is said to be started with complete subduction of the intermediate oceanic crust.*

The ongoing India-Asia collision for the last 60-50 Ma started following the closure of the Tethys ocean between two great masses since the Paleozoic, Laurasia in the north and Gondwana in the south. The related deformation has affected a vast area of southeast Asia (Fig. 1.3) and resulted in the most spectacular Himalayan-Tibetan orogen, comprising of Himalaya and Karakoram ranges in the south and the vast Tibetan plateau in the north and is more than 2500 km long, along the strike. This system is a part of the greater Himalayan-Alpine system that extends from the Mediterranean Sea in the west to the Sumatra arc of Indonesia in the east over a distance of more than 7000 km. The better known mountain ranges of this system are Atlas (NW Africa) Pyrenees, Apennines, Alps, Carpathians, Balkan, Caucasus, Zagros, Himalaya, Karakoram, Indo-Burmese mountain chains. The Himalayan-Tibetan system has been acknowledged by a vast community of all the branches of Earth scientists to be the most suitable and important system to understand collision related processes for the following reasons. First, collision being active today, geophysical and geological monitoring can be done and relationships demonstrated. (Armijo et al., 1989; Abbott et al., 1997; Bilham et al., 1997). Second, the contrasting style of deformation in Himalaya and Tibet helps in understanding the control of the lithospheric properties on deformation and strain partitioning (Bird, 1978; Davis et al., 1983; England and Houseman, 1986; Dalhen and Barr, 1989; Houseman and England, 1993; Houseman and England, 1996; Kong and Bird, 1996; McCaferey and Nalbek, 1998). Third, the variety of pre-, syn-, and post-collision magmatism associated with this system along with large scale thrusting, strike-slip and normal faulting and other regional structures help in understanding the processes deep in the lithosphere and the large scale dynamics of the collision (Tapponier et al.,1975; Valdiya, 1976; Misra, 1979; Honegger, et al., 1982; Arita, 1983; Trivedi et al., 1984; Le Fort, 1986; Hodges et al., 1988; Khan et al., 1989; Weinberg and Dunlop, 2000). Fourth, the preserved geological sequences of pre-collision oceanic basins at some places help in reconstructing the history of continental margin and oceanic basins (Brookfield and Andrews-Speed, 1984; Gaetani and Garzanti, 1991; Beck et al., 1995; Rowley, 1996; Acharyya, 1997; Searle et. al., 1997; Burbank et al., 1997; Najaman et al., 2001). Because of its immense size and elevations the Himalyan-Tibetan system is believed to have played a significant role in the global climate change and climate in turn might have affected the erosion rate and altered the dynamics of the Himalayan evolution. (Ruddiman and Kutzbach, 1989; Molnar and England, 1990; Molnar et al., 1993;). Therefore, earth scientists all over the world have been studying various aspects of this system in various geographical locations for more than a century (Lydekker, 1883; Hayden, 1907; Auden, 1935; Wadia, 1937; Heim and Ganser 1939; Ganser, 1964; Acharyya and Sastry, 1979; Tahirkheli and Jan, 1979). Studies done and information gathered from different locations help in building up a coherent and self-consistent picture of the spatial and temporal evolution of the Himalayan-Tibetan system and its implications to global Earth System processes.

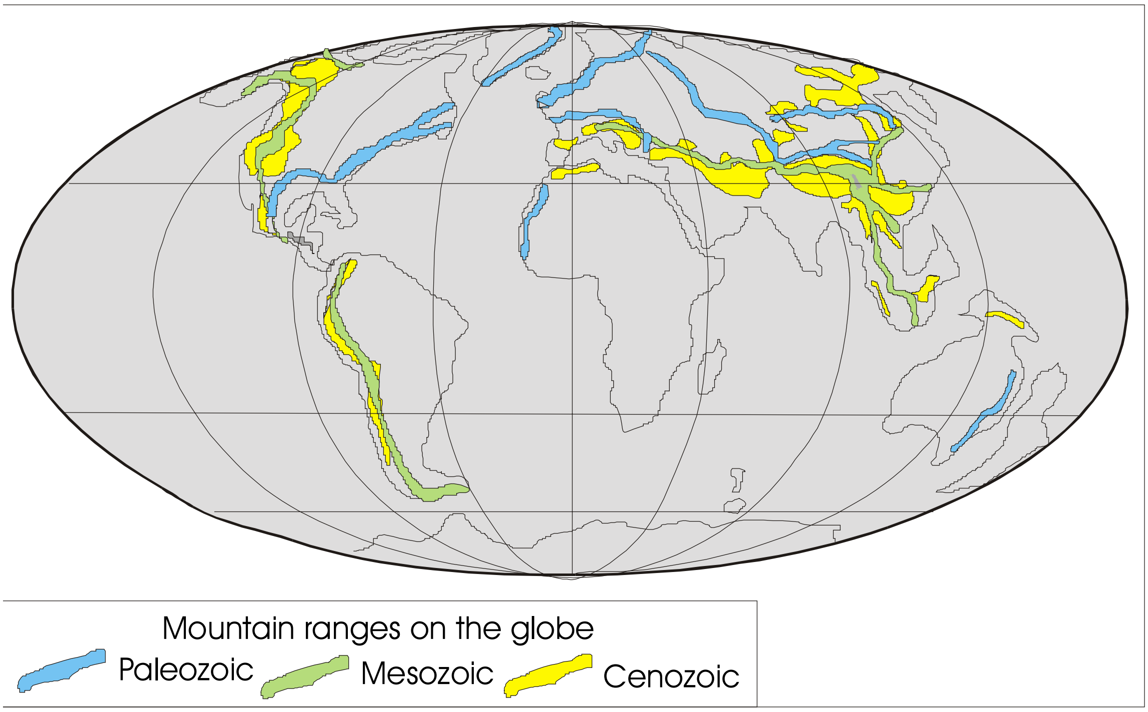

Fig. 1.2 *Phanerozoic mountain ranges on the globe.*

1.2 Motivation for the present study

The collision zone in Trans Himalaya, comprising of plate boundaries and associated sedimentation and magmatism, has proved to be an excellent natural laboratory to understand the various processes associated with continent-continent collision. It has yielded a wealth of geological and geophysical information regarding the present day structures, stratigraphy, seismic activity, geodetic changes; and with the help of recent technical advances, such as the GPS measurements, quite precise estimates of the present day crustal convergence and strain partitioning into different regions of the collision zone have been obtained. (Harrison et al., 1992; Wittlinger et al., 1998). Despite all this information and insights available; details of the precise timing and mechanisms responsible for the formation of Himalaya and Tibetan plateau remain subjects of considerable debate even today. This is because most of the information we have about the collision zone provides us the details of present day structures and activities, which can not be extrapolated back in time to understand the evolution of Himalaya and Tibet.

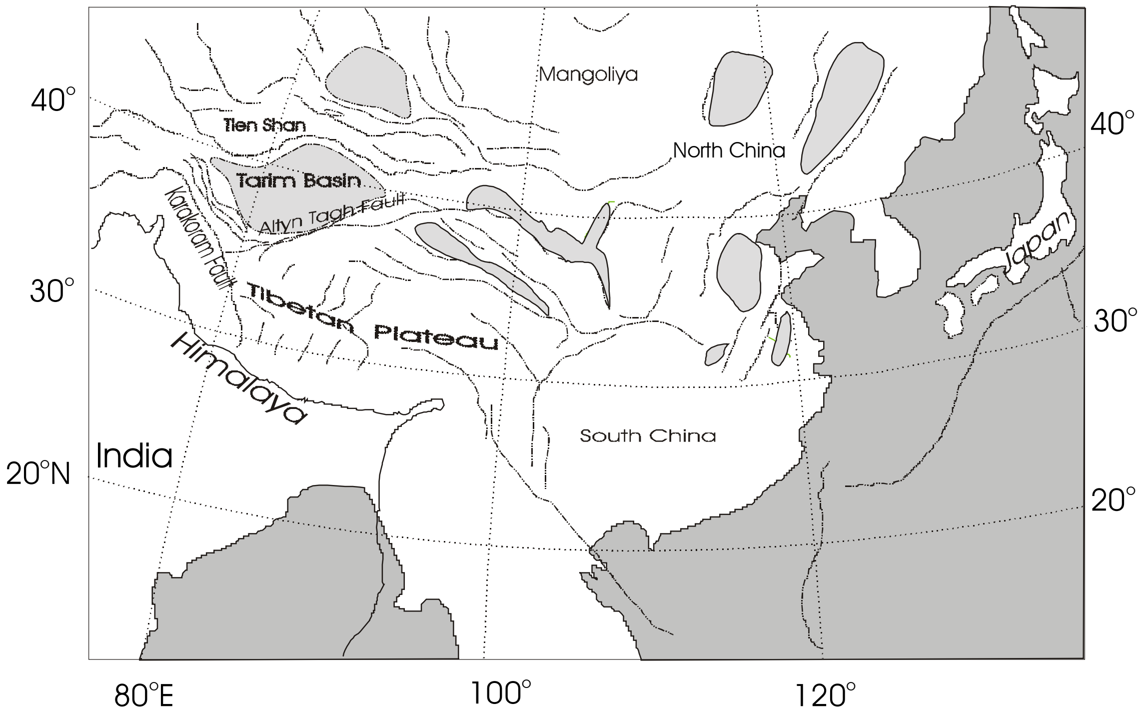

***Fig. 1.3** Regions affected by India-Asia collision. The lines show active faults (Yin and Harrison 2000).*

To fully appreciate the mechanism of the evolution of the collision zone to the present day level we must have constraints on crustal deformation over the entire period since the onset of collision. Though stratigraphic observations in some regions of the collision zone permit us to infer the timing of some of the large events such as ophiolite obduction and initiation of the collision, it is usually very difficult to correlate information from different regions. This is the main reason why the most fundamental question regarding the timing of the initiation of the collision has remained unsettled (Beck et al., 1995; Rowley, 1996; Searle et al., 1997). The consequent problems of deriving the continuous history of uplift and deformation in the collision zone since the initiation of the collision has led to the proposals of several theoretical tectonic models (Tapponier et al., 1975; Davis et al., 1983; England and Houseman, 1986; Dalhen and Barr, 1989; Harrison et al., 1992; Houseman and England, 1993) which are primarily aimed at explaining some of the key present day geological observations. Lack of time constraints for various processes over the history of the collision is, however, a major hurdle for a complete understanding of the collision process. This shortcoming has been recognized lately by several workers and recently several attempts to provide time constraints on the uplift and subsequent sedimentation, from samples selected from different Himalayan regions using various chronometers have been made (Searle et al., 1999). The Ladakh region of Trans Himalaya, area of the present study, is probably the best sector in the entire 2500 km long suture zone, because it has preserved almost the complete history of Paleozoic Indian passive margin to the post collision molasses (Ravishankar et al., 1989; Weinberg and Dunlop, 2000). Collision preceded a long episode of subduction of the Tethys oceanic lithosphere beneath the Asian continent, which gave rise to Trans Himalayan Batholith (THB) all along the southern margin of the Asian continent. Ladakh Batholith (LB) is part of this subduction related calc-alkaline plutonic magmatism (Honegger et al., 1982). LB now forms high mountain ridges separating the Nubra-Shyok valley from the Indus Valley (Fig. 2.1). The uplift of these deep-seated rocks to such an elevation requires large scale tectonic events which are caused by the ongoing collision; however, information about the timing and the rate of uplift is required to understand the response of collision and subsequent deformation. There have been several episodes of volcanism in the Ladakh region represented by the volcanic rocks of varying chemistry (Sharma 1991). These rocks form linear suites and their inter-relationship as well as their relationship with the plutonic volcanism is not clear. These vary from island-arc type Dras volcanics to baslatic-andesitic Shyok volcanics to the rhyolite of Khardung volcanics (Venkatesan et al., 1994; Rolland et al., 2000). Do they represent different tectonic settings at the time of their formation? Are they pre-collision or do they represent collision induced magmatism? These are some of the unanswered questions about these volcanic rocks. I have attempted to provide a geochronological framework for these rocks. Their thermal history might provide an important clue regarding their origin and inter-relationship. Apart from these rocks there are basalts of obducted oceanic lithosphere. These ophiolites of the southern margin of the LB are recognized to be the part of the continuous belt running all along the 2500 km of THB. The effect of the ongoing collision on these trapped ophiolites with respect to their radioactive clocks has not yet been explored. Absolute dating of rocks from the ophiolitic melange in principle should give the age of the formation of the ocean floor. The tectonic setting of this ocean floor, however, is difficult to ascertain due to variable geochemical signatures (Thakur and Bhatt, 1983; Hebert et al., 2000). The effect of collision related deformation on ophiolites being unknown, the interpretation of the absolute ages of ophiolites is difficult. However, temperature sensitive radio-isotopic technique such as ^{40}Ar-^{39}Ar might provide clues of the tectono-thermal history experienced by the rocks of the ophiolite suite. Similar ophiolites found along the northern margin of the Ladakh Batholith(LB), named as Shyok Suture, are truncated in eastern Ladakh. A recent study (Rolland et al., 2000) reveals that the chemistry of volcanics of the northern portion of Ladakh sector is different from that of the northern Kohistan sector of Pakistan, thus questioning the prevailing belief of Kohistan-Ladakh island arc.

The present study attempts to provide a scenario for the evolution of Ladakh sector along its northern and southern margins, cooling history of the plutonic rocks of LB, geochronological framework for the volcanism in Ladakh, and attempts to look for the signatures of the ongoing collision in the trapped ophiolites of both the sutures to build a scenario of thermochronological evolution the Ladakh terrain of Trans Himalaya in particular, and India Asia collision zone in general. For this, $^{40}Ar/^{39}Ar$ systematics is used, which is sensitive to the temperatures ranging from ~600^{o}C to 150^{o}C, the closure temperatures for Hornblende and K-feldspar. (McDougall and Harrison, 1999). In addition, for the first time, I have attempted to retrieve the thermochronological information from bulk rock samples instead of the conventional 'mineral closure temperatures versus age' technique, which is limited mainly to plutonic rocks due to the difficulty in mineral separation from the volcanic rocks. Such a time-temperature information is very useful in deciphering a nearly continuous deformational history. I have attempted to build a scenario for the collision zone evolution by synthesizing available thermochronological data from the different geographical locations of the India-Asia collision zone, including this study (Ladakh region). Such a reconstruction assumes that the change in the rate of cooling, as inferred from the thermochronological studies, indicates a change of processes responsible for the cooling. Rapid cooling periods would indicate high tectonic activity at that time and region. Thus thermochronological data can provide helpful constraints for building up a model for the evolution and crustal accommodation in India-Asia collision zone in time and space.

Geology of the Trans Himalaya in the Ladakh sector

2.1 Geotectonic subdivisions of Himalaya

The Himalaya can broadly be classified into four major geotectonic units (Fig. 2.1) (Ganser, 1964; Valdiya, 1984), which from south to north are,

1) Siwaliks or Sub Himalaya separated from the Indo-Gangetic plains by the Himalayan Frontal Fault (HFF) in south.
2) Lesser Himalaya is separated from the Siwalik by the Main Boundary Thrust (MBT)
3) Higher Himalaya or Himadri which is separated from the Lesser Himalaya by the Main Central Thrust (MCT) and the
4) Trans Himalaya or the Tethyan zone which is north of the Higher Himalaya.

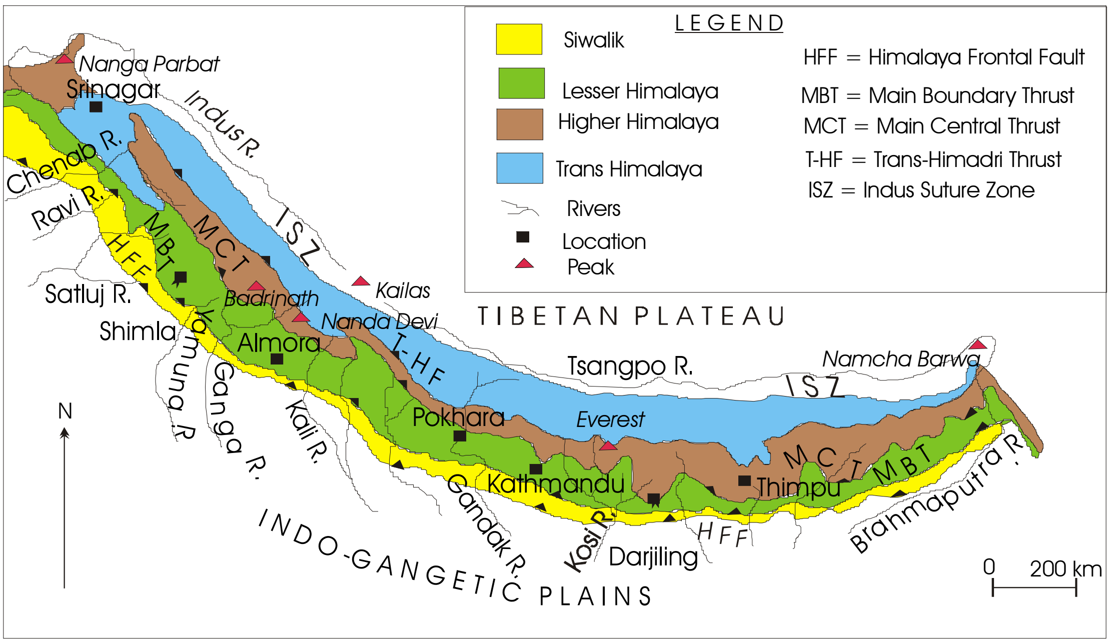

***Fig. 2.1** Geotectonic subdivisions of Himalaya (adapted from Valdiya, 1998).*

2.2 Subdivisions of Trans Himalaya

The Trans Himalaya, as the name suggests is the terrain lying beyond the main Himalayan ranges towards the north. The Trans Himalaya again can be subdivided into following units (Searle et al., 1987), which from south to north are

1) Continental passive margin sediments, (Lahoul supergroup and Zanskar-Spiti basin sediments in Ladakh) of the northern Indian margin
2) Indus Suture Zone including the arc-trench sediments, ophiolites and continental molasse deposits,
3) Trans Himalayan Batholith (Ladakh-Gangdese batholith) representing the subduction related calc-alkaline magmatism and
4) Shyok Suture Zone representing the suturing between the magmatic arc and the Asian margin.

All the above units of the trans Himalaya can be found in the Ladakh region (Fig. 2.2) of the northwestern Himalaya.

2.3 Geology of Ladakh

2.3.1. General Introduction

Ladakh, the land of many passes, of freezing high barren landscapes in Trans Himalaya is among the world's highest inhabited terrains. Situated on the northwestern Trans Himalaya, Ladakh has three major mountain ranges, Zanskar, Ladakh and Karakoram range with Higher Himalaya forming its southern border. Being in the rain-shadow region the annual rainfall is a mere 5 cm here and it is melting snow in summer, which sustains life. The temperatures go as low as $-30^{o}C$ in Leh and $-50^{o}C$ in Dras. With three months of subzero temperatures (Dec-Feb) and the rest of the months facing zero degree temperatures, it is a long and hard winter here. High aridity and low temperatures lead to sparse vegetation as a result the landscape is desert-like with sand dunes. In summer the temperature goes above $20^{o}C$. In the short intense summer, cultivation is sustained by melting snow and carefully harnessing the water. Apples, apricots and barley are grown here in summer. The major waterway of Ladakh is Indus which enters India from Tibet at Demchok, starting near Mt. Kailash. Its tributaries, the Zanskar, Shingo, Shyok, and Nubra and their river valleys form the main area of human habitation. Ladakh also has one of the largest and most beautiful natural lakes in the country. Pangong Tso, 150 km long and 4 km wide, is at the height of 4300 m. Tso Morari, a pearl shaped lake and Tso kar are the other brackish water lakes of Ladakh. Yaye Tso, Kiun Tso and Amtitla are among the fresh water lakes. Ladakh, covering an area of approximately 98,000 sq km of the northwest Trans Himalaya provides a complete section through all the major geological units of the Trans Himalaya (Fig. 2.2).

2.3.2. The passive continental margin deposits

The passive continental margin deposits are represented by the Paleozoic Lahoul supergroup and Mesozoic Zanskar supergroup. These are separated by the rift related Panjal Traps which erupted in Permian and are well exposed now in Kashmir valley. These are continental tholeiites and mildly alkaline flood basalts (Searle et al., 1987). With this rift in Permian, the Neo-Tethys passive margin evolved in Mesozoic. This period is represented by the thick Triassic platform carbonate and Jurassic transgression of the shelf marked by the fossiliferous Spiti shales. The shallow marine carbonate deposition continued up to late Cretaceous as represented in the Zanskar ranges and the Kangi-la flysch is overlying these shallow marine deposits representing the deep water conditions. The fossiliferous Eocene limestone of the Zanskar is believed to be the youngest shelf deposit of the Neo-Tethys margin (Mathur and Pant, 1983).

2.3.3. Indus Suture Zone

Indus suture zone contains the deep-sea sediments of the northern Indian plate and southern Tibetan plate separated by fore arc-trench sediments and overlain by ophiolitic mélanges and molasses (Fig. 2.2). In Ladakh area, the deep sea sediments are represented by Lamayuru complex which consists of Triassic to Cretaceous shales, sandstones, turbidites and deep sea radiolarian cherts (Searle et al., 1987 and the references therein). The Lamayuru complex is believed to represent the deep-sea facies of the Indian passive margin and are time equivalent of the Zanskar shelf deposits (Mathur and Pant, 1983). The Lamayuru complex grades into the fore arc Nindam formation. Nindam formation is intra oceanic deposits on the southern flank of Dras island arc (Fig. 2.3). It comprises volcanoclastic sediments and pelagic carbonates. The trace and rare earth element signatures of sediments are similar to that of Chalt and Dras volcanic rocks but are distinct

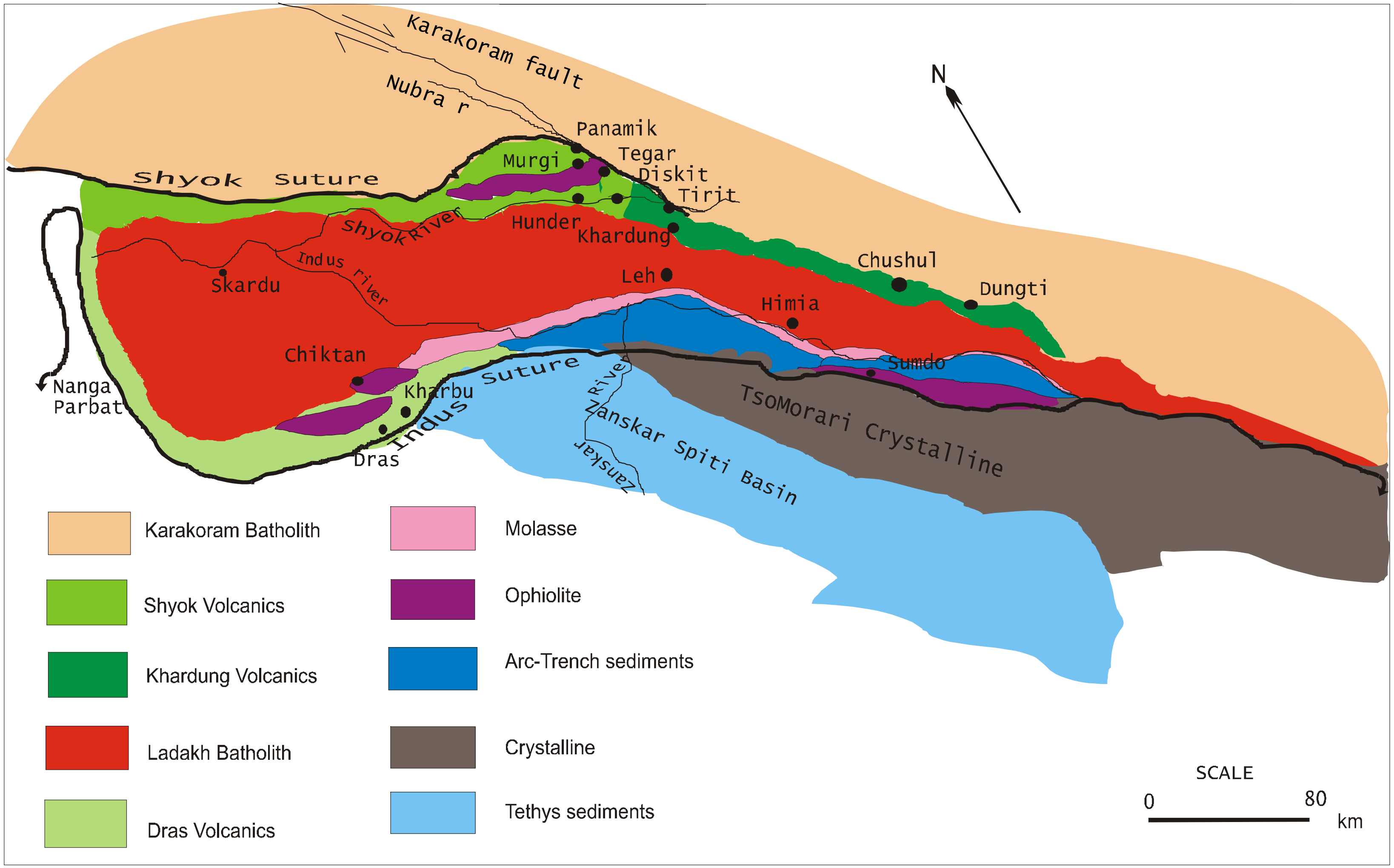

Fig. 2.2 *Geological map of Ladakh showing the sample locations (Modified fromSharma, 1991)*

from Khardung volcanics (Clift et al., 2000). Ophiolitic mélanges with exotic sedimentary blocks are characteristic features of the Indus Suture. Ophiolitic mélanges occur in two distinct tectonic settings (Searle et al., 1987). In the first it occurs as autochtonous unit within Indus Suture and in the other it occurs as allochtonous units forming nappes and klippes on the younger Tethyan sediments. In the western Ladakh (Fig. 2.3) two belts of Shergol ophiolites have been recognized to the north and south of the Nindam formations (Thakur and Bhat, 1983).

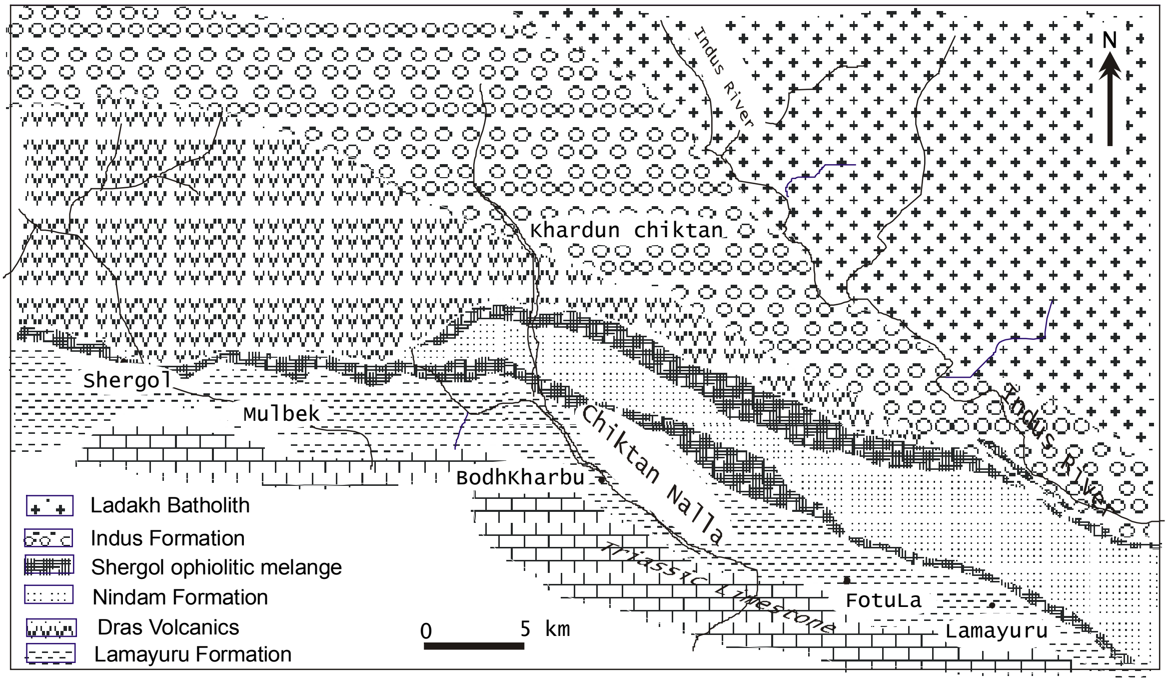

***Fig. 2.3** Geological map of western Ladakh (Thakur and Misra, 1983).*

The Shergol ophiolitic mélange exposed near the Bodhkharbu and Chiktan Nala comprises mainly serpentinites, peridotites, basic volcanics along with jasperoid shale, green sandstones and phyllites. In the eastern Ladakh, Zildat ophiolitic mélange is found to be thrusted over Tso Morari crystalline complex and is overlain by Nidar ophiolites (Fig. 2.4). Zildat ophiolitic mélange in Mahe-Sumdo nala section is composed of serpentinites, purple shale, exotic limestone and volcanics with pillow lavas (Thakur and Misra, 1983). Nidar ophiolite has thick units of ultramafics, gabbros, volcanics with pillow lavas, cherts and clastics. The allocthonous part of the Indus Suture ophiolites are well exposed in the Spongtang area of the Ladakh and is known as Spongtang klippe. This ophiolitic mélange is thrusted 30 km south of its main root zone in Indus Suture. It comprises of ultramafics, gabbro, serpentinites and some volcanics. The timing of the obduction of the Spongtang ophiolite onto the northern passive margin of the Indian plate has been debated hotly. Fuchs (1979), Keleman and Sonnenfeld (1983) and Reuber (1986) suggested a post early Eocene age of the obduction because the Spongtang ophiolite and its underlying thrust sheets comprising deep water sediments, alkalic volcanic rocks and mélanges have been thrusted over Paleocene-Early Eocene limestones. Searle (1986, 1988) first proposed that the post collisional restacking of the units obliterated the actual Late-Cretaceous Early Paleocene obduction event. Searle et al. (1997) presented field data and structural mapping in favor of a Cretaceous obduction.

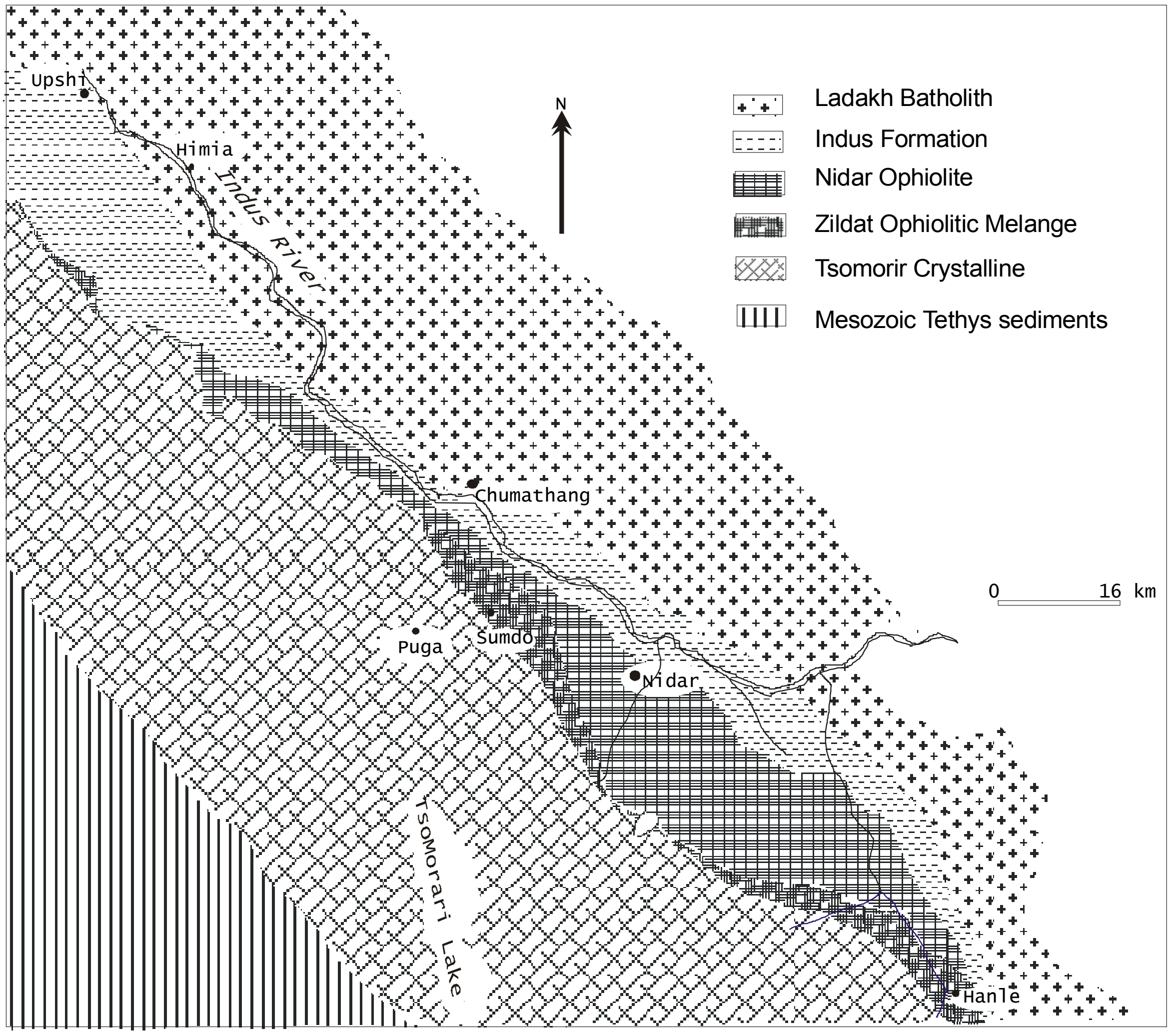

Fig. 2.4 *Geological map of eastern Ladakh (modified from Thakur & Bhat, 1983).*

The ophiolitic mélanges in Ladakh are overlain by another fore arc basin known as Indus Group or Indus Formation, south of the Ladakh batholith (Fig. 2.4). This fore arc seems to have evolved from middle Cretaceous to Eocene. (Thakur and Bagati, 1983; Garzanti and Van Haver, 1988). This basin in Ladakh represents a complex transition from marine to continental deposition conditions and thus becomes important to constrain the timing of initiation of the collision (Rowley, 1996). The transition from marine to continental deposition starts from the Eocene Indus clastics and Indus molasses overlying the Numulitic limestone. Hemis conglomerate from near the Hemis gompa south of Leh representing the continental Molasses has clasts from volcanic, plutonic, sedimentary and metasedimentary rocks. The major part of the detritus in the Indus group is supplied from the nearby source and the provenance lies to the north (Thakur and Bagati, 1983).

2.3.4. Ladakh Batholith

Ladakh Batholith is a part of 2500 km long Trans Himalayan Batholith (THB), that is mainly subduction related calc-alkaline magmatism evolved along the southern margin of the Eurasian plate in mostly Andean type tectonic setting except in the western sector of Kohistan batholith where it seems to have intruded into a Chalt-Dras island arc (Sharma, 1990; Honneger et al., 1982; Weinberg and Dunlop, 2000). Ladakh batholith is around 500 km long and 30-40 km wide (Fig. 2.2). The rocks range from gabbro norite to granites and leucogranites. Granodiorites and biotite bearing granites are the dominating rock types of the Ladakh batholith. At places the different rocks are quite intermingling and their intrusive relationship is difficult to ascertain (Ahmad et al., 1998). The Ladakh batholith is cut by andesitic and basaltic dykes.

The existing geochronological data range from 100 Ma to 40 Ma, frequently interpreted as the duration of subduction. The ending of the magmatism is widely used to constrain the age of initiation of the collision (Honnegger et al. 1982, Weinberg and Dunlop, 2000). However, younger ages have been obtained recently which probably are post-collision. The significant crustal anatexis also may be involved in the batholith formation as indicated by the previous isotopic studies (Honnegger et al., 1982; Weinberg and Dunlop, 2000).

2.3.5. North of the Ladakh Batholith

Shyok suture zone marks the northern boundary of the Ladakh batholith and separates it from the Karakoram batholith (Fig. 2.5). Shyok suture in Ladakh is the eastern continuation of the Northern Suture of the Kohistan sector of Pakistan. Kohistan-Ladakh sectors usually are believed to be Island arc type with Chalt volcanics of Kohistan sector and Shyok volcanics of the Ladakh representing the back arc basin sequences (Petterson and Windley, 1985; Upadhyay et al., 1999). A recent study, however, indicated that the Northern Kohistan is chemically quite different than the Northern Ladakh. This requires

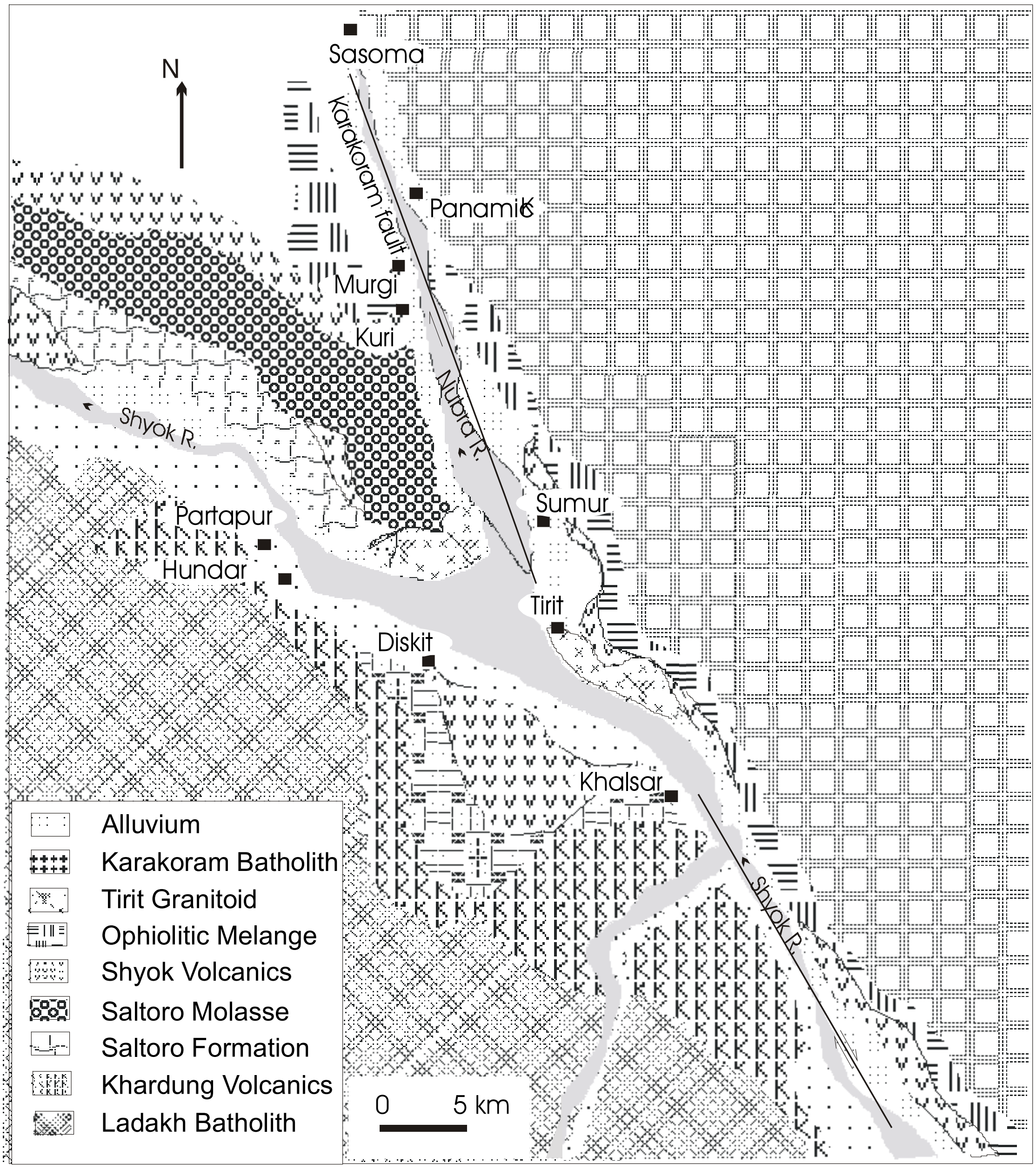

***Fig. 2.5** Geological map of Shyok Suture Zone in Northern Ladakh (modified from Upadhyay et al., 1999; Rai, 1982).*

a different evolutionary scenario of Northern Ladakh than the Northern Kohistan (Rolland et al., 2000). The relative timing of suturing along the two sutures bounding the Kohistan-Ladakh sector has remained controversial. While many workers believed Shyok suture to be older being closed in Cretaceous (Pudsey, 1986; Petterson and Windley, 1991; Treloar et al., 1996); Brookfield and Reynolds (1981) and Reynolds et al. (1983) suggested that it did not close until Miocene. Rai (1983), however, argued against any separate suturing along the Shyok suture. According to his interpretation Indus and Shyok zones are segments of one single suture, which has been cut by the Ladakh batholith. Shyok suture zone has volcano-sedimentary sequences and mélange zone exposed in Shyok-Nubra valley north of Ladakh batholith. The volcanics range from basalt to rhyolites and ignimbrites. Thakur (1981) grouped acidic and explosive rhyolites and ignimbrites in Khardung volcanics. These directly overlie the Ladakh batholith. Ophiolitic mélanges in Shyok suture zone is exposed in the Nubra valley and comprises serpentinites, shales, limestones and basic volcanics. Other volcanic units grouped under Shyok volcanics range from tholeiitic basalt to basaltic andesites to andesites. Continental sedimentation in Shyok suture is represented by Saltoro molasses (Fig. 2.5) and comprises shales, sandstones and conglomerates. Upadhyay et al. (1999) found it to be in thrust contact with the Shyok volcanics. All major units of Shyok suture zone are usually described from the Shyok Nubra valley, their characteristics and relationships are less clear to the east of the Nubra valley (Fig. 2.5). The Shyok suture is not found to the east of Ladakh. The eastern part appears to have evolved as a pure Andean type margin.

2.4 Fieldwork and samples

Fieldwork in Ladakh, to collect the samples, was carried out in months of August-September 1997. We traversed through the Lahoul-Spiti and Zanskar basins of Paleozoic-Mesozoic continental passive margin sediments. We reached Sabu 4 kms south east of Leh in three days from Manali after crossing four major passes, viz., Rohtang pass, Baralacha la (La meaning pass), Lachunglung la, and Tanglang la. Observations and samples were taken in five major traverses from the main Sabu camp (Fig. 2.6). Field observations and sample locations are described according to these traverses. Sample locations and descriptions are tabulated in Table 2.1. The longitudes and latitudes were obtained by a hand-held GPS (Global Positioning System).

2.4.1. Sabu-Leh-Khardung la –Khardung-Hunder

This route cuts across the almost NW-SE trending Ladakh ranges of Ladakh batholith and reaches Nubra-Shyok valley in northern Ladakh. On the southern margin of the batholith, near Sabu and Leh, the rocks are generally biotite granites with hornblende. The sample LK 24 was collected from *Shanti Stupa* in Leh (a Bodh stupa built by the Japanese). This is a coarse grained biotite hornblende granite. Some more mafic enclaves

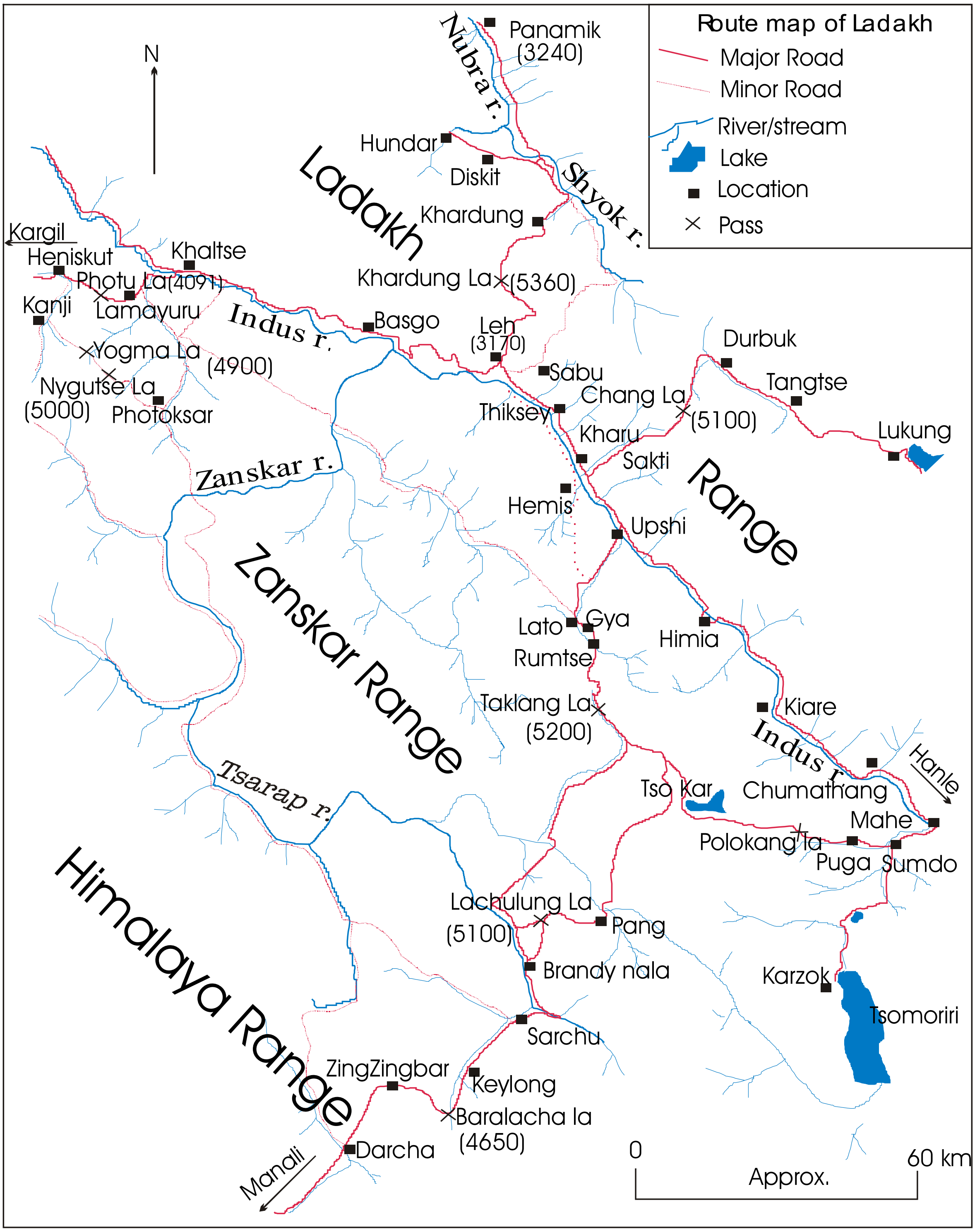

***Fig. 2.6** Route map of Ladakh showing important locations, rivers and passes (numbers in parentheses are altitude in meters) (Source:Lombard, 1981)*

were seen in the biotie granite of the *Shanti Stupa*. The granodiorites and biotite granites are found through out the width of the batholith. However, there are numerous basic as well as aplitic dykes found cutting it. Near South Pullu an ultramafic body was also seen within the batholith. Near the Khardung glacier, the granodiorites have pinkish shades giving them an appearance of monzonite. Acidic volcanics and rhyolites are dominant rocks towards the base of the batholith and are in tectonic contact with the main batholith near the Khardung village. Between the Khardung village and the Khalsar traffic check post (TCP) we found the signatures of the explosive volcanics in the form of ignimbrites, lapilli textures, tuffs, and volcanic breccias. They form the type locality for the Khardung volcanics (Fig. 2.7). Rhyolite samples, LK 88 and LK 90, of Khardung volcanics were collected near the Khardung village towards the Khalsar TCP.

Fig. 2.7 *Rhyolite and ignimbrite of Khardung Volcanics near Khardung village in northern Ladakh*

Sample LK86 is taken from further north, between Khalsar and Khardung and is a green colored volcanics at the contact between acidic Khardung volcanics and Shyok volcanics. Basic volcanics, at places green colored, grouped under Shyok volcanics are seen in contact with the acidic volcanics in Hunder Nala and also further north near the villages Scampuk and Partapur. A traverse along Nubra river was taken to observe and collect the samples from the various units of the Shyok suture zone.

2.4.1.1. Tirit-Diskit-Tegar-Panamik-Murgi

Tirit village is south east of the Shyok-Nubra confluence. Pink granite usually described as Tirit granite is exposed between Tirit and Khalsar TCP. Towards the north Tirit granite is in tectonic contact with the serpentinites near the Diskit village at the Shyok-Nubra confluence. Between Diskit and Tegar, ultramafics and serpentinites are seen. North of the Tegar towards Panamik ultramafics and serpentinites appeared to be intruded by doleritic dykes, basic volcanics, and acidic volcanics. At Panamik, porphyritic granitoids of Karakoram batholith appears to be in tectonic contact with the Shyok volcanics and ophiolitic mélange towards south. Porphyritic granodiorites of the Karakoram batholith are seen mylonitized along the Nubra river section due to probably Karakoram fault. The ophiolitic mélange of Shyok suture zone is exposed near the village Murgi (Fig. 2.8) which can be reached from Panamik by crossing the suspension bridge over the river Nubra (Fig. 2.6).

Fig.2.8 *Ophiolitic mélange near the village Murgi on the bank of Nubra river. Green colour is of serpentinization intermingling with the purple shale, chert and basalts.*

Sample LK 47 is taken from the mylonitized Karakoram batholith granitoids along the Nubra river section. This is mafic segregation and mainly consists of the micaceous minerals. Sample LK 48 is of a very fine-grained volcanics at the contact between

Karakoram fault related mylonitized granitoids and the Murgi mélange. LK 57 is medium grained basic volcanics 15 km north of Sumur towards Panamik. Samples LK67 and LK 68 are taken from a sharp contact between basic and acidic volcanics between Tegar and Panamik about 7 km south of Panamik. Sample LK 70 is a medium grained basic volcanics collected from between Panamik and Tegar.

2.4.2. Kharu-Sakti-Chnag la- Darbuk-Tangtse-Lukung (Pangong Tso)

This route cuts across the Ladakh batholith, and crosses the Ladakh ranges at Chang la. Near Sakti village, gabbroic and granitic bodies are intercalated with each other. 11 km from Sakti towards Chang la (Fig. 2.6), a large body of fine-grained black colored mafic rock is found as an enclave within the granite. Further north near Chang la, acidic dykes cutting the gabbros are found. The area north-east of the Chang la, from near Darbuk to Lukung, seems to have undergone large scale and wide spread deformation with migmatisation very clearly exposed between Tangtse and Lukung. Serpentinized and brecciated rocks are found near Tangtse while the mylonitization of granitoids with elongated phenocrysts of feldspars are seen near the Tangtse Indo-Tibet border police post, indicative of the widespread deformation, which could be related to the suturing along the Shyok Suture.

2.4.3. Shey-Thiksey-Upshi-Himia-Gaik-Kiari-Chumathang

This route runs parallel to the Indus river (Fig. 2.9) along the southern margin of the Ladakh bathoith. Near Thiksey Gompa Gabbro is the main phase of the bathoith, while near Upshi the pink granite with big crystals of K-feldspar dominates. Between Likche and Himia Muscovite-Biotite leucogranite, with some hornblende as well, appears to have intruded in the pre-existing granodiorites. Sample LK 198, of these two-mica bearing leucogranites is taken from near the Himia village. Near Gaik porphyritic granite with big phenocrysts of the K-feldspar grains is exposed. Near Kiari, the granodiorites are richer in hornblende and forms the quartz-monzodiorites. The exposed southern margin of Ladakh bathoith is most spectacular near Chumathang where leucocratic granites criss-cross the gabbro and diorite (Fig. 2.10).

Fig.2.9 *Indus river valley east of Leh. The red colour (between the two black lines) along the river is because of chert and marks the Indus Suture.*

Fig. 2.10 *Intermingling of the light colored granites and basic rocks in the southern margin of the Ladakh batholith, near Chumathang village in Eastern Ladakh.*

2.4.4. Mahe-Sumdo-Pugga-Polokangla-Tso Kar

This section cuts across the Indus formation at Mahe and then traverses through the Zildat ophiolitic mélange (Thakur and Misra, 1983) in Sumdo nala between Mahe and Sumdo village (Fig. 2.11).

Fig. 2.11 *Ophiolitic mélange at the Sumdo nala section. Light coloured exotic limestone is caught up in the ultramafics.*

At Sumdo, it is in tectonic contact with the Pugga formation of Tso-Morari crystalline. The Zildat ophiolitic mélange has ultramafics, volcanics and pillow lavas exposed in the Nala section. Sample LK 176 collected from the nala section is porphyritic with a few hornblende needles as phenocrysts. While the sample LK 182 is fine-grained volcanic collected from the same Nala section.

2.4.5 Leh-Bhodhkharbu-Shergol-Kargil-Dras

The southern margin of the Ladakh bathoilth in the western Ladakh has more mafic component in comparison to the southern margin of batholith in the eastern Ladakh. This route runs parallel to Ladakh batholith and traverses the Kargil igneous complex, Shergol ophiolite near Shergol and Chiktan and traverses the green colored Dras volcanics after Kharbu to Dras (Fig. 2.3). Sample LG 290 of Dras volcanics is from near Kharbu village.

Fig. 2.12 *Pillow lavas near the village Chiktan in the western Ladakh*

2.4.5.1 Hiniskut-Kanji-Yogma La-Nyigutse La-Spongtang river

This is a trek route to the Spongtang Klippe ~ 25 km south of the main road (Fig.2.6). This route cuts across a thick band of limestone, with shale and sandstones in between upto the Spongtang river. Klippe which is made up of peridotites and serpentinites with gabbro and basalt rests over the Eocene limestones which form the SW-NE trending sharp peaks as seen in the Fig. 2.13.

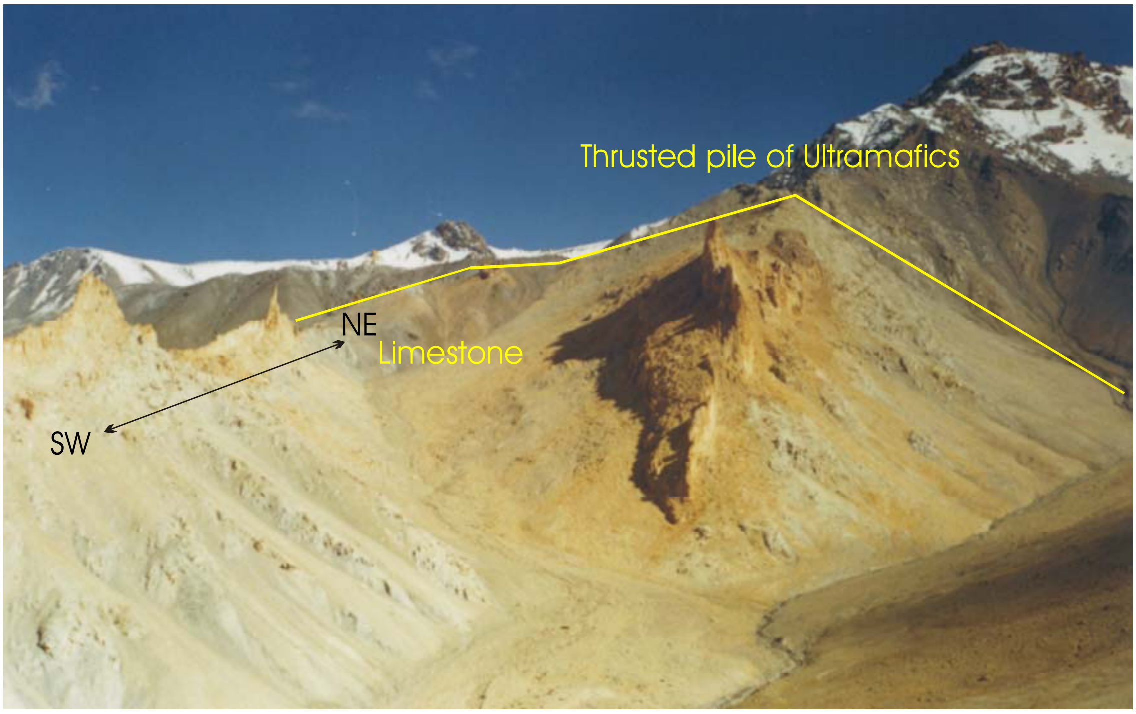

Fig. 2.13 *Spongtang klippe. Light yellow coloured sharp peaks are of Limestones, the dark coloured ultramafics are seen to be thrusted over these younger limestones.*

Table 2.1 *Location and description of samples*

Sample	**Location**				**Tectonic setting**	**Description**
	Longitude (°E)	Latitude (°N)	Altitude (m) ±100 m	Village name		
LK198	78°5.1’	33°29.2’	3870	Himia	Ladakh batholith	coarse grained, muscovite, biotite and hornblende bearing granite leucogranite
LK198-Muscovite	78°5.1’	33°29.2’	3870	Himia	Ladakh batholith	Hand picked >95% white muscovite of ~1 mm.
LK24	77°34.5’	34°10.4’	3630	Leh	Ladakh batholith	Coarse grained biotite granite
LK24-Biotite	77°34.5’	34°10.4’	3630	Leh	Ladakh batholith	Hand picked >99% biotite grains of~1 mm
LK182	77°36.9’	33°15.3’	4200	Between Sumdo and Mahe	Indus suture zone	Basalt from ophiolitic mélange
LK176	77°45.2’	33°50.1’	4210	Between Sumdo and Mahe	Indus suture zone	Basalt from ophiolitic mélange with small phenocrysts of pyroxenes
LK209	76°31.7’	34°25.6’	3150	Chiktan	Indus suture zone	Pillow lava belonging to Shergol ophiolite
LG290	-	-	-	Dras	Dras volcanics	Green colored basic volcanic rock.

LK47	77°31.4’	34°45.7’	3250	Murgi	Karakoram fault	Mafic segregation along the fault within the Karakoram porphyritic granite.
LG166	77o27.7’	34o35.2’	3180	Hunder	Shyok suture zone	Andesitic basalt
LG197	77°36.9’	34°38.4’	3090	Tegar	Shyok suture zone	Basalt
LG188	77°37.1’	34°38.1’	3090	Tegar	Shyok suture zone	Basalt
LK48	77°31.4	34°46.1’	3250	Murgi	Shyok suture zone	Mylonite in the suture zone
LK57	77°34.2	34°43.1’	3240	Between Panamik and Tegar	Shyok suture zone	Dolerite, with plagioclase and pyroxenes
LK67	77°34.5’	34°42.4’	3180	Between Panamik and Tegar	Shyok suture zone	Dolerite in tectonic contact with serpentinites
LK68	77°34.7’	34°42.1’	3170	Between Panamik and Tegar	Shyok suture zone	Fine grained basic volcanic rock
LK70	77°35.1’	34°41.5’	3110	Between Panamik and Tegar	Shyok suture zone	Dolerite
LK86	77°37.1’	34°35.2’	3550	Between Khalsar and Khardung	Khardung volcanics	Green colored basic volcanics in contact with the acidic volcanics.
LK88	77°38.2’	34°29.1’	3600	Khardung	Khardung volcanics	Rhyolite
LK90	77°38.9’	34°24.2’	3810	Khardung	Khardung volcanics	Rhyolite

LG87	-	-	--	Chushul	Khardung volcanics	Acidic volcanic rock
LG601	-	-	-	Dungti	Khardung volcanics	Acidic volcanic rock

Chapter Three

^{40}Ar-^{39}Ar geochronology and thermochronology: theoretical and experimental aspects

3.1 Fundamentals

The $^{40}Ar/^{39}Ar$ dating system is based on the decay scheme of the isotope ^{40}K. ^{40}K is one of the three naturally occurring isotopes of potassium (K). Potassium is produced during nucleosynthesis by the s-process. ^{40}K comprises of 0.01167 (±0.00004) atomic % of Potassium, with ^{39}K being the major isotope (93.2581 ± 0.0029 at.%) and ^{41}K making up the balance (6.7302 ± 0.0029 atomic %) (Garner et al 1975). ^{40}K, with 19 protons and 21 neutrons, decays spontaneously with a half life of 1250 Ma into ^{40}Ca and ^{40}Ar. It is the branch yielding radiogenic argon ($^{40}Ar^*$) which is utilized for the K-Ar and $^{40}Ar/^{39}Ar$ dating methods. About 89.5% of ^{40}K atoms decay by electron (β-) emission into ^{40}Ca yielding 1.33MeV of energy. The remaining atoms (~10.5%) decay into ^{40}Ar dominantly by orbital electron capture releasing 1.51MeV of energy, but only a very small percentage of atoms (0.16%) decay directly to the ground state of stable ^{40}Ar, most of them (10.32%) decay into the excited state releasing an energy of 0.05 MeV, the excited state comes to the ground state by releasing further γ-rays of energy 1.46 MeV. The remaining small number of atoms (0.001%) decay by emission of a positron β^+.

K-Ar dating method has been applied to a variety of geological problems during the last 40-50 years, because potassium is widely distributed being an essential or minor element in many minerals and is the eighth most abundant element in the earth's crust. Potassium with atomic number 19 falls in the group 1a of alkali elements in the periodic table. It has an atomic radius of 2.03 Å and ionic radius of 1.33 Å. Ar is a noble gas and usually doesn't react or form bonds with other elements found in minerals. This makes the K-Ar dating viable unlike the K-Ca decay scheme, where Ca is very common in rocks and it becomes highly difficult to detect the radiogenic Ca. Ar has three naturally occurring isotopes ^{40}Ar, ^{38}Ar and ^{36}Ar and the atmospheric ratio of $^{40}Ar/^{36}Ar$ is used to correct for the initial ^{40}Ar present in the sample other than the radiogenic $^{40}Ar^*$. This ratio is recommended by Steiger and Jager (1977) for use in geochronology as 295.5 and is derived from the values of atomic abundances given by Neir (1950) as ^{40}Ar 99.600%, ^{38}Ar 0.0632 ± 0.0001% and ^{36}Ar 0.3364 ± 0.0006%. Any mineral containing K will accumulate the radiogenic $^{40}Ar^*$ in course of time. In the laboratory the total ^{40}Ar is measured and accumulated $^{40}Ar^*$ can be calculated after applying the correction for the atmospheric argon and for the other known sources of ^{40}Ar. The number of atoms of daughter produced (D), number of parent atoms remaining (N) and the decay constant (λ) will then provide the time elapsed (t) since the daughter started getting accumulating in the sample according to the following equation:

$$t = \frac{1}{\lambda}\ln(1+\frac{D}{N}) \tag{3.1}$$

As decay constant λ is the total decay constant for ^{40}K yielding ^{40}Ca and ^{40}Ar, the above equation has to be modified for the fraction of decays yielding ^{40}Ar, which is the ratio of decay constants for electron capture (λ_e) and positron decay (λ_e') to the total decay constant. Hence taking only that fraction of total number of parent ^{40}K atoms which decay to ^{40}Ar, i.e. $[\{(\lambda_e+\lambda_e')/\lambda\}^{40}K]$, the above equation (3.1), for K-Ar dating, becomes:

$$t = \frac{1}{\lambda}\ln(1+\frac{\lambda}{\lambda e+\lambda e'}\frac{^{40}Ar^*}{^{40}K}) \tag{3.2}$$

The time 't' then can be related to geologically meaningful event, e.g. for a volcanic rock, 't' would be the age of eruption because as soon as the lava erupts on the surface it cools and starts accumulating the $^{40}Ar^*$. But for a mineral of a plutonic rock this time 't' may not be the age of crystallization as a significant amount of time elapses before it cools to the temperature low enough to retain the $^{40}Ar^*$ and 't' is said to be the 'cooling age' of that mineral.

3.1.1. Fundamental assumptions for K-Ar dating system

As with all other isotope dating methods, there are a number of assumptions that are made for K-Ar dating. These assumptions also apply to the ^{40}Ar-^{39}Ar method, though the latter provides greatly increased opportunities for testing these by performing step-heating experiments. The principal assumptions are given below.

1. The parent nuclide ^{40}K, decays at a rate independent of its physical state and is not affected by differences in pressure or temperature. This is a major assumption, common to all dating methods based on radioactivity. Available evidences suggest that it is well founded (Friedlander et al., 1981).
2. The $^{40}K/K$ ratio in nature is constant at any given time. As ^{40}K is rarely measured directly for dating purposes, this is an important underlying assumption. Isotopic measurements of K in terrestrial and extra-terrestrial samples indicate that the assumption is valid, at least to the extent that no authenticated differences greater than 1.3% have been reported in the $^{39}K/^{41}K$ ratio.
3. The radiogenic argon measured in the sample is produced by *in situ* decay of ^{40}K in the interval since the rock crystallized or re-crystallized. Violations of this are not uncommon but can be verified by the ^{40}Ar-^{39}Ar step-heating method.
4. Corrections can be made for non-radiogenic ^{40}Ar present in the rock being dated. For terrestrial rocks the general assumption is that all such argon is atmospheric in composition with $^{40}Ar/^{36}Ar$ being 295.5.
5. The sample must have remained a closed system since the event being dated. $^{40}Ar/^{39}Ar$ technique is robust enough to provide useful insight into the thermal histories if the samples do not satisfy this assumption.

3.1.2. The ^{40}Ar-^{39}Ar dating method

The K-Ar dating method requires two separate experiments for measuring parent ^{40}K and daughter ^{40}Ar as they are different elements. The ^{40}Ar-^{39}Ar method is modification of K-Ar technique which obviates this requirement of two separate measurements by converting the parent isotope to the same element as the daughter. The sample is irradiated by fast neutrons in a nuclear reactor to convert some of ^{39}K into ^{39}Ar. The fixed natural ratio $^{39}K/^{40}K$ provides an estimate for the parent ^{40}K by the measurement of ^{39}Ar. In order to know the conversion factor of ^{39}K to ^{39}Ar and to take care of other interfering nuclear reactions a sample of known K-Ar age and pure salts of K and Ca are irradiated along with the sample. The unknown age of the sample is then derived by comparison with the monitor sample.

The amount of $^{39}Ar_k$ i.e. number of atoms produced from ^{39}K, depends upon, duration of the irradiation, Δ, neutron flux of energy E, $\varphi(E)$, and neutron capture cross section at energy E for the reaction $^{39}K(n,p)^{39}Ar$, $\sigma(E)$ and the relation can be expressed as (Mitchell, 1968)

$$^{39}Ar_k = {}^{39}K\Delta \int \varphi(E)\sigma(E)dE \tag{3.3}$$

The rearranged K-Ar age equation

$$^{40}Ar^* = {}^{40}K\frac{\lambda_e + \lambda_e'}{\lambda}[(\exp \lambda t) - 1] \tag{3.4}$$

and the $^{39}Ar_k$ production equation give

$$\frac{^{40}Ar^*}{^{39}Ar_k} = \frac{^{40}K}{^{39}K}\frac{\lambda_e + \lambda_e'}{\lambda}\frac{1}{\Delta}\frac{[\exp \lambda t) - 1]}{\int \varphi(E)\sigma(E)dE} \tag{3.5}$$

This can further be simplified by introducing a dimensionless parameter J (Grasty and Mitchell, 1966) such that

$$J = \frac{^{39}K}{^{40}K}\frac{\lambda}{\lambda_e + \lambda_e'}\Delta \int \varphi(E)\sigma(E)dE \tag{3.6}$$

which simplifies the equation (3.5) as

$$\frac{^{40}Ar^*}{^{39}Ar_k} = \frac{(\exp \lambda t) - 1}{J} \tag{3.7}$$

which upon rearrangement gives the estimate of ‘t’ as

$$t = \frac{1}{\lambda}\ln(1 + J\frac{^{40}Ar^*}{^{39}Ar_K}) \tag{3.8}$$

This equation shows that just by measuring the ratio $^{40}Ar^*/^{39}Ar_K$, the age ‘t’ can be calculated, provided J is known, which can easily be calculated by irradiating a sample of known ‘t’ as

$$J = \frac{(\exp \lambda t - 1)}{^{40}Ar^*/^{39}Ar_K} \tag{3.9}$$

This modification in the conventional K-Ar technique improved the precision of measurement, as ratios can be measured with more precision than the abundances. This requires a very small quantity of sample and it also solves the problem of sample inhomogeneity. As it is clear that the ^{40}Ar-^{39}Ar method relies upon a known age sample which is used to monitor the neutron fluence, this ***monitor sample*** is very critical. Usually the following criteria are followed for choosing a monitor sample. 1) It should have uniform $^{40}Ar^*$ to ^{40}K ratio distributed homogeneously in order to calculate the accurate and precise K-

Ar age of this sample. 2) It should be sufficiently coarse grained to minimize the health hazards due to the radioactivity after the irradiation. 3) It should be available in sufficient quantity. Several mineral standards of different ages are used by different laboratories as monitor samples McDougall and Harrison, 1999; Renne, 2000). The total fusion Ar-Ar ages are more precise and accurate than the K-Ar ages but they don't provide any additional information than the K-Ar ages. A major advancement was achieved when it was realized that after irradiation the sample need not be fused in a single step, instead it can be degassed incrementally in various steps and the gas released at each step can be analyzed for isotopic ratio for obtaining 't' and thus an age spectrum of many apparent ages can be obtained instead of a single total fusion age or K-Ar age.

This technique known as '***step heating***' or '***incremental heating***' technique (Merrihue and Turner, 1966) has additional advantage of providing the inner distribution of ^{40}Ar* relative to ^{39}K which in turn is related to ^{40}K. In principle radiogenic Ar and the parent ^{40}K or ^{39}Ar should be released in equal proportions in each step if the sample has not lost any radiogenic argon subsequent to its crystallization. These ratios or apparent ages when plotted against the cumulative % of ^{39}Ar released, would provide flat pattern in the age spectrum called as ***plateau age***. Any deviation from the plateau age shows the redistribution of ^{40}Ar* relative to ^{40}K. Since the diffusion of Ar is comparatively easier than the diffusion of K, any heating or metamorphism subsequent to crystallization will result in the loss of ^{40}Ar*, which then will get reflected in the age spectrum by lower ages in the corresponding temperature steps. The post-crystallization thermal disturbances experienced by the sample as revealed by the step heating experiment have been very useful in solving various geological problems and make this ^{40}Ar-^{39}Ar technique a more robust tool compared to the conventional K-Ar dating method.

3.2 ^{40}Ar/^{39}Ar thermochronology

The fact that the 't' obtained by the ^{40}Ar-^{39}Ar approach can be related to the thermal history experienced by the sample gave rise to a new field of ^{40}Ar-^{39}Ar thermochronology. The fundamental basis of the ^{40}Ar-^{39}Ar thermochronology is that the loss of radiogenic argon from the sample is a temperature dependent diffusion process.

3.2.1. Diffusion theory and diffusion equation

Random molecular motion tends to equilibrate the molecular/atomic concentration in a finite volume and this leads to the diffusion of Ar from areas of high concentration to areas of the low concentration in the sample. Fick's first law describes this molecular diffusion on basis of an analogy with the Fourier's law of heat conduction. This is represented as

$$\frac{n}{A_x} = F = -D\frac{\partial C}{\partial X} \tag{3.10}$$

where n is number of molecules, A_x is cross sectional area, F is flux across the unit area, D is the proportionality constant called diffusion constant, C is the concentration. The minus sign indicates that flow is from high concentration to low concentration. The change in concentration with time t in the three space coordinates can be derived and is represented as

$$\frac{\partial C}{\partial t} = D(\frac{\partial^2 C}{\partial X^2} + \frac{\partial^2 C}{\partial Y^2} + \frac{\partial^2 C}{\partial Z^2}) \tag{3.11}$$

This is referred to as Fick's second law. The solution of the above equation for different geometries and boundary conditions gives us the distribution of concentration at any time t within the solid of that geometry. These solutions then can be converted into the expressions for fractional loss after time t starting with a homogeneous distribution of concentration in the solid. For example the expression for a sphere of radius r would be

$$f = 1 - (6/\pi^2)\sum_{1}^{\infty}(1/n^2)\exp(-n^2\pi^2 Dt/r^2) \tag{3.12}$$

Where f is the fractional loss. Here D is taken as constant with time. These expressions for fractional loss for solids of different geometries are given in McDougall and Harrison (1999). This equation can be used to calculate theoretical age spectra for those solids who have experienced partial loss of radiogenic argon at some time t. However, it has been shown that the diffusion coefficient is dependent on temperature and follows the Arrhenius equation. Hence in the case of constant diffusion coefficient it is assumed that the temperature remains constant.

3.2.2. Arrhenius equation

The temperature dependence of diffusion coefficient is given as

$$D = D_0 \exp(-E/RT) \tag{3.13}$$

Where D_0 is the frequency factor ($D=D_0$ at $T=\infty$), E is the activation energy required to cross the threshold so that an atom can move in a crystalline lattice and the T is the absolute temperature. This equation will become an equation of straight line on taking the logarithm (to the base 10) of both sides as

$$\log D = \log D_0 - \frac{E}{2.303R}\frac{1}{T} \tag{3.14}$$

Arrhenius plot is obtained by plotting –logD versus 1/T. It will give a straight line with slope as E/2.303R and intercept on y as $-\log D_{0.}$. This equation can be coupled with the solutions of diffusion equation that provide the concentration distribution at time t or the fractional loss *f*. Thus we can have a relationship between the diffusion coefficient D, temperature T and time t such as

$$\frac{E}{RT} = \ln(\frac{tD_0 / r^2}{Dt / r^2}) \tag{3.15}$$

Here the dimensionless parameter Dt/r^2 is given by the expression of fractional loss *f*. In this way we can assign a temperature T to the age t obtained for the system which undergone a fractional loss because of a square thermal pulse, i.e. temperature increased from T=0 to T. This forms the basis of thermochronology. Though this relationship is valid only for the diffusion coefficient D which doesn't change with time, i.e. temperature remains constant which is not very realistic scenario geologically, it can be extended to any realistic thermal history by just introducing time-dependent D, defined as

$$\zeta = \int_0^t \frac{D(t)}{r^2} dt \tag{3.16}$$

for (Dt/r^2) in equation (3.15) (Dodson, 1973; Lovera, et al., 1989) . This will introduce a time constant τ, according to the thermal history chosen, and the equation (3.15)will become as

$$\frac{E}{RT} = \ln(A\tau D_0 / r^2) \tag{3.17}$$

Where A is a geometric constant (as the solution of diffusion equation (3.11) depends upon the geometry of grain) and τ is a function related to the form of integrated thermal history, e.g. if we assume the thermal history to be linear in 1/T (t=1/T), then time dependent diffusion coefficient can be written with a time constant τ such as $D=D_o\exp(-E/RT_o-t/\tau)$ or $D= D(0)\exp(-t/\tau)$, where D(0) is the initial diffusion coefficient. Here τ is defined as the time in which the diffusion coefficient D will become 1/e times the initial. T is some characteristic temperature of the system. This temperature T corresponding to age t indicates that at this temperature the retention of the daughter atoms became complete and the diffusive loss stopped. This is called the closure temperature.

3.2.3. Concept of closure temperature and equation

Minerals and rocks crystallize at high temperatures. At such high temperatures the radiogenic argon diffuses out of the system as soon as it forms from the decay of ^{40}K. The temperature at which the radiogenic argon starts to accumulate within the system and stops getting lost is called the closure temperature for argon. For volcanic rocks this temperature is achieved almost instantaneously as they cool very fast but for the minerals and rocks forming very deep inside the earth there is a significant time delay to reach the closure temperature. For such slowly cooling systems the age calculated gives the time at which the system attained its closure temperature. This concept of closure temperature or blocking temperature was given by the Dodson (1973) and is represented diagrammatically below (Fig. 3.1). This diagram shows that in a slowly cooling mineral the daughter-to-parent ratio (D/P) is zero at very high temperature and passes through a partial accumulation zone (the curved portion in the lower diagram) and then increases constantly with time. The age calculated in lab (t_c) is the intercept of the constant growth line of D/P on the time axis and the corresponding temperature T_c is called the closure temperature for the daughter element.

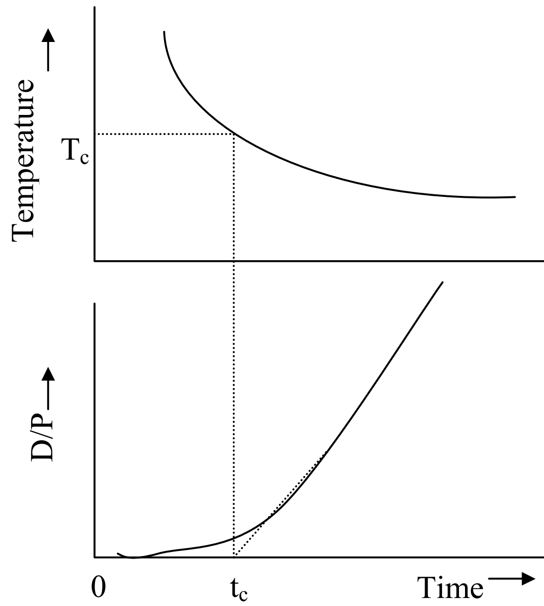

Fig. 3.1 *Illustration of closure temperature concept. T_c is the closure temperature and t_c is the time. The diffusive loss of daughter (D) ceases when the system is cooled to T_c at time t_c, After that daughter to parent ratio (D/P) increases with the constant rate, corresponding to the decay constant.*

Dodson (1973) has derived the expression for the closure temperature as

$$T_c = \frac{E/R}{\ln[\frac{ART_c^2 D_0 / r^2}{EdT/dt}]} \tag{3.18}$$

This expression requires an initial assumption of cooling history (dT/dt), however, it has been shown (Lovera et al., 1993) that the closure temperature is highly insensitive to the cooling history. This expression can be extended to the time dependent diffusion coefficient as well. This allows us to assign temperature to the age calculated for a mineral. If we analyze three different minerals from a same rock then we will have three time-temperature points for that rock and that provides us the cooling history of that rock as depicted in the following diagram (Fig. 3.2).

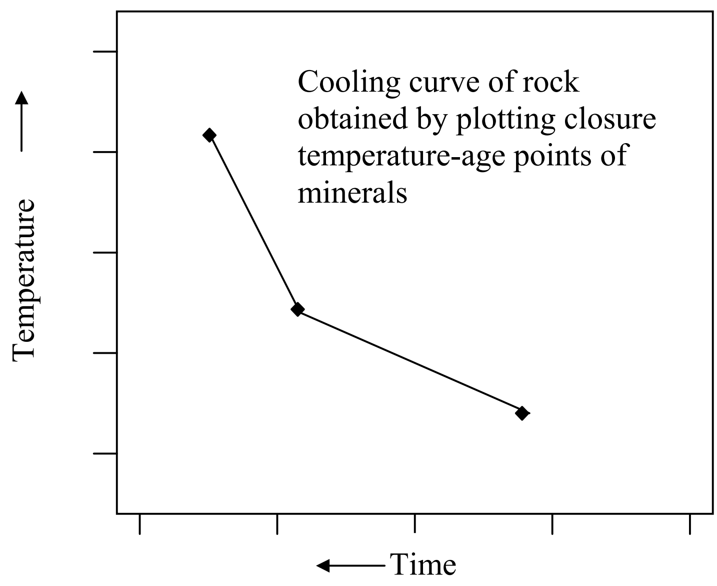

***Fig.3.2** Cooling history diagram as derived by plotting the age-closure temperature, pairs of different minerals. This is a traditional method of thermochronology.*

3.2.4. Assumptions

This approach of obtaining the cooling history requires the following assumptions.

1. The laboratory degassing follows the same volume diffusion process that governed the loss of radiogenic argon in nature.
2. Minerals are stable under vacuum heating.
3. Minerals have not experienced the subsequent loss of argon below the closure temperature.

4. Minerals were not recrystallized.

Age spectrum also provides us the information of the cooling history experienced by the sample. A theoretical age spectrum can be constructed using the diffusion properties of the sample obtained from the Arrhenius plot (as discussed in section 3.2.2), which will match the age spectrum obtained in the laboratory if the cooling history assumed to construct the theoretical spectrum is correct.

3.3 Multi Diffusion Domain (MDD) Model

It has been observed for many K-feldspars that the Arrhenius plots are not always straight lines as predicted by the above single site diffusion model**.** This has been explained by Lovera et al. (1989) by the multi diffusion domain (MDD) model. The MDD model, apart from the fundamental assumption that argon diffusion in the laboratory follows the same mechanism as in nature, is based on the following assumptions

1. The sample is composed of non-interacting, discrete diffusion domains of simple geometries.
2. The domain boundaries have zero argon concentration.
3. The parent ^{40}K is distributed homogeneously within each domain.
4. Cooling starts at very high temperatures and is very slow.

The age spectra and Arrhenius plots for the MDD can be calculated by adding up the argon released from each separate domain. This extension has been done by Lovera et al. (1989) who presented a mathematical expression for calculating the age spectrum and the Arrhenius plot. The diffusion parameters and the distribution of domains of sample having multi diffusion domains are difficult to calculate from the Arrhenius plot alone, due to its non-linearity. The Arrhenius plot of such a sample would be nonlinear because of simultaneous release of argon from all the diffusion domains and to quantify the contribution from each of the domain a different way of plotting, independent of the heating schedule would be required (Lovera et al., 1991).

3.3.1 Log(r/r_0) plot

Lovera et al. (1991) proposed a new way of plot, known as log(r/r_o) plot. This plot is constructed by first estimating log (D/r_o^2), as the intercept of linear portion of the Arrhenius plot, on y-axis. Each successive D/r^2 is calculated according to eq. 3.12 taking the appropriate geometry of domains into consideration. Subtracting $\log(D/r^2)$ from the $\log(D/r_o^2)$ gives $2\log(r/r_o)$. It is then plotted after dividing by 2 with cumulative % of ^{39}Ar released. This provides an estimate of gas content of each separate domain size and is independent of laboratory heating schedule.

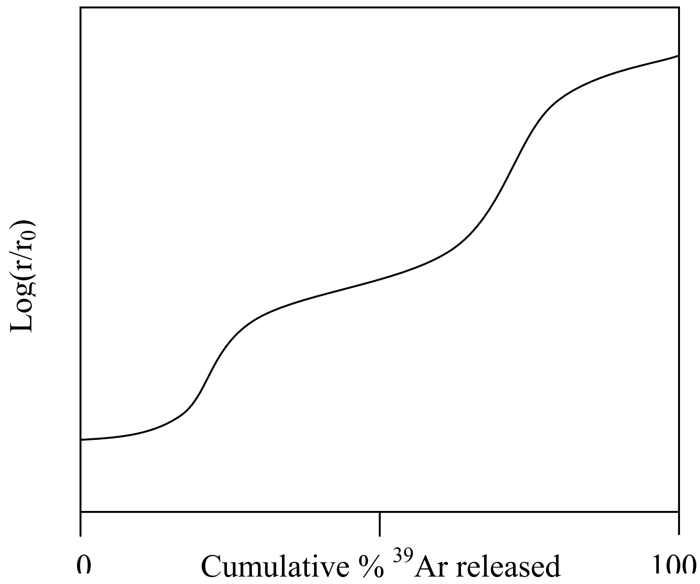

Fig. 3.3 *Log (r/r_o) plot. The local plateaus correspond to the sizes and the steep rises, from one plateau to another, correspond to the gas content of different diffusion domains.*

This plot (Fig. 3.3) shows the sizes in terms of the local plateaus and the gas contents of each domain is represented by the steep rises from one domain to another domain. Once the distribution of the domains is known from the above plot one can construct a theoretical age spectrum for different cooling histories to obtain the best fit with the age spectrum obtained in the laboratory and hence the corresponding cooling history can be ascertained. The MDD model thus provides the continuous cooling history from a single mineral instead of a temperature-time point.

The MDD model was developed for K-feldspars, however, it has been used for whole rocks in the present study. The rationale for using this model for whole rocks is that different minerals may be taken to represent the different diffusion domains which satisfy all the necessary criteria for using the MDD model. Most importantly, the rock must be devoid of any mineral such as biotite, which tends to break down under vacuum heating.

Recently (Lee, 1995), has proposed another process of argon loss which is called Multi Path (MP) model. MP model takes into account the defects and cracks in crystal that can lead to non-volume diffusion loss of argon. However, this model is not used here.

3.4. Experimental Aspects

3.4.1. Sample Preparation

Whole rock samples were first examined under petrographic microscope and fresh sample chips were crushed and powdered in a stainless steel mortar and pestle to 100-150 μm size. From the homogenized powder a 600-700 mg aliquot was prepared. Mineral separation was done using the standard procedure of density and magnetic separations using heavy liquid and isodynamic Franz magnetic separator respectively. The final separation was done by hand picking coarse grains under a stereomicroscope. The whole rock and minerals then were cleaned and washed using 0.05N HCl in an ultrasonic bath to remove carbonate impurities. Samples were ultrasonicated with water several times to ensure removal of all HCl. The dried sample powder then was packed in aluminum foils along with the monitor sample and pure CaF_2 and K_2SO_4 salts and sealed in quartz vials. To monitor the neutron fluence variation in the reactor a 99.99% pure Ni wire was kept in each vial. The sealed vials were put in an aluminum reactor can and sent for the irradiation.

3.4.2. Irradiation of the sample

The samples were irradiated in the APSARA reactor of Bhabha Atomic Research Centre (BARC) Mumbai. This is a light water-moderated reactor of 1MW power. The total neutron flux is 10^{12} neutron/cm^2/sec out of which 50-60% is fast neutron flux. The irradiation is carried out in the D-4 position of the reactor, which is the core position and receives the maximum flux with the minimum variation. The irradiation was done for 100 hrs cumulative in two batches. The maximum and minimum durations of the irradiation in a step was 0.25 hrs and 6 hrs respectively. The maximum flux variation was determined by the ^{58}Co activity, produced from ^{58}Ni by the ^{58}Ni (n,p) ^{58}Co reaction. The maximum variation is found to be 5% horizontally and 6% vertically. The irradiated samples were cooled to bring the activity to a safe handling level. The samples were then packed in aluminum foils and stored in the sample tree of the extraction unit.

3.4.3. Interfering nuclear reactions

A sample consisting of a variety of elements gives rise to a wide range of nuclear reactions; however only those producing argon are of interest here. Isotopes of argon can be produced by interaction of neutrons with isotopes of calcium, potassium, argon, and chlorine (Merrihue and Turner, 1966; Mitchell, 1968; Brereton, 1970; Turner, 1971a). Out of these reactions many are of minor significance due to the small abundance of the target isotope in the sample or due to higher energy required for the reactions. The most important reactions for the ^{40}Ar/^{39}Ar dating are tabulated below (Table 3.1).

3.4.3.1 Reactions with calcium

Three argon isotopes ^{36}Ar, ^{37}Ar and ^{39}Ar are produced from reaction with calcium. Corrections are made for the ^{36}Ar and ^{39}Ar with the help of ^{37}Ar, which is neither present in atmospheric argon and nor produced in a significant amount during the irradiation, from ^{39}K. A pure calcium salt, CaF_2, is irradiated along with the sample and (^{36}Ar/^{37}Ar) and (^{39}Ar/^{37}Ar) ratios are measured in it, which then are used for obtaining the correction factors, after correcting for the atmospheric ^{36}Ar.

Table 3.1 *Important nuclear reactions producing argon isotopes by neutron bombardment* [a,b] *(from McDougall and Harrison, 1999).*

Argon Isotope Produced	**Target Element**	
	Calcium	**Potassium**
^{36}Ar	**^{40}Ca(n,nα)^{36}Ar (-7.04, 96.94)**	
^{37}Ar	**^{40}Ca(n,α)^{37}Ar (+ 1.75, 96.94)**	
^{39}Ar	**^{42}Ca(n,α)^{39}Ar (+0.34, 0.65)**	**^{39}K(n,p)^{39}Ar (+0.22, 93.26)**
^{40}Ar		**^{40}K(n,p)^{40}Ar (+2.29, 0.01167)**

[a] *Apart from these reactions, ^{36}Ar is also produced from ^{35}Cl, ^{37}Ar from ^{39}K and ^{36}Ar, ^{39}Ar from ^{38}Ar and ^{40}Ar from ^{43}Ca, ^{44}Ca and ^{41}K in insignificant amounts. ^{38}Ar is produced from ^{42}Ca, ^{39}K, ^{41}K, ^{40}Ar and ^{37}Cl, however usually not corrected for as it doesn't interfere the final results.*

[b] *In brackets are given the energy associated with the reaction (MeV) and the target isotope abundance (atom%)*

Thus while the correction factor $(^{39}Ar/^{37}Ar)_{Ca}$ is straight forward = $(^{39}Ar/^{37}Ar)_m$ in the CaF_2 (after correcting for the decay of ^{37}Ar and ^{39}Ar), where subscript 'm' stands for the measured, the correction factor for ^{36}Ar is obtained after correcting for the atmospheric ^{36}Ar with the help of ^{40}Ar as $(^{36}Ar/^{37}Ar)_{Ca} = \{^{36}Ar_m - ^{40}Ar_m/295.5\}/^{37}Ar$, since all the ^{40}Ar present in the CaF_2 is of atmospheric origin. Here the ^{37}Ar value used is the one after the decay correction {half life($t_{1/2}$) =35.1 days} during the irradiation and subsequent to it.

3.4.3.2. Reactions with potassium

The most important reaction for ^{40}Ar/^{39}Ar dating is with ^{39}K, ^{39}K(n,p)^{39}Ar. Besides this, ^{40}Ar is also produced in significant amounts from ^{40}K according to the reaction ^{40}K(n,p)^{40}Ar. The correction factor for $^{40}Ar_K$ is derived by measuring argon ratios in the irradiated pure potassium salt, K_2SO_4. The ^{40}Ar measured in this salt then is corrected for the atmospheric ^{40}Ar and the correction factor is obtained as

$$(^{40}Ar/^{39}Ar)_K = \{^{40}Ar_m - ^{36}Ar_m X\ 295.5\}/^{39}Ar \tag{3.19}$$

Here it is assumed that all the ^{36}Ar measured in the potassium salt is of atmospheric origin.

3.4.4 Decay correction

^{37}Ar and ^{39}Ar produced in the reactor are radioactive. It is required to correct for their decay during and subsequent to irradiation of the sample until the time of analysis. As the half life of ^{39}Ar is 269 ± 3 yrs, no significant error is introduced during the time scale of irradiation to analysis(~1 year) if left uncorrected. However, the half life of ^{37}Ar is only 35.1 ± 0.1 days (Stoener et al., 1965) and the decay correction of ^{37}Ar is very important to arrive at the correct result. The relevant general equation for the decay factor after Brereton (1972) and Dalrymple et al. (1981) is

$$\text{Decay Factor} = \frac{\lambda t e^{\lambda t'}}{(1 - e^{-\lambda t})} \tag{3.20}$$

Where t is the duration of irradiation and t' is the time elapsed between the end of the irradiation and the analyses. The above equation is valid only when the irradiation is done continuously, though usually the irradiation is done in segments of various durations. In the latter case the equation used is given by Wijbrans (1985) as:

$$\text{Decay Factor} = \lambda \sum_{i=1}^{n} t_i \Big/ \sum_{i=1}^{n} \{(1 - e^{-\lambda t_i}) / e^{\lambda t_i}\} \tag{3.21}$$

Where t_i is the duration of irradiation of segment i, t_i' is the time elapsed between the end of i^{th} segment and the analysis of the sample, n is the total number of such segments, and λ is the decay constant for ^{37}Ar.

3.4.5 The Calculation of $^{40}Ar^*/^{39}Ar_K$

The final calculation of the age takes care of the above decay factors and reactor-produced argon isotopes. After the analysis of the sample, the total ^{40}Ar measured, $^{40}Ar_m$, would have all the components as

$$^{40}Ar_m = {}^{40}Ar^* + {}^{40}Ar_A + {}^{40}Ar_K \qquad (3.22)$$

where superscript * indicates the radiogenic component and the subscripts 'A' and 'K' indicate atmospheric and potassium produced components of ^{40}Ar. Hence

$$^{40}Ar^* = {}^{40}Ar_m - {}^{40}Ar_A - {}^{40}Ar_K \qquad (3.23)$$

And the total ^{36}Ar measured, $^{36}Ar_m$ will have components of atmospheric ^{36}Ar, $^{36}Ar_A$ and calcium produced ^{36}Ar, $^{36}Ar_{Ca}$ as

$$^{36}Ar_m = {}^{36}Ar_A + {}^{36}Ar_{Ca} \qquad (3.24)$$

with the atmospheric ratio as $\{^{40}Ar/^{36}Ar\}_A = 295.5$

Then

$$^{40}Ar_A = 295.5\,[\,^{36}Ar_m - {}^{36}Ar_{Ca}] \qquad (3.25)$$

substituting it in the eq.3.23 we get

$$^{40}Ar^* = {}^{40}Ar_m - 295.5\,{}^{36}Ar_m + 295.5\,{}^{36}Ar_{Ca} - {}^{40}Ar_K \qquad (3.26)$$

The total ^{39}Ar measured, $^{39}Ar_m$, would have potassium produced ^{39}Ar, $^{39}Ar_K$, and Ca produced as $^{39}Ar_{Ca}$, i.e.

$$^{39}Ar_m = {}^{39}Ar_K + {}^{39}Ar_{Ca}$$

or

$$^{39}Ar_K = {}^{39}Ar_m - {}^{39}Ar_{Ca} \qquad (3.27)$$

Dividing eq.(3.26) by eq. (3.27) and dividing both numerator and denominator on the right hand side by $^{39}Ar_m$ we get

$$\frac{^{40}Ar^*}{^{39}Ar_K} = \frac{(^{40}Ar/^{39}Ar)_m - 295.5(^{36}Ar/^{39}Ar)_m + 295.5(^{36}Ar_{Ca}/^{39}Ar_m) - (^{40}Ar_k/^{39}Ar_m)}{1-(^{39}Ar_{Ca}/^{39}Ar_m)} \qquad (3.28)$$

As $$\frac{^{36}Ar_{Ca}}{^{39}Ar_m} = \frac{^{36}Ar_{Ca}}{^{37}Ar_{Ca}}\frac{^{37}Ar_m}{^{39}Ar_m} \qquad (3.29)$$

$$= [\frac{^{36}Ar}{^{37}Ar}]_{Ca} [\frac{^{37}Ar}{^{39}Ar}]_{Ca} \qquad (3.30)$$

because $^{37}Ar_{Ca} = {}^{37}Ar_{m,}$ and as

$$\frac{^{39}Ar_{Ca}}{^{39}Ar_m} = [\frac{^{39}Ar}{^{37}Ar}]_{Ca} [\frac{^{37}Ar}{^{39}Ar}]_m \qquad (3.31)$$

because $^{37}Ar_{Ca} = {}^{37}Ar_{m,}$ and as

$$\frac{^{40}Ar_K}{^{39}Ar_m} = [\frac{^{40}Ar}{^{39}Ar}]_K \frac{^{39}Ar_K}{^{39}Ar_m} \qquad (3.32)$$

$$= [\frac{^{40}Ar}{^{39}Ar}]_K [1 - \frac{^{39}Ar_{Ca}}{^{39}Ar_m}] \qquad (3.33)$$

Substituting eq. (3.30), (3.31) and (3.33) in the eq. 3.28 one gets

$$\frac{^{40}Ar^*}{^{39}Ar_K} = \frac{(^{40}Ar/^{39}Ar)_m - 295.5(^{36}Ar/^{39}Ar)_m + 295.5(^{36}Ar/^{37}Ar)_{Ca}(^{37}Ar/^{39}Ar)_m}{1-(^{39}Ar/^{37}Ar)_{Ca}(^{37}Ar/^{39}Ar)_m} - [\frac{^{40}Ar}{^{39}Ar}]_K$$

(3.34)

This equation is used to calculate the age at the each temperature step.

3.4.6. Argon extraction and purification

An argon extraction and purification system was developed indigenously (Venkatesan et al., 1986). Fig. 3.4 shows the schematic of this system. It is composed of a high vacuum line with two ion pumps, one diffusion pump, and one rotary pump, a furnace assembly in which a sample can be heated in a controlled manner, getter system for purification, isolation valves and charcoal trap cooled at liquid nitrogen temperature to move the gas from one section to another section. The furnace (Fig. 3.5) is a single vacuum chamber. It consists of a molybdenum crucible electrically heated by a concentric, tantalum mesh filament surrounded by tantalum radiation shields. The temperature of the crucible is controlled by a variac, which is calibrated with the help of an optical pyrometer. The temperatures are calibrated within ± 10^{o}C. The outer SS jacket of furnace is connected to cold water supply. Samples are dropped into the crucible from a glass sample holder connected to the upper flange of the furnace.

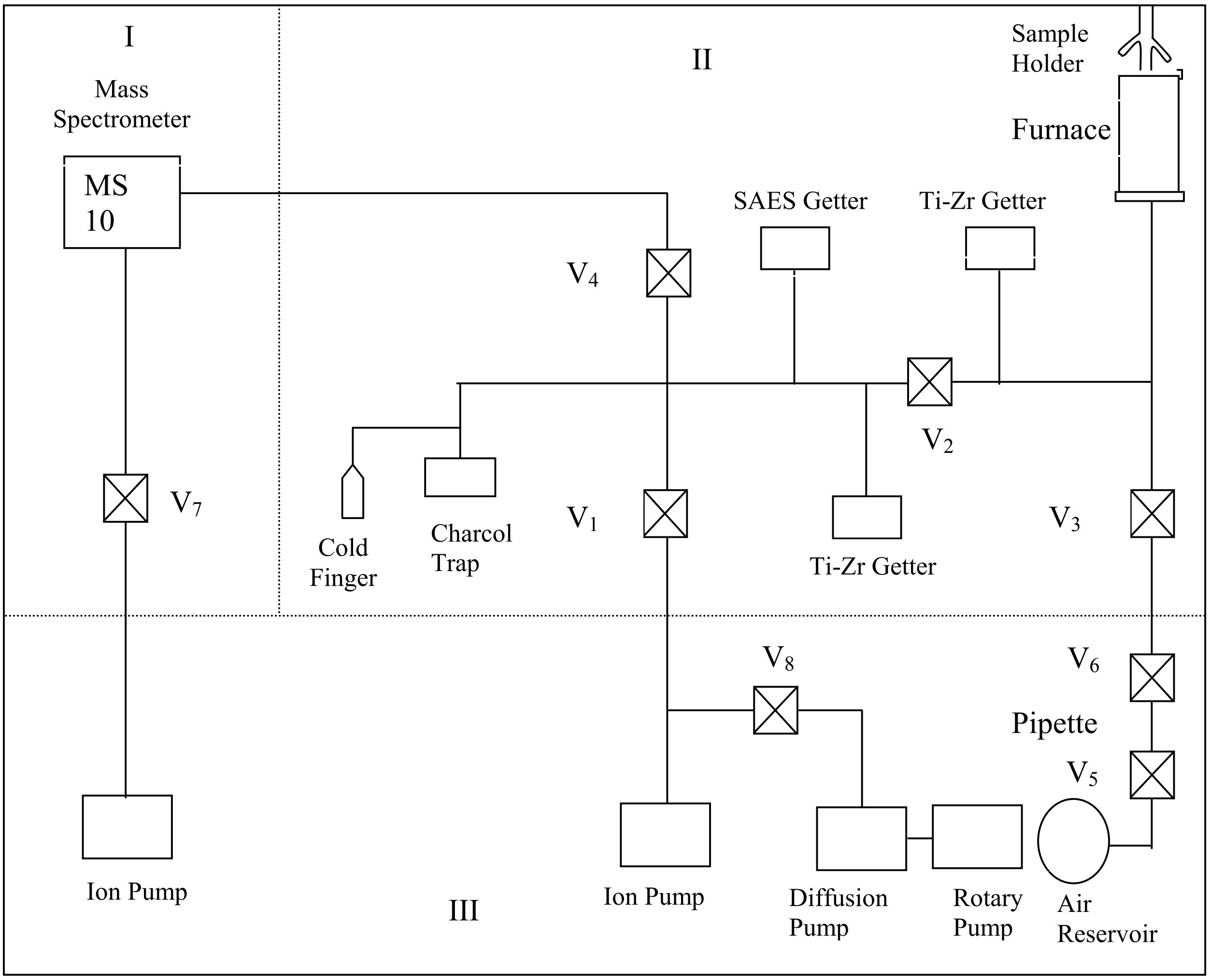

***Fig.3.4** Schematic diagram of the complete Argon Gas Extraction-Purification system. I: Mass Spectrometer, II: Extraction System and III: Pumping System.*

The gas purification system consists of four valves V_1 to V_4 and three getters, all interconnected and fitted into a single rectangular stainless steel block (Fig. 3.6). The gas is extracted from the sample by heating the sample for 55 min. at each temperature step. The released gas first comes into contact with Ti-Zr getter which is kept hot, most of the active gasses are either chemically combined or adsorbed by this getter. This cleaned gas then is allowed to react with another Ti-Zr getter and SAES getter by opening the valve V_2 (Fig. 3.4). The first Ti-Zr getter, in meantime is reduced to room temperature to adsorb the hydrogen.

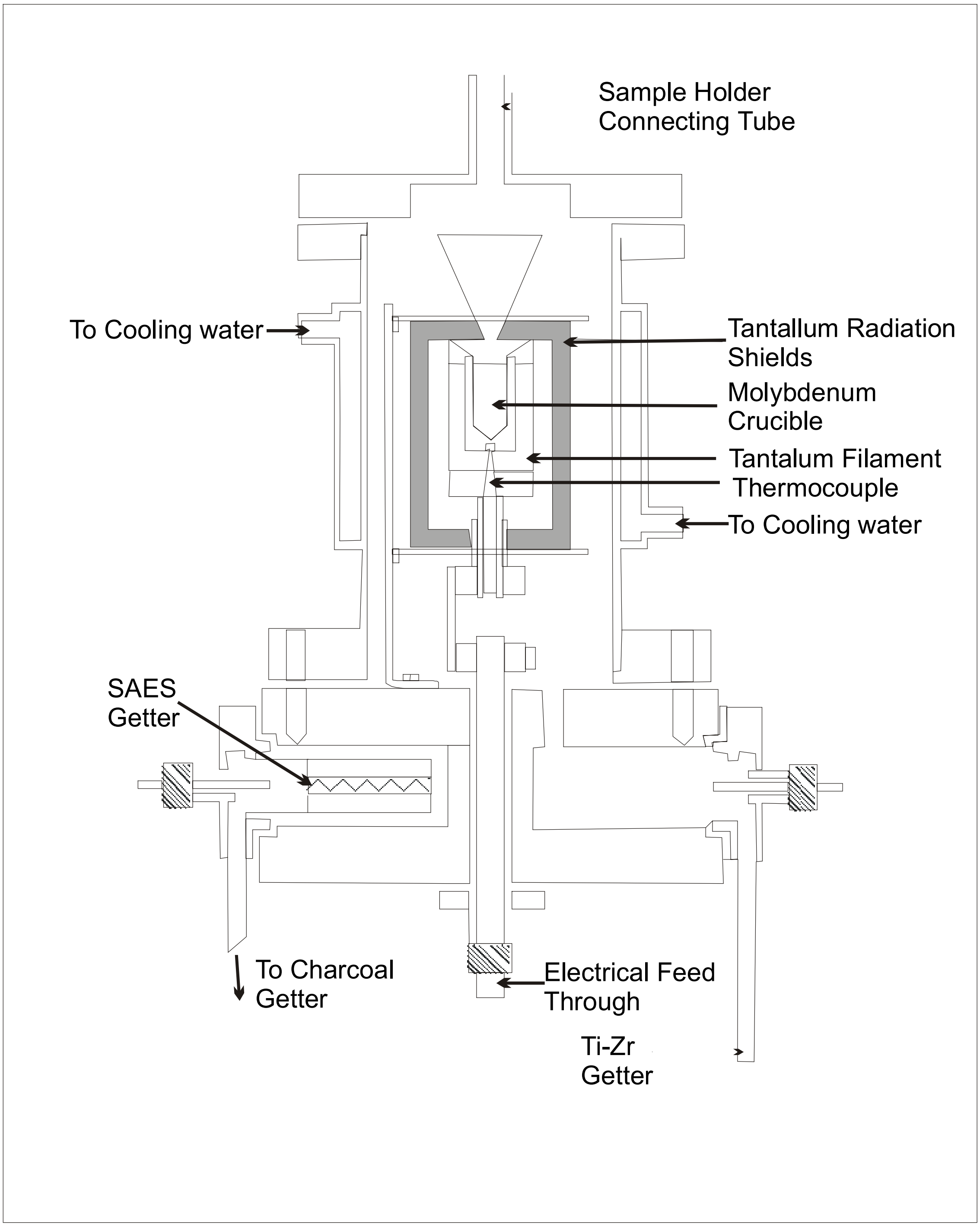

Fig.3.5 *A section through furnace and extraction unit.*

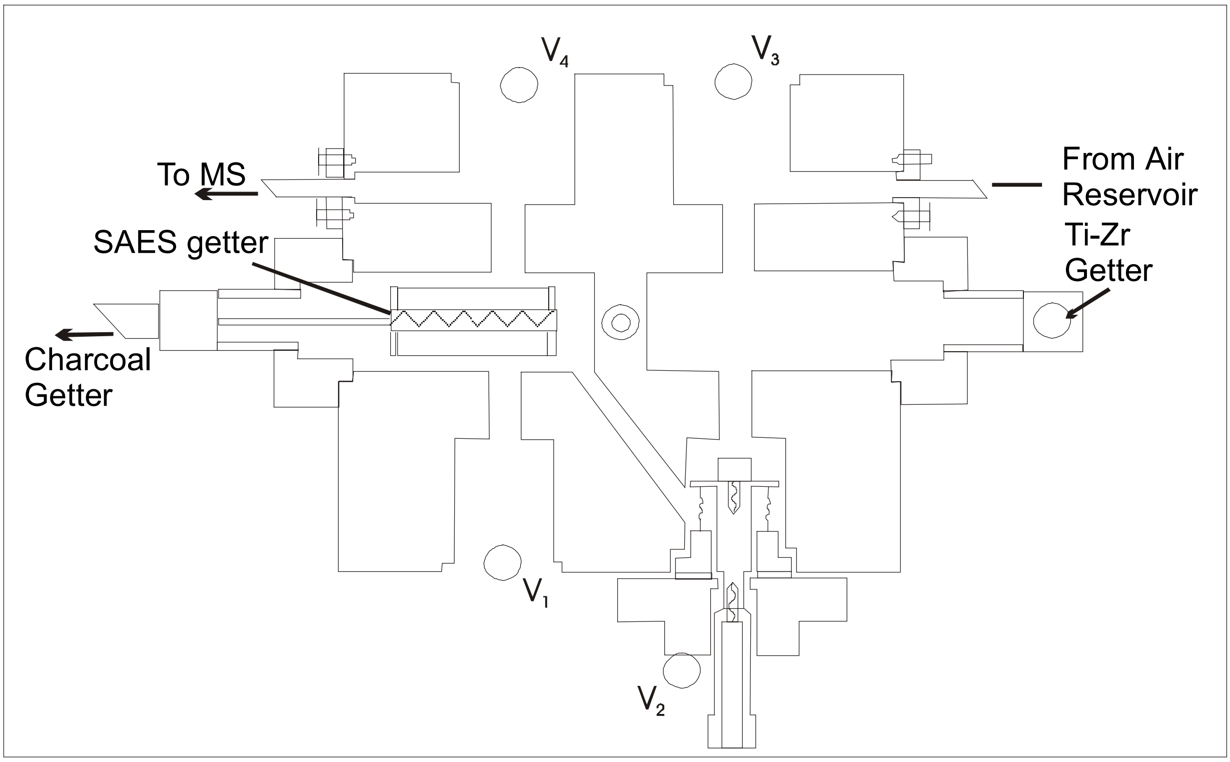

Fig.3.6 *Middle section of the S-S block showing assembly of the one of the valves*

The purified gas then is adsorbed on charcol which is kept at liquid nitrogen temperature. 15 min are given for this collection to ensure that almost all the purified gas is collected on the charcoal. It is then passed through cold finger kept at liquid nitrogen temperature to remove water vapour before admitting into the mass spectrometer, by opening V_4. After the gas gets equilibrated the V_4 is closed and the remaining unwanted gas is pumped by opening V_1 (Fig. 3.4). The gas is extracted and purified in this manner for usually 19-20 temperature steps starting at 400^{o}C and going up to 1400^{o}C at 50^{o}C intervals.

3.4.7. Analysis, Data acquisition and Reduction

The purified gas is analyzed in AEI MS10 (180^{o} deflection, 5cm radius) having 1.8 kilogauss permanent magnetic field and is operated in static mode. Ions of masses 40, 39, 38, 37 and 36 are collected by varying the accelerating voltage on a Faraday cup. The ion currents (pico amperes) are dropped across very high resistances of 10^{11} ohms to 10^{10} ohms according to the amount of gas.

The data acquisition of the resulting voltages is done sequentially through a computer. Peak heights and relative timings of peak measurements from the time of sample introduction (t_o) are fed to a curve-fit program to compute isotopic ratios and abundances corresponding to time zero (t_o). The ratios measured are corrected for system blanks for each temperature step. The system blanks are measured before and after the sample for 10 to 12 steps and the blanks are estimated for the other steps by interpolation. System blanks are measured following the same procedure as is used for the sample but without sample. The ^{40}Ar blank for the present work varied from 0.2 to 20 % of the sample gas for temperature steps up to about 1200^{o}C and increases up to 30% and occasionally to 40% in the fusion step. Table 3.2 gives a typical blank variation in different steps for a sample.

Table 3.2 *Typical system blanks in percentage (Sample LK198)**

TEMP.(^{o}C)	^{39}Ar	^{36}Ar	^{37}Ar	^{40}Ar
450	.00	.00	.00	1.38
500	.00	.00	.00	2.39
550	.00	.00	.00	2.33
600	.00	.00	.00	1.54
650	.00	.00	.00	3.16
700	.00	.00	.00	1.79
750	.00	.00	.00	1.97
800	.00	.00	.00	1.99
850	.00	.00	.00	1.81
900	.00	.00	.00	2.11
950	.00	.00	.00	1.82
1000	.00	8.11	.00	1.41
1050	.00	5.99	.00	1.05
1100	.00	4.11	.00	.70
1150	.00	9.21	.00	2.81
1200	.00	22.07	.00	9.35
1250	.00	20.05	.00	9.60
1300	.00	42.55	.00	27.64
1400	.00	34.04	.00	34.45
TOTAL	.00	7.26	.00	3.35

* The blanks are measured for each sample.

The blank corrected ratios are then corrected for mass discrimination (MD) based on analysis of atmospheric argon (Air Standard) introduced from a pipette system connected to the extraction line. Each sample was preceded and followed by an Air Standard analyses and the average MD values were found for correcting the measured ratios. Mass spectrometer signal was calibrated with the known amount of $^{40}Ar^*$ by repeated measurements of the monitor sample McClure Mountain Hornblende (MMHb-1). This helps in knowing the abundance of an isotope, and is called 'sensitivity for argon' and found to be varying from (0.1 to 0.8) $\times 10^{-7}$ ccSTP/mV.

Errors are calculated by quadratically propagating the errors in the measured ratios, blanks and interfering isotopes. Each box in the age spectra does not include error in J but the errors quoted on the plateau age and the integrated age includes error in J. All the errors quoted are 2σ. Plateau age is weighted mean of the apparent ages of at least four consecutive steps which are within 2σ and consist of minimum 50% of gas released. Weighted means are calculated using the method given by Bevington (1969) where $1/\sigma_i^2$ (σ_i is the standard deviation for the i^{th} step) is taken as the weight. Isochron ages are calculated using the two-error regression method outlined by York (1969) of data points corresponding to plateau steps. The typical error on the age of the samples analyzed is less than 10%.

Chapter Four

Results

4.1 Presentation of Results

4.1.1. Age Spectrum and Plateau Age

The step heating experiment yields apparent ages of gas fractions released at different temperatures. Turner et al. (1966) first plotted the apparent age at each temperature step against the cumulative % of ^{39}Ar released. This plot has since then become a standard way of presenting the results of the step heating experiment and is known as the age spectrum. This plot enables one to test the underlying assumptions (Chapter 3, 3.1.1). If the sample has remained a closed system since its crystallization and not subjected to subsequent thermal disturbance, and if potassium was distributed uniformly, all the steps would yield concordant ages and would result in a flat (**Plateau**) age spectrum. Deviation from flatness would indicate subsequent disturbances.

To distinguish between undisturbed and disturbed systems, many criteria were proposed for the identification of a plateau in an age spectrum (Dalrymple & Lanphere, 1974; Fleck et al., 1977; York et al., 1981; Foland et al., 1986; Snee et al., 1988; Dallmeyer and Lecorche, 1990). However, there is no uniform convention on the definition of a plateau. I have defined the plateau in the age spectrum as a portion that has four or more consecutive steps with apparent ages within 2σ comprising of at least 50 % of the total ^{39}Ar released. While the apparent ages don't include error in ***J***, the plateau age is calculated by taking a weighted mean of apparent ages including the error in ***J.*** Plateau-like ages are calculated wherever there are plateau-like features but the above criterion for plateau is not strictly met.

4.1.2. Isochron Plot

Merrihue and Turner (1966) first employed the technique of isotope correlation diagram to the step heating results for simultaneously assessing the sample age and isotopic composition of the trapped argon. This has provided an independent check for the model assumption that the trapped argon is of atmospheric composition. The isochron is derived by plotting the total $^{40}Ar/^{36}Ar$ measured in each step (after correcting for the nuclear interferences), constituting the plateau, against the $^{39}Ar_K/^{36}Ar$ (proxy for the parent ^{40}K). This approach is similar to the conventional Rb/Sr isochron method. A linear regression is done with due weightage for the errors in both the ratios. (York, 1966, 1969). In the case where ^{36}Ar is in small amount, it is measured with poor precision compared to ^{40}Ar and ^{39}Ar. Thus the presence of ^{36}Ar in both the axes results in highly correlated errors. To circumvent this problem another way of plotting was suggested (Turner, 1971b; Roddick et al., 1980) in which $^{36}Ar/^{40}Ar$ is plotted against $^{39}Ar/^{40}Ar$. This is called inverse isochron. However, essentially both the plots should give same age and trapped ratio. I have presented here only isochron plots for the concordant age steps forming plateau, wherever plateau ages were derivable.

4.1.3. Criterion of the Goodness of Fit

A criterion of Mean Square of Weighted Deviate (**MSWD**) is used to test the goodness of fit of straight line to the data (McIntyre et al., 1966). The data are weighted according to the inverse weighted variance. A MSWD much less than the expected value of 1 suggests that experimental errors may be overestimated (Wendt and Carl, 1991), while if the value of MSWD is much higher than unity, a linear relationship between the data may not exist or experimental errors may be underestimated (McDougall & Harrison, 1999).

4.2 Monitor Sample

Results presented here are with respect to the widely used monitor sample McClure Mountain hornblende (MMhb-1), with an age of 520.4 ± 1.7 Ma based on the average results of K-Ar analyses from 15 different laboratories (Alexander et al., 1978; Samson and Alexander, 1987). There has been some debate, however, over the true age of this standard lately (Baksi et al 1996) with U.S. Geological Survey reporting an age of 513.9

± 2.3 Ma based on K-Ar data (Dalrymple et al 1993). Renne et al., (1998) have recommended an age of 523.1 ± 2.6 Ma (neglecting the error in the decay constant) based on intercalibration of other primary standards. I have also analysed another standard LP-6 biotite (Table 4.1) for intercalibration with respect to the MMhb-1. The total fusion age obtained, 124.1 ± 2.2 (2σ error) Ma, with respect to the 520.4 ± 1.7 Ma age of the MMHb-1, is within errors of the average K-Ar age of 127.9 ± 2.2 Ma (2σ error) based on several interlaboratory analyses of LP-6 (Odin et al 1982).

Table 4.1 *Argon isotopic composition and total age of LP6 Biotite. The error in age is with error in **J**.* ***J= .002296 ± .000014,*** *correction factors are* $(^{36}Ar/^{37}Ar)_{Ca}$ *=0.00016;* $(^{39}Ar/^{37}Ar)_{Ca}$*= 0.00075, and* $(^{40}Ar/^{39}Ar)_{K}$*= 0.046.*

$^{36}Ar/^{39}Ar$ ± 1σ	$^{40}Ar/^{39}Ar$ ± 1σ	^{40}Ar*%	$^{37}Ar/^{39}Ar$ ± 1σ	$^{40}Ar/^{36}Ar$ ± 1σ	AGE(Ma) ± 1σ
0.01115	34.32	90.40	0.00786	3079.1	124.1
0.00043	0.21		0.00032	121.3	1.1

The results obtained using the different ages of the monitor samples, however, can be readily compared by recalculating relative to the new age to avoid the confusion by using the following equation (Renne, 2000; Dalrymple et al., 1993):

$$t_u = \frac{\ln[R(e^{\lambda t_{s2}} - 1) + 1]}{\lambda}$$

where t_u is the unknown age of a sample, R is the ratio of the $^{40}Ar^*/^{39}Ar_K$ value of the sample to that of the standard, and t_{s2} is the new age of the standard. The value of R can be determined by substitution using the original value (t_{s1}) for the age of the standard:

$$R = \frac{\{\frac{^{40}Ar^*}{^{39}Ar_K}\}_u}{\{\frac{^{40}Ar^*}{^{39}Ar_K}\}_s} = \frac{\{e^{\lambda t_u} - 1\}}{\{e^{\lambda t_{s1}} - 1\}}$$

The samples used in the present study were irradiated in the three irradiation batches. The J values, correction factors and mean sensivities for each irradiation, are obtained as discussed in the last chapter and are tabulated in Table 4.2. ***J*** values for the individual samples are given with the corresponding data tables. The difference in J values within a batch of irradiation reflects the neutron flux variation. The flux variation is calculated wit the help of Ni wire discussed in chapter 3.

Table 4.2 *Correction factors and mean sensitivity of the irradiation batches.*

SAMPLES IN THE IRRADIATION BATCH	CORRECTION FACTORS			MEAN SENSITIVITY (ccSTP/mV)
	$(^{36}Ar/^{37}Ar)_{Ca}$	**$(^{39}Ar/^{37}Ar)_{Ca}$**	**$(^{40}Ar/^{39}Ar)_{K}$**	
LK209, LK182, LK176, LK 24, LK24B, LK198, LK198M, LK48	0.00034	0.00071	0.046	$0.8x10^{-7}$
LK47, LK57, LK67, LK68, LK70, LK86, LK88, LK90	0.00016	0.00075	0.069	$0.7x10^{-7}$
LG290, LG188, LG166, LG197, LG 601, LG 87	0.00015	0.00068	0.079	$0.2x10^{-7}$

Results of the samples from all the major geological units of the Trans Himalaya of Ladakh sector have been presented here, from south to north.

4.3 Indus Suture Zone

The Indus Suture Zone is characterized by sporadic occurrences of ophiolites and ophiolitic mélanges (Fig. 2.2). In Ladakh, this is represented by two main ophiolitic bodies, Shergol ophiolite (Fig.2.3) in the west and Zildat and Nidar ophiolites (Fig.2.4) in the east. Samples from both west and east Ladakh have been analyzed and the results have been presented in the tables 4.3 to 4.5 and figures 4.1 to 4.3. Sample details have been presented in the chapter 2. Sample LK 209 is a pillow lava taken from the village Chiktan in the western Ladakh (Fig.2.2). It has yielded a plateau age of 128.2 ± 2.6 Ma for the first six steps consisting of more than 60% of ^{39}Ar released. The isochron age for this, 126.9 ± 7.6 Ma, is within errors of the plateau age with the trapped ratio of

$^{40}Ar/^{36}Ar$ as 296.9 ±8.4 Ma (Table 4.3 & Fig.4.1). The higher temperature steps have yielded higher ages; however, the integrated age is within errors of the plateau age. The concordance of all the three ages, viz. plateau, isochron and integrated age, for this sample is interpreted to yield the age of formation. The subsequent redistribution of the radiogenic argon within the whole rock could have given rise to the disturbed high temperature part of the spectrum.

Sample LK182 is taken from the Sumdo Nala in the eastern Ladakh (Fig.2.3). This sample yielded a cooling pattern of rising apparent ages from ~14 Ma to ~ 38 Ma, for ~99.5 % of ^{39}Ar released from 450^{o}C temperature step to 950^{o}C. (Table 4.4 &Fig. 4.2). It yielded a plateau-like age at the maximum temperature steps (900^{o}C & 950^{o}C) consisting of 23% of the ^{39}Ar released. The cooling pattern of this basalt sample is interpreted to be due to a subsequent resetting tectono-thermal event. Further interpretation and derivation of the cooling history of the sample is done by modeling the age spectrum using the Multi Diffusion Model (MDD), discussed in detail in chapter 5. The inferred cooling history is rapid cooling at ~40Ma followed by slow cooling between 38 and 18 Ma and again subsequent fast cooling.

The sample from LK176, from the same Sumdo Nala (Fig.2.3), yielded a four step plateau age of 46.8 ± 0.7 Ma for the middle temperature steps (from 600 to 750^{o}C), consisting of 64.4% of ^{39}Ar released. The isochron age of 46.8 ± 1.3 Ma, for this sample, is same as the plateau age with the trapped $^{40}Ar/^{36}Ar$ ratio of 295.8 ± 11.9 (Table 4.5 & Fig 4.3). The MDD model by assuming monotonic cooling, yields an age spectrum which matches well with the experimentally derived age spectrum for 80 % of the gas released (see chapter 5). The corresponding cooling curves show two-step cooling, starting with an instantaneous cooling at 50 Ma followed by slow cooling from 100^{o}C.

Besides the above samples, I attempted to analyze samples of serpentinites and ultramafics of the lower units of the ophiolites of the suture zone to retrieve the timing of the serpentinization and the tectono-thermal history experienced by the ultramafics. A total number of seven samples of serpentinites and one sample of the ultramafic were studied but the experiment did not give any meaningful data because of the high content of trapped gases with very low K content masking the signal.

4.4 Dras Volcanics

Sample LG 290 is also taken from near the Kharbu village of the western Ladakh (Figs. 2.2 & 2.3). Overall the age spectrum forms the pattern of rising ages like a cooling pattern. However, a plateau-like age of 85.6 ± 0.6 Ma for 8 steps comprising more than 80% of the ^{39}Ar released can be derived (Table 4.6 & Fig. 4.4). The plateau like age is consistent with the earlier estimates of the age of the Dras Volcanics.

Table 4.3** Argon isotopic composition and apparent ages of sample LK97/209 (Chiktan Pillow Lava) at different temperature steps. The errors in ages are without and with (bracketed) errors in **J**. **J= .002369 ± .000028

TEMP. (^{O}C)	^{36}Ar/^{39}Ar ± 1σ	^{40}Ar/^{39}Ar ± 1σ	AGE(Ma) ± 1σ	^{39}Ar%	^{40}Ar*%	^{37}Ar/^{39}Ar ± 1σ	^{40}Ar/^{36}Ar ± 1σ
450	1.182	376.17	111.0	3.11	7.12	3.470	318.16
	.021	7.01	13.0(13.1)			.067	6.10
500	.4038	148.66	121.14	9.44	19.73	2.9371	368.12
	.0049	.87	6.33(6.48)			.0059	4.81
550	.2638	110.28	133.06	17.84	29.31	2.5796	418.01
	.0010	.64	2.34(2.79)			.0074	2.64
600	.1954	89.49	130.80	12.30	35.48	11.123	458.00
	.0016	.56	2.44(2.86)			.037	4.34
650	.16612	79.23	124.40	12.37	38.04	13.114	476.96
	.00059	.47	1.68(2.20)			.081	2.99
700	.1394	72.46	128.89	7.07	43.16	12.421	519.85
	.0017	.54	2.43(2.84)			.025	6.96
750	.10206	53.83	98.41	4.07	43.97	26.805	527.44
	.00079	.40	1.41(1.81)			.054	5.02
800	.2241	86.74	85.58	2.17	23.65	33.68	387.03
	.0030	.58	4.16(4.27)			.15	5.74
850	.4885	168.58	100.7	1.53	14.37	16.70	345.11
	.0089	1.42	10.7(10.7)			.31	6.58
900	.5825	194.10	91.53	1.29	11.32	21.77	333.22
	.0031	1.22	5.44(5.54)			.20	2.58
950	.3772	147.46	147.58	2.08	24.41	48.01	390.92
	.0045	1.17	6.10(6.33)			6.93	4.77
1000	.2154	101.18	153.64	2.92	37.10	89.39	469.79
	.0022	.88	3.59(3.99)			.43	5.85
1050	.2312	112.52	179.61	7.70	39.28	38.99	486.69
	.0020	.69	3.16(3.75)			.11	4.91
1100	.2401	120.21	199.10	7.19	40.98	22.525	500.72
	.0019	.77	3.31(3.99)			.045	4.88
1150	.2168	114.63	204.02	2.57	44.10	20.84	528.7
	.0048	1.44	7.44(7.78)			.16	13.2
1200	.128	81.13	175.8	2.19	53.26	26.43	632.2
	.013	4.09	22.0(22.1)			.28	73.0
1250	.038	56.59	184.3	1.63	80.24	31.14	1495.5
	.022	6.58	35.9(36.0)			.21	897.1
1300	.017	51.87	189.5	2.54	90.14	32.14	2995.7
	.021	6.36	34.5(34.6)			.10	3724.6
TOTAL	.25903	110.78	140.65	100.00	30.90	17.74	427.67
	.00098	.31	1.57(2.24)			.15	1.96

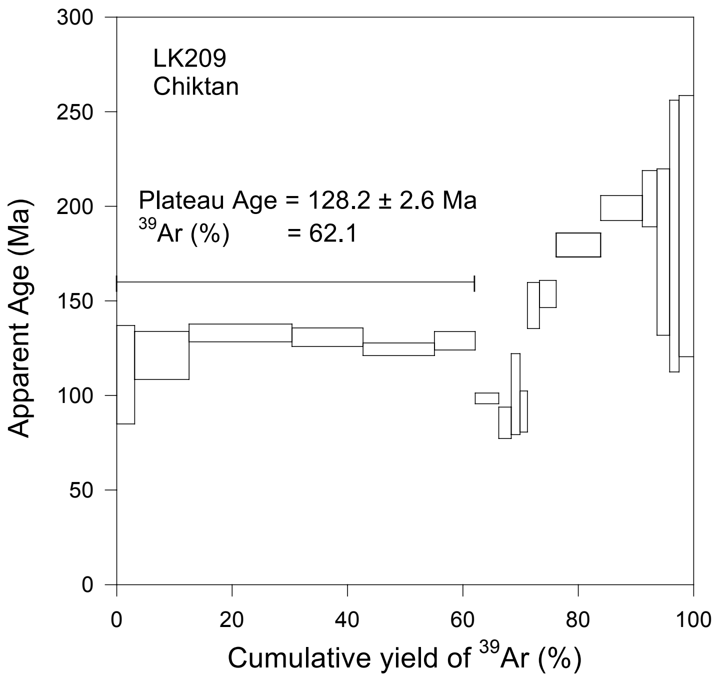

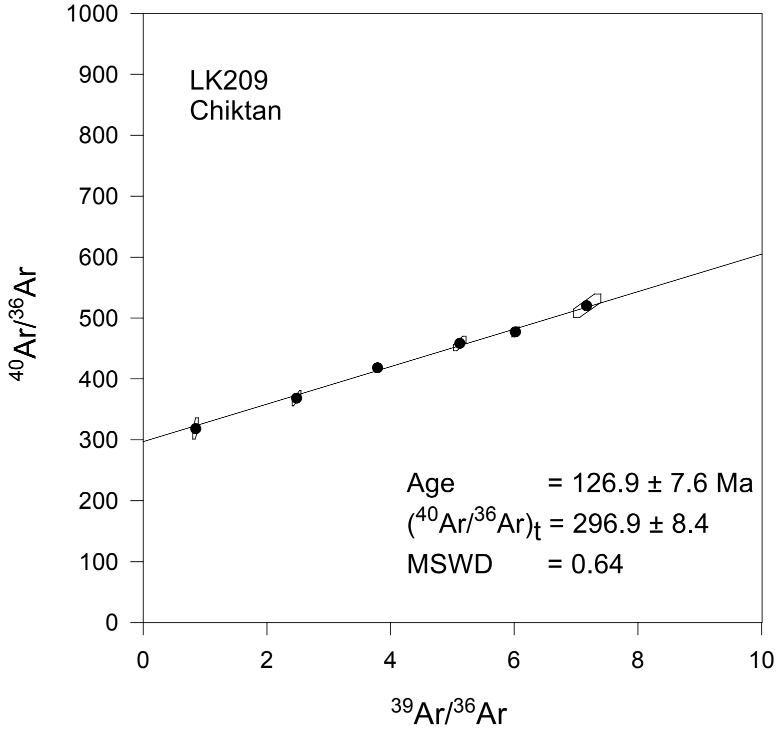

Fig. 4.1 *for the sample LK209. Errors in apparent ages are 2σ without including error in J. Plateau age includes error in J.*

(Bottom) $^{40}Ar/^{36}Ar$ vs. $^{39}Ar/^{36}Ar$ correlation diagram is also shown with isochron age ($\pm 2\sigma$), $^{40}Ar/^{36}Ar$ trapped ratio and MSWD value.

Table 4.4** Argon isotopic composition and apparent ages of sample LK97/182 (Sumdo Nala) at different temperature steps. The errors in ages are without and with (bracketed) errors in **J**. **J= .002113 ± .000032

Temp. °C	$^{36}Ar/^{39}Ar$ ± 1σ	$^{40}Ar/^{39}Ar$ ± 1σ	Age(Ma) ± 1σ	^{39}Ar%	$^{40}Ar^*$%	$^{37}Ar/^{39}Ar$ ± 1σ	$^{40}Ar/^{36}Ar$ ± 1σ
450	0.011013	6.89	13.79	0.47	52.74	0.2477	625.3
	0.000087	0.10	0.39(0.44)			0.0055	10.4
500	0.003397	5.973	18.85	2.90	83.20	0.2650	1758.5
	0.000030	0.038	0.13(0.31)			0.0013	18.5
550	0.001864	6.907	24.07	8.45	92.03	0.15152	3706.1
	0.000012	0.040	0.13(0.38)			0.00030	29.8
600	0.000763	8.369	30.78	22.90	97.30	0.05572	10961.4
	0.000012	0.048	0.16(0.49)			0.00023	180.3
650	0.003079	9.728	33.30	27.72	90.65	0.05015	3159.0
	0.000025	0.056	0.18(0.53)			0.00031	29.8
700	0.0008544	9.815	36.09	14.19	97.43	0.06657	11487.1
	0.0000074	0.057	0.18(0.57)			0.00056	115.6
750	0.001927	10.988	39.28	5.37	94.82	0.13536	5701.1
	0.000050	0.064	0.22(0.63)			0.00027	151.1
800	0.002510	10.94	38.48	7.27	93.22	0.2452	4360.8
	0.000038	0.10	0.21(0.61)			0.0015	69.3
850	0.003676	11.182	38.08	5.40	90.28	1.3069	3041.4
	0.000080	0.065	0.23(0.61)			0.0047	68.1
900	0.00242	10.674	37.57	3.92	93.30	1.5736	4412.4
	0.00015	0.063	0.26(0.62)			0.0031	270.2
950	0.01440	14.31	37.95	1.06	70.28	10.783	994.2
	0.00067	0.39	0.98(1.13)			0.036	48.5
1000	0.0438	32.96	74.77	0.15	60.75	72.91	752.9
	0.0053	2.07	9.48(9.54)			0.15	102.3
1050	0.064	48.16	107.9	0.08	60.58	89.06	749.7
	0.014	4.01	20.7(20.7)			1.36	174.6
1100	0.131	99.1	216.9	0.07	61.00	90.05	757.8
	0.049	12.4	64.7(64.7)			0.28	300.9
1400	0.126	153.4	396.3	0.08	75.77	57.27	1219.7
	0.082	16.3	86.3(86.5)			0.11	805.5
TOTAL	0.002494	9.629	33.58	100.00	92.35	0.6195	3860.2
	0.000075	0.028	0.12(0.52)			0.0013	116.7

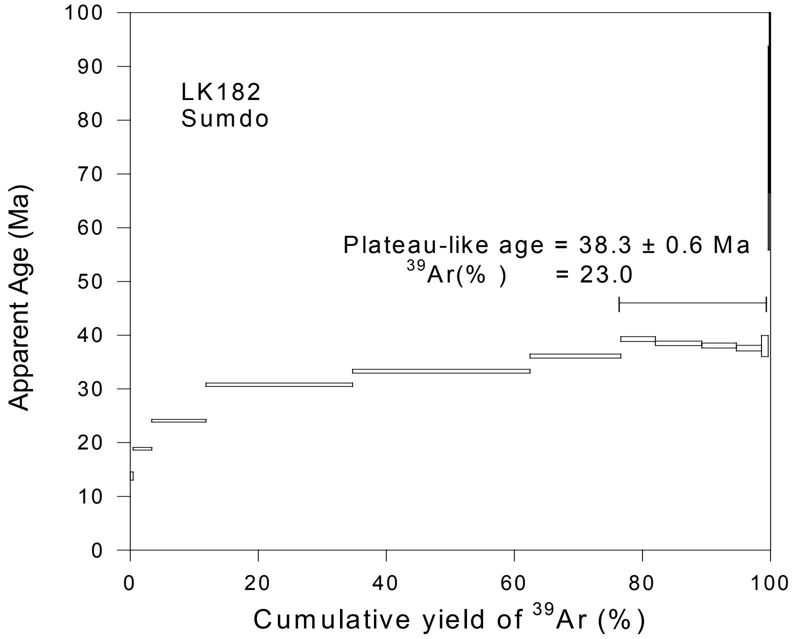

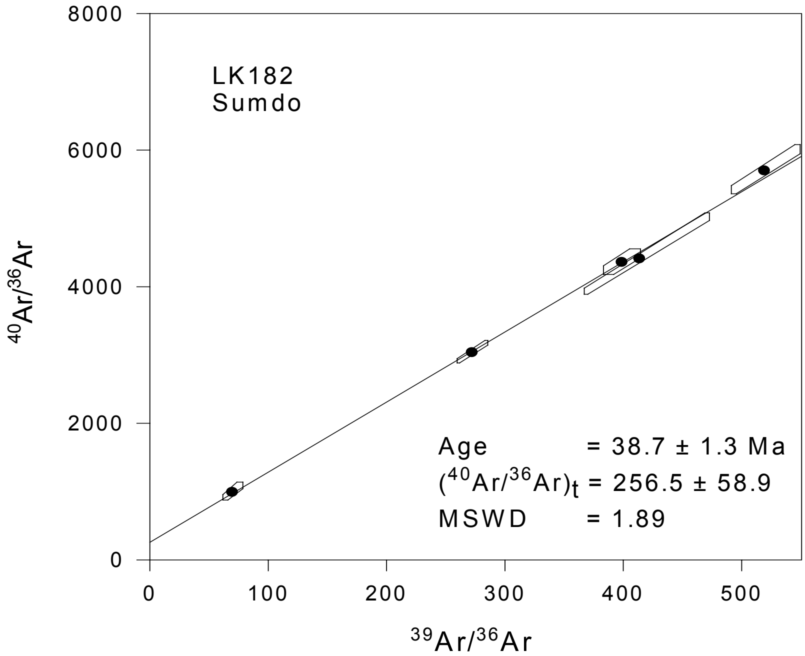

Fig. 4.2
the sample LK182. Apparent age boxes have 2σ errors without including error in J. The plateau-like age includes error in J.
(Bottom) $^{40}Ar/^{36}Ar$ vs. $^{39}Ar/^{36}Ar$ correlation diagram is also shown with isochron age($\pm 2\sigma$) , $^{40}Ar/^{36}Ar$ trapped ratio and MSWD value.

Table 4.5** Argon isotopic composition and apparent ages of sample LK176 (Sumdo Nala) at different temperature steps. The errors in ages are without and with (bracketed) errors in **J**. **J= .002256 ± .000027

Temp. ^{o}C	^{36}Ar/^{39}Ar ± 1σ	^{40}Ar/^{39}Ar ± 1σ	Age(Ma) ± 1σ	^{39}Ar%	^{40}Ar*%	^{37}Ar/^{39}Ar ± 1σ	^{40}Ar/^{36}Ar ± 1σ
450	.0506	39.48	97.13	.60	62.13	2.274	780.2
	.0013	.55	2.18(2.45)			.051	21.6
500	.03385	16.66	26.87	3.95	39.94	3.398	491.99
	.00038	.11	.59(.67)			.016	6.27
550	.017570	12.965	31.36	7.57	59.96	1.784	737.94
	.000091	.088	.33(.50)			.067	5.98
600	.01230	15.077	45.97	12.48	75.90	1.2575	1226.0
	.00023	.089	.41(.68)			.0039	23.8
650	.04560	25.21	47.14	17.46	46.56	.7514	552.91
	.00059	.15	.84(1.00)			.0033	7.65
700	.00809	14.154	47.24	13.16	83.10	.5357	1748.8
	.00014	.084	.34(.65)			.0023	32.6
750	.006743	13.642	46.79	21.34	85.39	.5559	2023.1
	.000024	.080	.28(.61)			.0022	12.6
800	.01642	14.996	40.81	9.63	67.64	3.036	913.27
	.00013	.092	.35(.59)			.019	8.72
850	.03232	19.53	40.14	5.75	51.09	16.111	604.14
	.00026	.13	.53(.71)			.032	5.92
900	.03061	18.70	38.88	4.06	51.64	21.584	611.0
	.00085	.14	1.11(1.20)			.043	17.4
950	.08201	30.10	23.72	2.00	19.49	38.786	367.04
	.00058	.24	1.10(1.14)			.078	3.80
1000	.0597	39.02	84.96	1.10	54.79	126.80	653.6
	.0032	.24	3.76(3.88)			.49	35.3
1050	.0339	32.98	91.13	.90	69.64	211.15	973.4
	.0057	1.80	8.77(8.83)			2.31	171.1
TOTAL	.02226	17.588	44.26	100.00	62.61	6.930	790.30
	.00013	.041	.21(.56)			.022	4.94

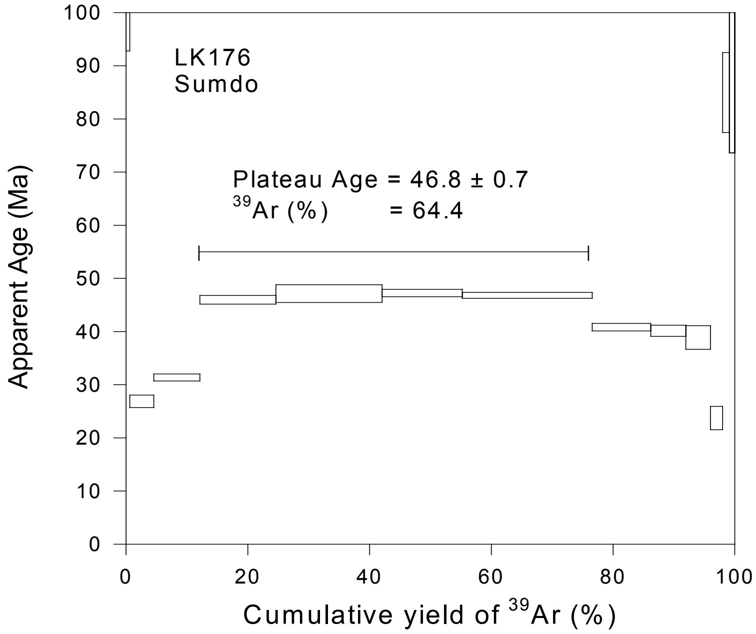

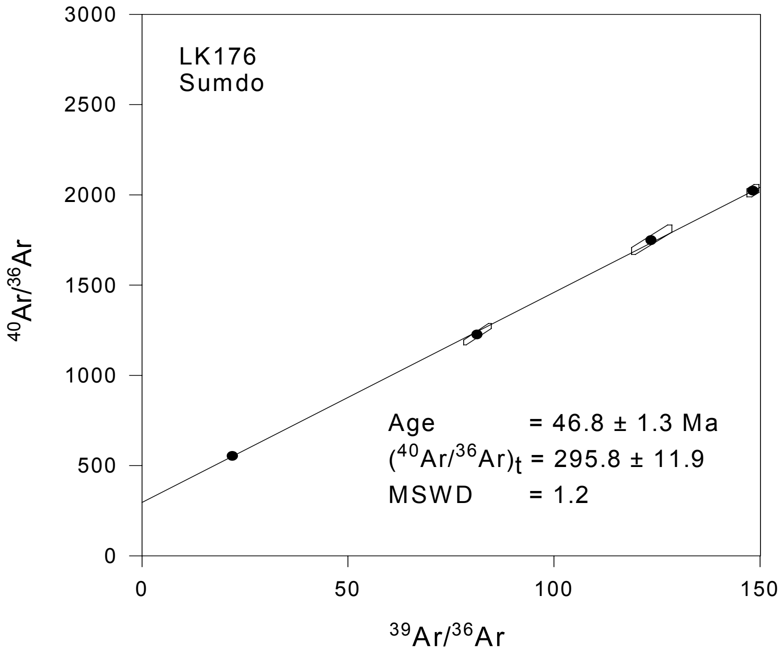

Fig. 4.3 *(Top) Ar/ Ar step heating results shown as apparent age spectrum for the sample LK176. Error in each apparent age is 2σ without including error in J. The error in plateau age includes error in J.*

(Bottom) $^{40}Ar/^{36}Ar$ vs. $^{39}Ar/^{36}Ar$ correlation diagram is shown with isochron age ($\pm 2\sigma$), $^{40}Ar/^{36}Ar$ trapped ratio and MSWD value.

Table 4.6** Argon isotopic composition and apparent ages of sample LG290 (Kharbu, Dras Volcanics) at different temperature steps. The errors in ages are without and with (bracketed) errors in **J. J= .002447 ± .000013

Temp. ^{o}C	$^{36}Ar/^{39}Ar$ ± 1σ	$^{40}Ar/^{39}Ar$ ± 1σ	Age(Ma) ± 1σ	^{39}Ar%	$^{40}Ar^{*}$%	$^{37}Ar/^{39}Ar$ ± 1σ	$^{40}Ar/^{36}Ar$ ± 1σ
500	.1571	53.26	29.98	.91	12.86	4.448	339.11
	.0033	.92	5.78(5.78)			.013	9.22
550	.0419	15.10	11.99	1.20	18.05	4.597	360.6
	.0025	.66	4.34(4.34)			.011	26.7
600	.01752	13.18	34.99	3.19	60.73	3.4894	752.5
	.00094	.26	1.64(1.65)			.0070	43.0
650	.00669	16.97	64.98	9.85	88.35	3.8590	2537.4
	.00031	.13	.63(.72)			.0077	117.6
700	.00398	20.16	81.88	9.55	94.16	3.8645	5059.6
	.00031	.14	.68(.80)			.0077	401.3
750	.00342	20.12	82.40	11.21	94.97	5.068	5879.0
	.00027	.14	.62(.75)			.010	462.1
800	.00264	20.22	83.79	6.35	96.14	7.605	7650.5
	.00047	.17	.90(1.00)			.015	1367.4
850	.00464	20.56	82.73	4.87	93.33	7.269	4428.7
	.00062	.14	.93(1.02)			.015	587.8
900	.03558	30.09	84.38	10.00	65.05	6.942	845.60
	.00032	.19	.81(.92)			.014	9.08
950	.02744	28.45	87.60	11.97	71.50	10.457	1036.8
	.00027	.18	.73(.86)			.021	11.7
1000	.00685	22.68	88.92	17.09	91.07	11.077	3310.6
	.00018	.14	.56(.73)			.022	87.6
1050	.00721	23.67	92.63	9.19	91.00	12.503	3282.8
	.00033	.17	.75(.89)			.025	151.2
1100	.0647	36.06	73.27	1.02	46.99	37.352	557.4
	.0038	.89	6.10(6.12)			.075	35.9
1200	.0791	54.41	132.02	2.15	57.04	39.501	687.9
	.0017	.58	3.05(3.12)			.079	16.6
1400	.1841	94.92	170.48	1.46	42.69	38.839	515.6
	.0047	1.82	9.13(9.17)			.078	16.4
TOTAL	.01803	24.607	83.14	100.00	78.35	9.1447	1365.0
	.00014	.059	.29(.52)			.0060	10.8

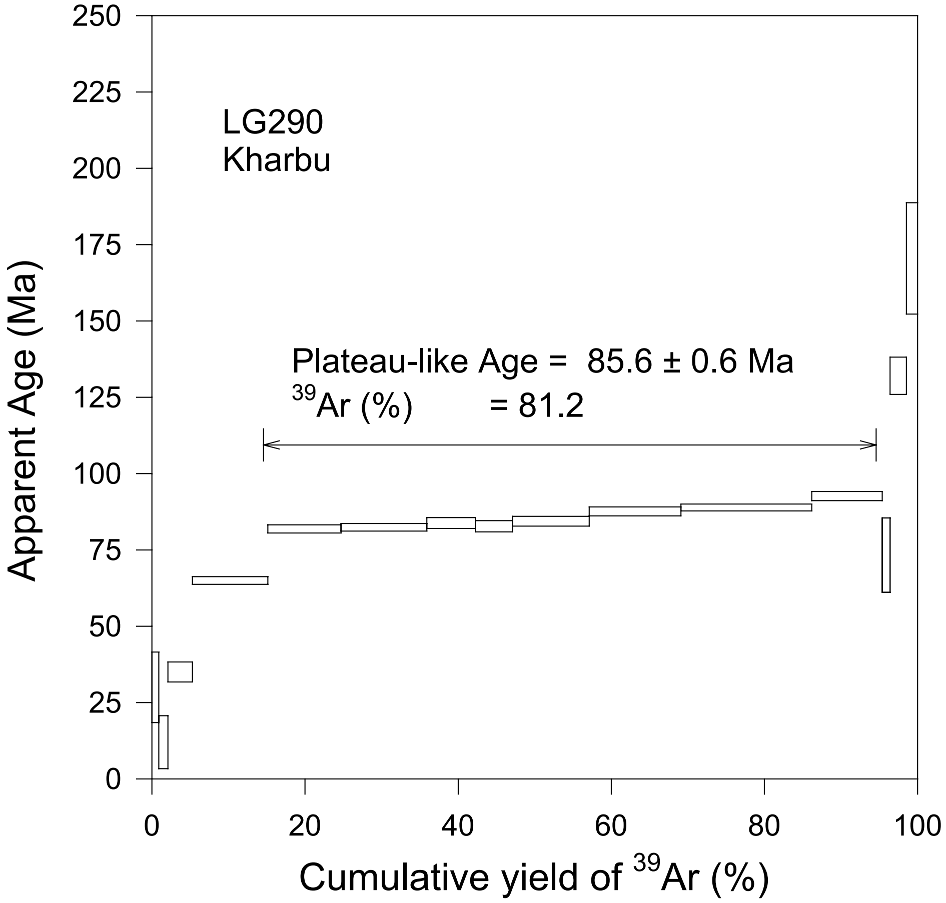

***Fig. 4.4** $^{40}Ar/^{39}Ar$ step heating results shown as apparent age spectrum for the sample LK290. The vertical side of the each box is 2σ error in apparent age without including error in J. Error in plateau-like age includes error in J.*

4.5 Ladakh Batholith

Sample LK 24 is a granodiorite from the Shanti Stupa in the vicinity of Leh (Fig.2.2). Whole rock analysis of this sample yielded a complex age spectrum with the three consecutive middle temperature steps (900, 950 & 1000^{o}C) yielding a maximum plateau-like age of 46.3 ± 0.6 Ma consisting of 51% of ^{39}Ar released (Table 4.7 & Fig 4.5). The three point isochron yields an age of 47.3 ± 1.2 Ma with the trapped argon ratio very close to atmospheric as 273.9 ± 20.0.

A biotite (LK24B) separated from this granodiorite yielded an excellent plateau age as 44.6 ± 0.3 Ma for the 13 consecutive steps consisting of 93% of the ^{39}Ar released (Table 4.8 & Fig. 4.6). The corresponding isochron yielded an age of 44.6 ± 0.7Ma with the trapped ratio as 309.5 ± 47.8 and MSWD of 0.63.

Sample LK198 is of a Leucogranite taken from the village Himia in the eastern Ladakh (Figs. 2.2 & 2.4). A cooling pattern for intermediate to higher temperatures (700^{o}C to 1100^{o}C) with a plateau like segment (at 1050^{o}C & 1100^{o}C steps) consisting of 32% of ^{39}Ar released can be seen for the intermediate steps (Table 4.9 & Fig. 4.7). Small amount (~ 10%) of ^{39}Ar was released at initial and final temperature steps.

Muscovite separated from this rock yielded an excellent plateau age of 29.8 ± 0.2 Ma consisting of 100% of ^{39}Ar released (Table 4.10 & Fig. 4.8). Its isochron yielded an age of 29.8 ± 0.4 Ma with the trapped ratio as 288.8 ± 5.3, which is very close to the atmospheric ratio. The MSWD for the fit is 0.39.

Table 4.7 *Argon isotopic composition and apparent ages of sample LK24 (Leh, Ladakh Batholith)at different temperature steps. The errors in ages are without and with (bracketed) errors in* ***J. J= .002256 ± .000016***

Temp. °C	^{36}Ar/^{39}Ar ± 1σ	^{40}Ar/^{39}Ar ± 1σ	Age(Ma) ± 1σ	^{39}Ar%	^{40}Ar*%	^{37}Ar/^{39}Ar ± 1σ	^{40}Ar/^{36}Ar ± 1σ
500	.16419	55.00	26.19	1.47	11.78	.1967	334.98
	.00088	.33	1.45(1.46)			.0072	2.50
550	.06299	26.43	31.53	2.53	29.57	.12480	419.59
	.00022	.15	.56(.60)			.00057	2.59
600	.04755	23.55	38.25	4.94	40.34	.09223	495.27
	.00025	.14	.53(.59)			.00063	3.59
650	.010805	12.927	39.18	5.82	75.30	.07354	1196.39
	.000037	.075	.26(.38)			.00074	7.36
700	.01417	13.656	38.12	4.27	69.33	.1060	963.4
	.00019	.079	.35(.44)			.0023	14.1
750	.023864	16.825	39.34	4.02	58.09	.16382	705.06
	.000083	.098	.35(.44)			.00050	4.36
800	.03880	20.84	37.73	4.76	44.97	.2734	536.98
	.00018	.12	.45(.52)			.0011	3.70
850	.05378	26.03	40.78	6.02	38.94	.5569	483.99
	.00019	.15	.54(.61)			.0022	2.96
900	.018589	16.886	45.78	12.31	67.47	1.8963	908.39
	.000086	.098	.35(.47)			.0038	6.20
950	.006169	13.500	46.90	26.61	86.50	4.0312	2188.4
	.000025	.080	.28(.43)			.0081	14.4
1000	.00984	14.33	45.90	12.43	79.71	2.0099	1456.7
	.00015	.11	.40(.51)			.0040	24.5
1050	.03253	19.30	38.99	8.25	50.18	2.2158	593.18
	.00025	.15	.57(.63)			.0044	6.01
1100	.04551	22.25	35.46	3.70	39.56	1.2352	488.89
	.00064	.24	1.18(1.20)			.0025	8.51
1150	.0600	25.42	31.07	1.26	30.29	2.534	423.9
	.0021	.64	3.51(3.51)			.021	18.0
1200	.0414	21.45	37.16	.76	43.01	3.424	518.6
	.0031	1.13	5.78(5.79)			.063	47.7
1250	.0453	21.65	33.29	.58	38.13	3.634	477.6
	.0047	1.58	8.38(8.38)			.019	60.3
1300	.0237	16.50	38.23	.27	57.54	4.244	695.9
	.0055	1.64	9.21(9.21)			.028	176.3
TOTAL	.024546	17.731	42.14	100.00	59.09	1.9476	722.35
	.000068	.040	.16(.33)			.0024	2.45

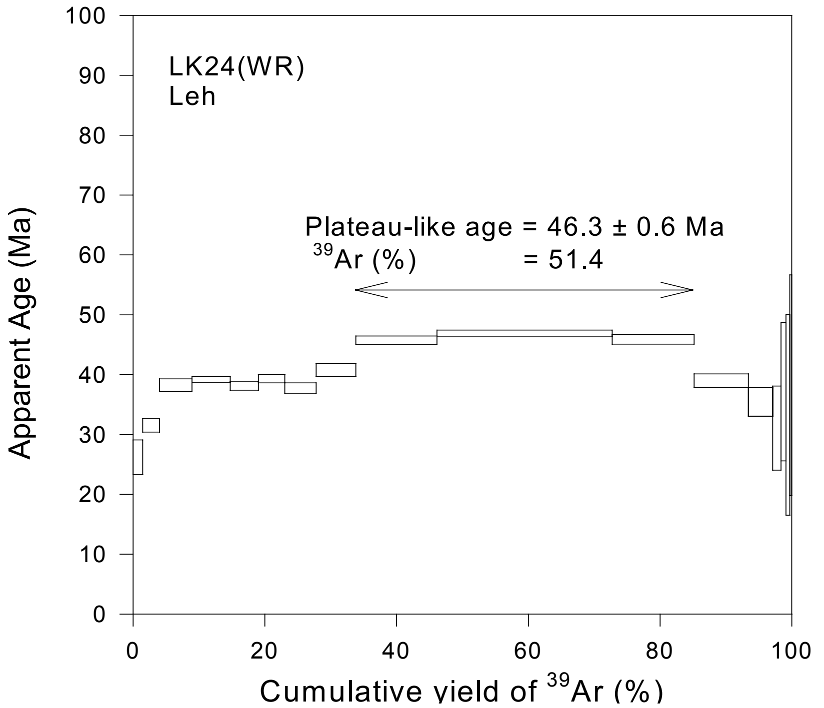

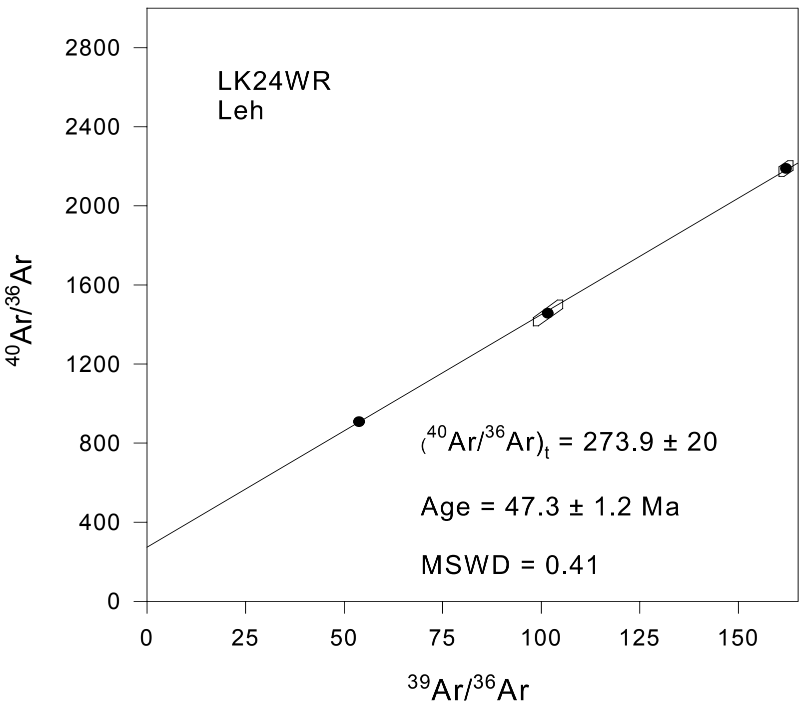

Fig. 4.5 *(Top) Ar/ Ar step heating results shown as apparent age spectrum for the sample LK24WR. Vertical side of each box is 2σ error in apparent age without including error in J. The plateau-like age ($\pm$ 2σ) includes error in J.*
(Bottom) ^{40}Ar/^{36}Ar vs. ^{39}Ar/^{36}Ar correlation diagram is shown with isochron age ($\pm$ 2σ), ^{40}Ar/^{36}Ar trapped ratio and MSWD value.

Table 4.8** Argon isotopic composition and apparent ages of sample LK24B (Biotite, Ladakh Batholith, Leh) at different temperature steps. The errors in ages are without and with (bracketed) errors in **J**. **J= .002237 ± .000016

Temp. ^{o}C	^{36}Ar/^{39}Ar ± 1σ	^{40}Ar/^{39}Ar ± 1σ	Age(Ma) ± 1σ	^{39}Ar%	^{40}Ar*%	^{37}Ar/^{39}Ar ± 1σ	^{40}Ar/^{36}Ar ± 1σ
450	.06023	22.24	17.85	.34	19.99	.1738	369.32
	.00027	.20	.82(.83)			.0060	3.65
500	.02256	11.99	21.36	.70	44.41	.08516	531.59
	.00013	.11	.43(.45)			.00065	5.49
550	.013291	12.732	35.18	1.84	69.15	.01369	957.97
	.000062	.081	.29(.38)			.00061	7.04
600	.004585	11.755	41.48	3.57	88.47	.0107	2563.7
	.000091	.070	.27(.39)			.0021	52.7
650	.003647	12.296	44.70	8.87	91.24	.02706	3371.6
	.000065	.071	.26(.40)			.00028	62.4
700	.000815	11.444	44.65	12.28	97.90	.003521	14044.5
	.000023	.066	.23(.39)			.000048	410.6
750	.001454	11.652	44.72	10.20	96.31	.01581	8014.0
	.000038	.068	.24(.39)			.00026	211.3
800	.001522	11.734	44.96	6.03	96.17	.01021	7709.0
	.000050	.069	.24(.40)			.00049	253.9
850	.003075	12.147	44.78	7.67	92.52	.04084	3950.0
	.000039	.071	.25(.40)			.00077	53.8
900	.00231	12.042	45.26	8.45	94.33	.04149	5211.0
	.00034	.070	.47(.56)			.00017	773.5
950	.001437	11.580	44.46	15.36	96.33	.05667	8059.5
	.000033	.067	.23(.39)			.00011	188.8
1000	.000874	11.408	44.43	16.25	97.74	.0402	13049.0
	.000063	.066	.24(.39)			.0015	949.6
1050	.000610	11.360	44.55	8.17	98.41	.07106	18632.4
	.000042	.067	.24(.39)			.00048	1301.9
1150	.0019	11.08	41.97	.20	94.96	2.946	5858.3
	.0018	.80	3.79(3.80)			.055	5560.3
TOTAL	.002374	11.762	44.082	100.00	94.04	.04864	4954.5
	.000034	.022	.086(.318)			.00029	70.6

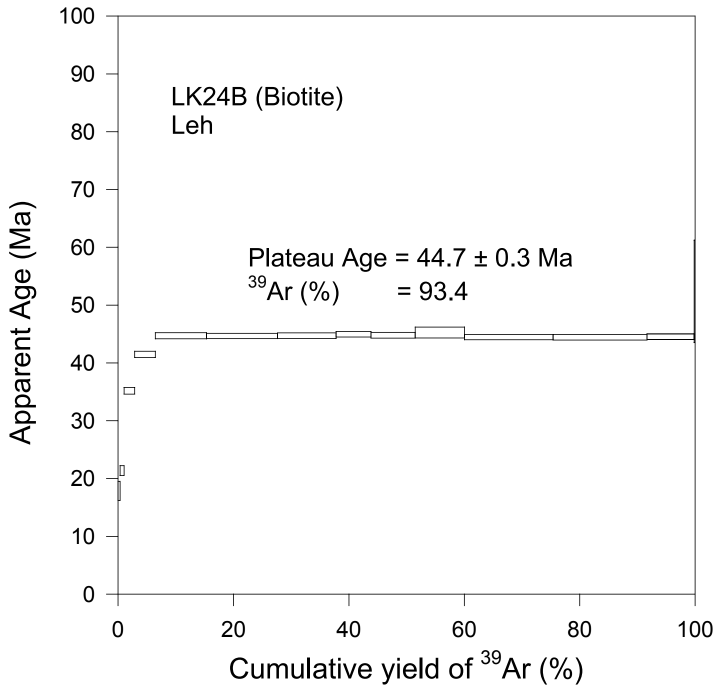

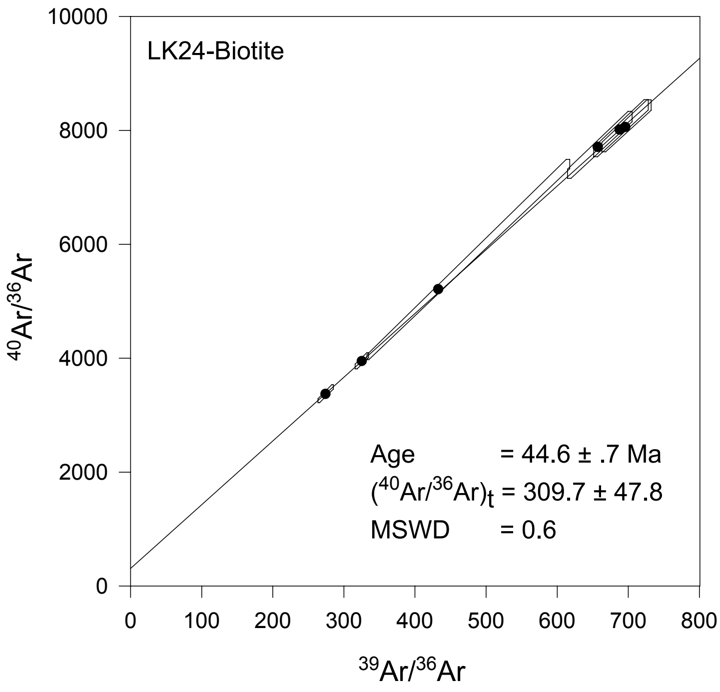

Fig. 4.6 *(Top) $^{40}Ar/^{39}Ar$ step heating results shown as apparent age spectrum for the sample LK24B. The vertical width of the each box is 2σ error in apparent age without including error in J. The plateau age includes error in J.*
(Bottom) $^{40}Ar/^{36}Ar$ vs. $^{39}Ar/^{36}Ar$ correlation diagram is also shown with isochron age ($\pm 2\sigma$), $^{40}Ar/^{36}Ar$ trapped ratio and MSWD value.

Table 4.9 *Argon isotopic composition and apparent ages of sample LK97/198 (Himia, Ladakh Batholith) at different temperature steps. The errors in ages are without and with (bracketed) errors in* ***J. J= .002429 ± .000015***

Temp. °C	$^{36}Ar/^{39}Ar$ ± 1σ	$^{40}Ar/^{39}Ar$ ± 1σ	Age(Ma) ± 1σ	$^{39}Ar\%$	$^{40}Ar^{*}\%$	$^{37}Ar/^{39}Ar$ ± 1σ	$^{40}Ar/^{36}Ar$ ± 1σ
450	.0720	39.89	79.75	1.15	46.65	.0474	553.88
	.0012	.24	1.74(1.80)			.0021	9.92
500	.02359	13.930	30.24	1.63	49.96	.1747	590.56
	.00012	.087	.36(.41)			.0037	4.53
550	.019120	12.198	28.47	2.20	53.68	.2064	637.97
	.000066	.076	.30(.34)			.0018	4.18
600	.04454	18.22	22.03	2.39	27.76	.21717	409.08
	.00029	.11	.54(.55)			.00043	3.45
650	.006190	6.266	19.34	3.53	70.81	.1639	1012.3
	.000064	.042	.18(.22)			.0010	12.1
700	.004645	5.558	18.25	4.19	75.30	.1747	1196.51
	.000019	.034	.13(.17)			.0024	8.02
750	.006020	6.242	19.45	6.44	71.50	.12157	1036.96
	.000026	.038	.15(.19)			.00024	7.15
800	.005244	6.324	20.80	6.61	75.50	.08515	1206.05
	.000018	.039	.15(.20)			.00017	7.79
850	.004677	6.547	22.49	7.72	78.89	.09668	1399.76
	.000020	.040	.15(.21)			.00019	9.62
900	.004227	7.220	25.98	6.56	82.70	.10547	1707.9
	.000015	.045	.17(.23)			.00048	11.1
950	.005022	7.946	28.10	7.50	81.33	.1088	1582.3
	.000026	.048	.19(.25)			.0011	11.8
1000	.005347	9.129	32.78	9.13	82.69	.1087	1707.4
	.000088	.054	.23(.31)			.0027	29.5
1050	.005641	9.999	36.15	12.00	83.33	.09653	1772.5
	.000051	.059	.23(.32)			.00019	18.4
1100	.005293	9.845	35.93	20.91	84.11	.08697	1860.0
	.000029	.057	.22(.31)			.00059	14.0
1150	.01342	13.947	43.22	4.75	71.57	.2506	1039.5
	.00017	.090	.40(.48)			.0023	14.4
1200	.02458	20.19	55.79	1.09	64.04	.3486	821.6
	.00071	.24	1.33(1.37)			.0029	25.7
1250	.02958	21.09	53.32	1.11	58.56	.4562	713.0
	.00075	.26	1.41(1.45)			.0077	20.0
1300	.0354	22.65	52.59	.49	53.76	.5031	639.1
	.0026	.88	4.99(5.00)			.0057	53.6
1400	.0686	33.30	56.19	. 61	39.11	.762	485.3
	0036	1.76	8.71(8.71)			.021	36.0
TOTAL	.008957	9.760	30.905	100.00	72.88	.12978	1089.68
	.000036	.021	.095(.211)			.00037	4.85

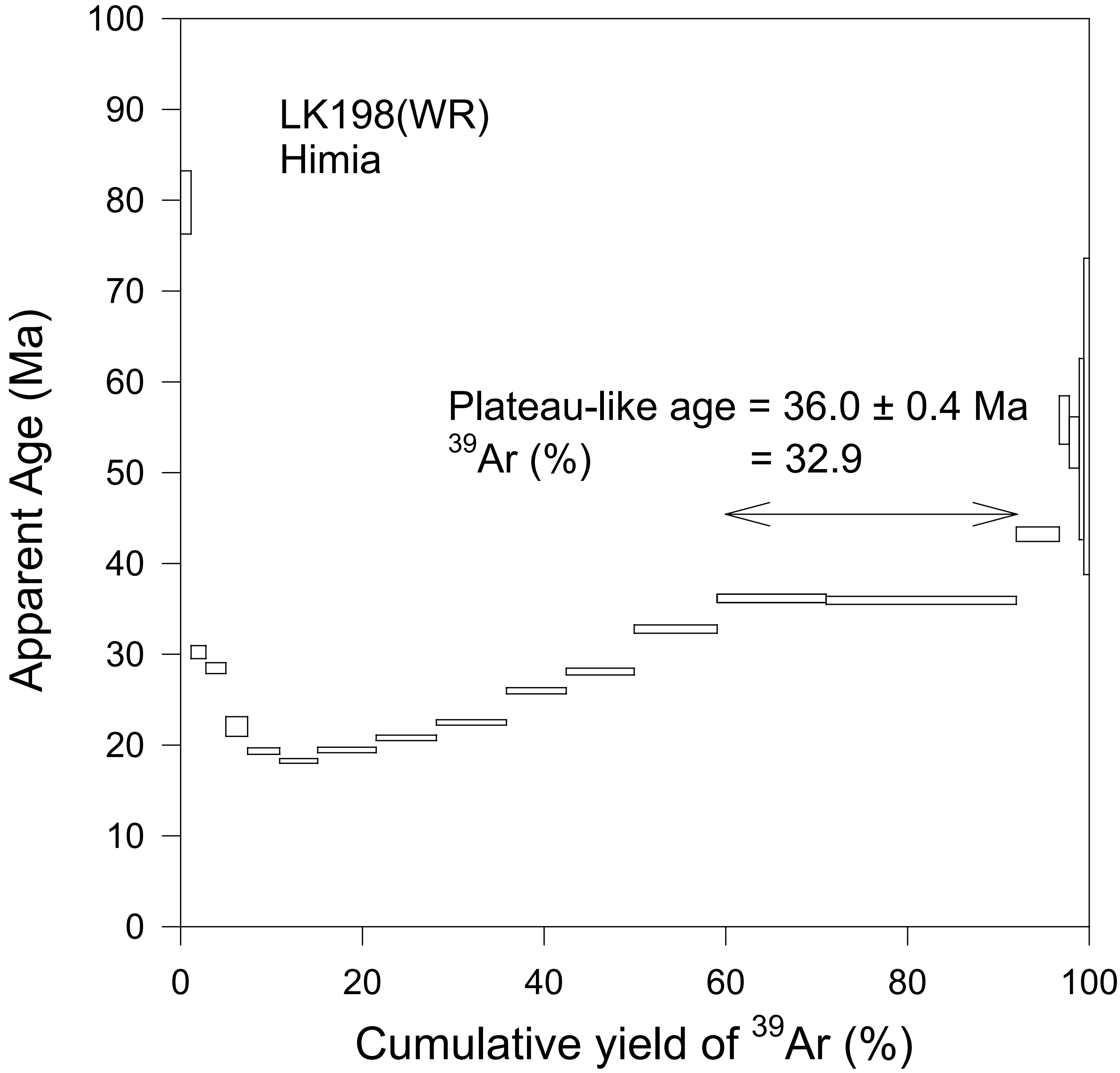

Fig. 4.7 *$^{40}Ar/^{39}Ar$ step heating results shown as apparent age spectrum for the sample LK198WR. The vertical width of the each box is 2 σ error in apparent age without including error in J. The plateau-like age includes error in J.*

Table 4.10** Argon isotopic composition and apparent ages of sample LK97198M (Muscovite, Ladakh Batholith, Himia) at different temperature steps. The errors in ages are without and with (bracketed) errors in **J. J= .002429 ± .000015

Temp.	$^{36}Ar/^{39}Ar$ ± 1σ	$^{40}Ar/^{39}Ar$ ± 1σ	Age(Ma) ± 1σ	$^{39}Ar\%$	$^{40}Ar^{*}\%$	± 1σ	$^{40}Ar/^{36}Ar$ ± 1σ
550	.04292	19.27	26.98	.36	34.19	.0677	448.99
	.00015	.17	.68(.70)			.0019	4.13
600	.04987	22.21	30.57	.80	33.64	.03644	445.31
	.00	.19	.74(.76)			.00085	3.92
650	.010811	10.299	29.08	1.41	68.98	.0143	952.65
	.000037	.070	.26(.31)			.0011	6.73
700	.003942	8.509	30.05	4.51	86.31	.011322	2158.5
	.000014	.051	.18(.26)			.000062	13.5
750	.0009092	7.555	29.82	13.93	96.44	.003287	8309.6
	.0000034	.044	.16(.24)			.000054	52.1
800	.0004053	7.406	29.82	21.44	98.38	.006099	18271.4
	.0000026	.043	.15(.24)			.000064	149.6
850	.0009839	7.521	29.60	16.77	96.13	.02830	7644.5
	.0000097	.044	.15(.24)			.00040	84.5
900	.0008032	7.509	29.76	21.34	96.84	.009458	9349.1
	.0000062	.043	.15(.24)			.000042	85.8
950	.0007518	7.582	30.12	11.21	97.07	.003839	10085.6
	.0000054	.044	.16(.24)			.000052	89.1
1000	.000137	7.466	30.39	6.15	99.46	.00605	54394.6
	.000027	.045	.16(.25)			.00062	10806.3
1050	.000850	7.480	29.59	1.74	96.64	.01092	8799.6
	.000100	.061	.26(.32)			.00018	1033.8
1100	.01977	13.80	32.53	.34	57.65	.0628	697.7
	.00079	.25	1.37(1.39)			.0013	30.5
TOTAL	.0016086	7.766	29.840	100.00	93.88	.010985	4827.9
	.0000047	.018	.062(.192)			.000082	16.9

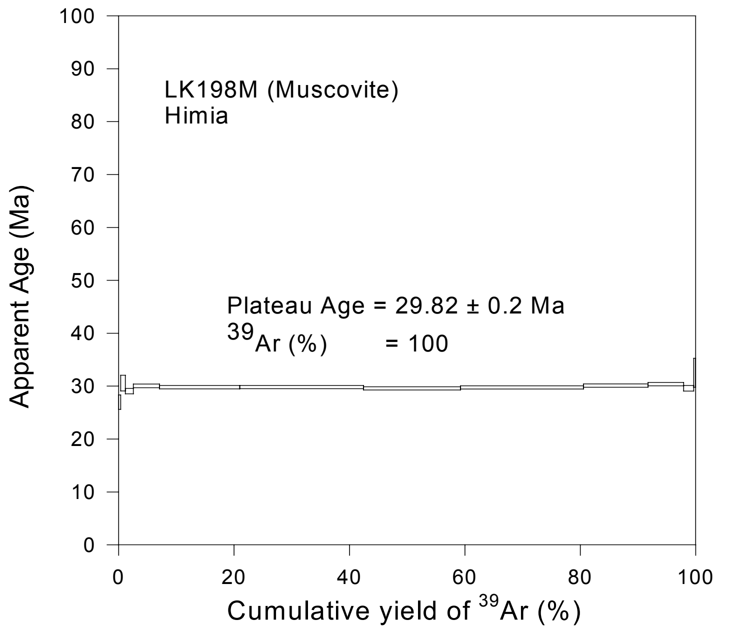

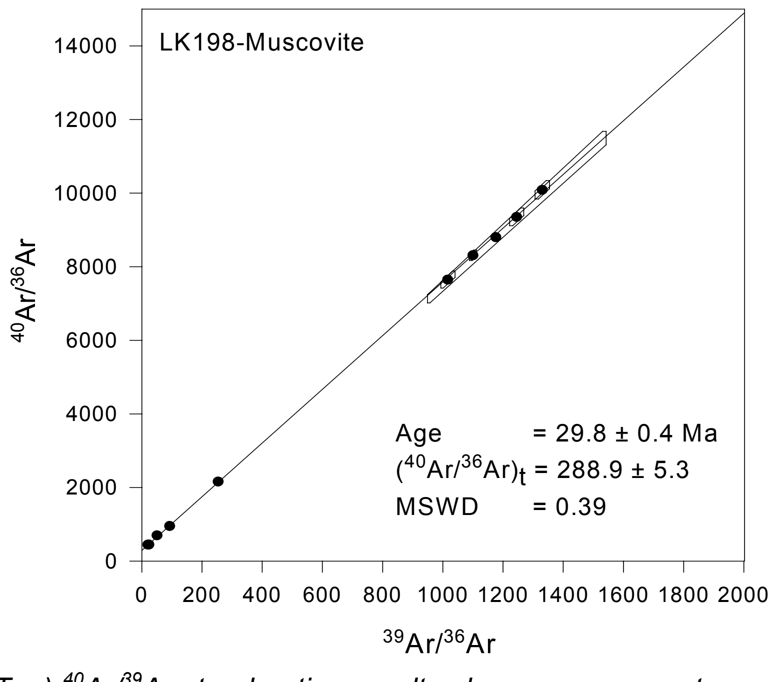

Fig. 4.8 *(Top) $^{40}Ar/^{39}Ar$ step heating results shown as apparent age spectrum for the sample LK198M. The vertical width of the each box is 2σ error in apparent age without including error in J. The plateau age includes error in J.*
(Bottom) $^{40}Ar/^{36}Ar$ vs. $^{39}Ar/^{36}Ar$ correlation diagram is also shown with isochron age ($\pm 2\sigma$), $^{40}Ar/^{36}Ar$ trapped ratio and MSWD value.

4.6 North of the Ladakh Batholith

4.6.1. Shyok Suture Zone

A total of nine samples were analyzed to cover all the variation in the chemistry of Shyok Suture Zone volcanics, which ranges from tholeiitic basalts to basaltic andesite.

Sample LK 48 is taken from the ophiolitic mélange of the Shyok suture zone near the village Murgi (Figs. 2.2 & 2.5). This has yielded cooling pattern of the rising apparent ages from ~13 Ma to ~ 20 Ma from 650^{o}C to 950^{o}C (Table 4.11 & Fig. 4.9). A very small amount of gas (<1%) released in the first and last step yielded high apparent ages, ~ 30 Ma and ~80 Ma respectively, indicating probably the small amount of excess argon present in the sample.

Sample LK57 from near the village Panamik (Figs. 2.2 & 2.5) yielded a complex age spectrum (Table 4.12 & Fig. 4.10). Overprinting of subsequent tectono-thermal events can be made out from the age spectrum. The apparent ages start from ~ 10 Ma (at 450^{o}C) and go up to ~20 Ma (at 650^{o}C) for the first ~ 40% of the gas released. The apparent ages again become as low as ~ 14 Ma at the seventh temperature step (700^{o}C) and then rise up to as high age as ~ 100 Ma at the maximum temperature step indicating perhaps a superposition of two events. A similar pattern gets repeated for the sample LK 67 which also yielded a disturbed age spectrum. (Table 4.13 & Fig. 4.11), which looks like two separate cooling patterns. The first cooling pattern starts from ~ 12 Ma (at 500^{o}C) and goes up to ~18 Ma (650^{o}C) consisting ~ 30% of the total gas released. The second pattern of the rising ages starts at middle temperature steps from ~11 Ma age and goes up to ~60 Ma consisting of the remaining 70% of the gas released.

Another sample LG 188 taken from the vicinity of the village Tegar (Figs.2.2 & 2.5) yielded a cooling pattern (Table 4.14 & Fig. 4.12) with the apparent ages rising from ~ 14 Ma (at 650^{o}C step) to ~30Ma (at 1200^{o}C step). The same cooling pattern is reproduced by the another sample from the same area, LK68 for the first ~ 60% of the total gas released, however, there is another cooling pattern superimposed, starting from the middle temperature steps at the apparent age ~20 Ma to a very high age of more than 200 Ma, for the remaining ~40% of the gas released (Table 4.15 & Fig. 4.13). Sample

LG 196, taken from the vicinity of the same village however yielded an excess argon pattern with the minimum age as ~30 Ma (Table 4.16 & Fig 4.14).

A basalt sample LG 166 from the village Hunder (Fig 2.2) yielded a typical excess argon pattern with the lower and higher temperature steps yielding very high ages (Table 4.17 & Fig. 4.15). The minimum age at the middle temperature steps of ~50 Ma could be the upper bound on the formation age of this sample. Sample LK 70 from near the village Tirit (Fig. 2.2) also yielded a complex age spectrum and appeared to have two superimposed cooling patterns (Table 4.18 & Fig. 4.16). The first spectrum starts from the apparent age of ~20 Ma (450^{o}C step) and goes up to ~35 Ma (650^{o}C) for the first ~ 55% of the gas released and again the ages become lower than ~25 Ma and then rise to as high values as ~ 100 Ma.

4.6.2. Karakoram Fault Zone

A micaceous segregation from a sheared granite from the Karakoram batholith, LK 47 was collected near the village Murgi (Figs. 2.2 & 2.5). Being crushed and segregated in a fault zone this sample had a large amount of trapped gases, and had to be degassed up to 700^{o}C. It could be analyzed starting from temperature 750^{o}C. However it yielded a very good plateau age of 13.9 ± 0.1 Ma consisting of nine consecutive steps and 99.5% of ^{39}Ar released (Table 4.19 & Fig. 4.17). The isochron of this sample yielded an age of 14.0 ± 0.3 Ma with trapped ratio as 283.6 ± 24.2 and MSWD of 0.2.

Table 4.11 *Argon isotopic composition and apparent ages of sample LK48 (Murgi,Shyok Suture Zone) at different temperature steps. The errors in ages are without and with (bracketed) errors in J. The errors quoted are in 1σ.* ***J****= .002253 ± .000014*

Temp. °C	$^{36}Ar/^{39}Ar$ ± 1σ	$^{40}Ar/^{39}Ar$ ± 1σ	Age(Ma) ± 1σ	^{39}Ar%	$^{40}Ar^*$%	$^{37}Ar/^{39}Ar$ ± 1σ	$^{40}Ar/^{36}Ar$ ± 1σ
500	.05212	22.29	27.78	.41	30.90	1.47	427.67
	.00027	.14	.55(.58)			.14	3.22
550	.02638	11.701	15.81	2.57	33.39	.194	443.60
	.00011	.079	.30(.32)			.018	3.24
600	.06699	24.20	17.82	4.97	18.21	.096	361.29
	.00048	.14	.72(.73)			.012	3.18
650	.016419	8.115	13.21	7.56	40.21	.3880	494.25
	.000057	.052	.19(.21)			.0036	3.32
700	.023944	10.646	14.45	13.70	33.54	.04604	444.62
	.000083	.063	.23(.25)			.00047	2.77
750	.022677	10.484	15.31	15.92	36.08	.09996	462.31
	.000079	.062	.23(.24)			.00089	2.88
800	.01400	8.030	15.75	18.16	48.47	.160	573.49
	.00020	.048	.28(.30)			.013	8.56
850	.004167	5.867	18.74	25.72	79.01	.1078	1407.74
	.000017	.035	.13(.17)			.0023	9.51
900	.006475	7.501	22.56	9.11	74.49	.623	1158.4
	.000052	.052	.20(.24)			.012	11.9
950	.04340	17.91	20.54	.77	28.39	6.63	412.64
	.00024	.39	1.57(1.57)			.20	9.23
1000	.0996	47.70	72.80	.29	38.32	15.35	479.1
	.0033	1.09	5.67(5.68)			.79	19.3
1150	.276	131.30	192.0	.28	37.98	21.22	476.4
	.015	4.29	18.5(18.5)			.43	28.4
1250	.077	114.88	340.4	.16	80.26	4.02	1496.7
	.035	5.97	39.7(39.8)			.17	692.0
1400	.038	14.51	13.6	.34	23.23	2.620	384.9
	.022	7.81	41.1(41.1)			.070	306.8
TOTAL	.01846	9.923	18.07	100.00	45.04	.3619	537.64
	.00011	.036	.19(.22)			.0047	3.75

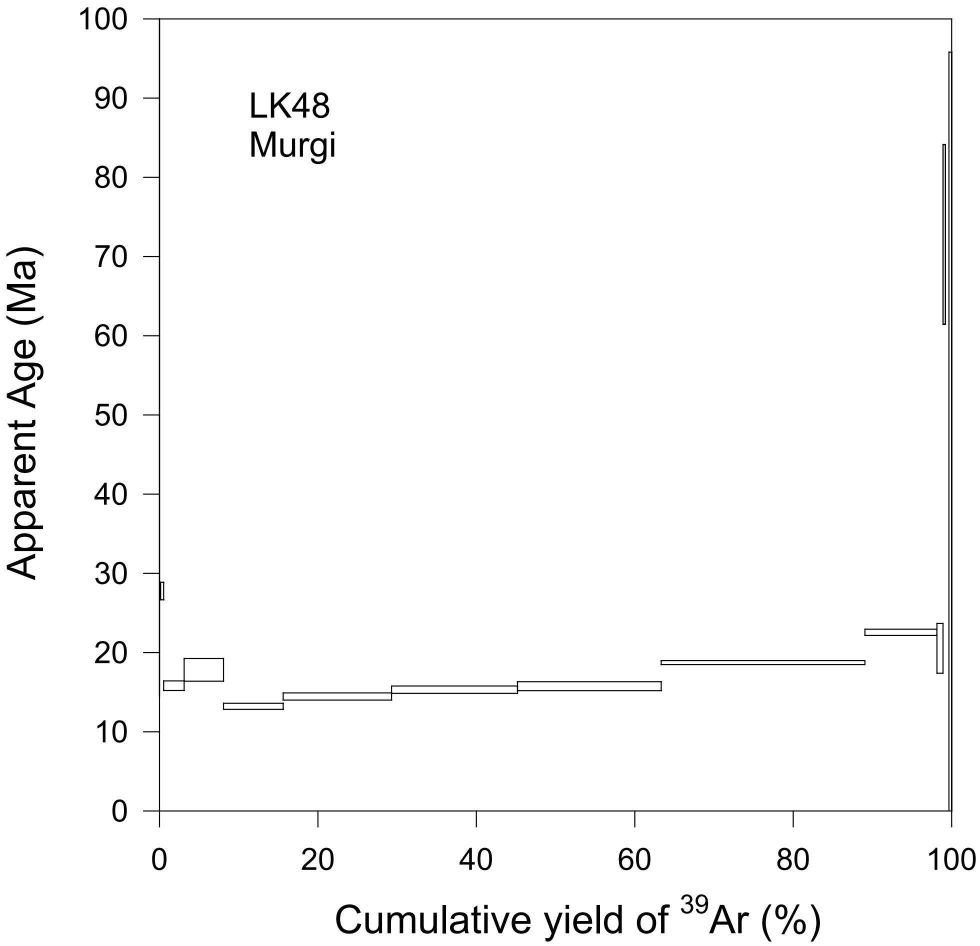

Fig. 4.9 *^{40}Ar/^{39}Ar step heating results shown as apparent age spectrum for the sample LK48. The vertical side of the each box is 2σ error in apparent age without including error in J.*

Table 4.12** Argon isotopic composition and apparent ages of sample LK57 (between Panamik and Tegar, Shyok Suture Zone)at different temperature steps. The errors in ages are without and with (bracketed) errors in **J**. The errors quoted are in 1σ. **J= .002342 ± .000014

Temp. °C	$^{36}Ar/^{39}Ar$ ± 1σ	$^{40}Ar/^{39}Ar$ ± 1σ	Age(Ma) ± 1σ	$^{39}Ar\%$	$^{40}Ar^*\%$	$^{37}Ar/^{39}Ar$ ± 1σ	$^{40}Ar/^{36}Ar$ ± 1σ
400	0.02977	13.188	18.45	2.91	33.29	1.177	442.98
	0.00046	0.079	0.064(0.064)			0.015	7.30
450	0.00671	4.079	8.83	4.62	51.40	1.7221	608.0
	0.0013	0.029	0.19(0.20)			0.0058	12.3
500	0.00702	4.450	10.00	4.29	53.38	1.371	633.8
	0.00010	0.034	0.18(0.19)			0.047	10.2
550	0.004142	5.177	16.62	9.42	76.36	0.8375	1250.0
	0.000019	0.032	0.12(0.16)			0.0017	8.99
600	0.00389	5.410	17.90	4.87	78.75	0.90	1390.8
	0.00013	0.039	0.22(0.24)			0.14	46.8
650	0.017174	9.988	20.63	12.97	49.19	0.6305	581.56
	0.000079	0.066	0.22(0.25)			0.0042	4.01
700	0.003929	4.764	15.15	5.99	75.63	0.781	1212.6
	0.000031	0.036	0.14(0.17)			0.011	12.8
750	0.00558	5.018	14.18	3.14	67.16	1.487	899.8
	0.00014	0.054	0.28(0.29)			0.043	25.0
800	0.004152	5.251	16.92	7.45	76.64	1.7712	1264.7
	0.000063	0.037	0.16(0.19)			0.0089	20.8
850	0.004224	5.540	18.03	8.58	77.47	2.3065	1311.45
	0.000016	0.037	0.14(0.18)			0.0046	9.39
900	0.005648	6.849	21.75	12.98	75.63	4.494	1212.71
	0.000035	0.042	0.16(0.20)			0.054	9.92
950	0.01045	8.596	23.11	5.31	64.06	6.680	822.2
	0.00040	0.063	0.55(0.56)			0.053	32.0
1000	0.01435	10.558	26.48	4.27	59.82	7.583	735.5
	0.00045	0.083	0.63(0.65)			0.26	23.5
1050	0.02089	16.33	42.38	30.70	62.18	9.271	781.42
	0.00019	0.12	0.50(0.56)			0.029	8.78
1100	0.01887	24.53	78.32	1.82	77.27	12.392	1299.9
	0.00076	0.24	1.30(1.37)			0.025	53.9
1150	0.01759	28.29	94.97	2.40	81.62	10.46	1607.7
	0.00056	0.28	1.26(1.37)			0.10	53.8
1200	0.01621	27.70	94.25	2.26	82.71	9.410	1708.9
	0.00059	0.35	1.53(1.62)			0.019	66.1
1250	0.019	23.31	73.2	0.92	75.86	9.33	1224.2
	0.017	0.94	20.9(20.9)			0.10	1106.3
1300	0.0293	27.24	76.83	1.43	68.22	10.15	929.8
	0.0013	0.72	3.32(3.35)			0.18	49.1
1350	0.0892	41.72	63.73	0.74	36.82	11.169	467.7
	0.0033	1.59	7.55(7.56)			0.097	24.8
TOTAL	0.1116	9.352	25.39	100.00	64.73	3.416	837.9
	0.00017	0.034	0.26(0.30)			0.011	13.4

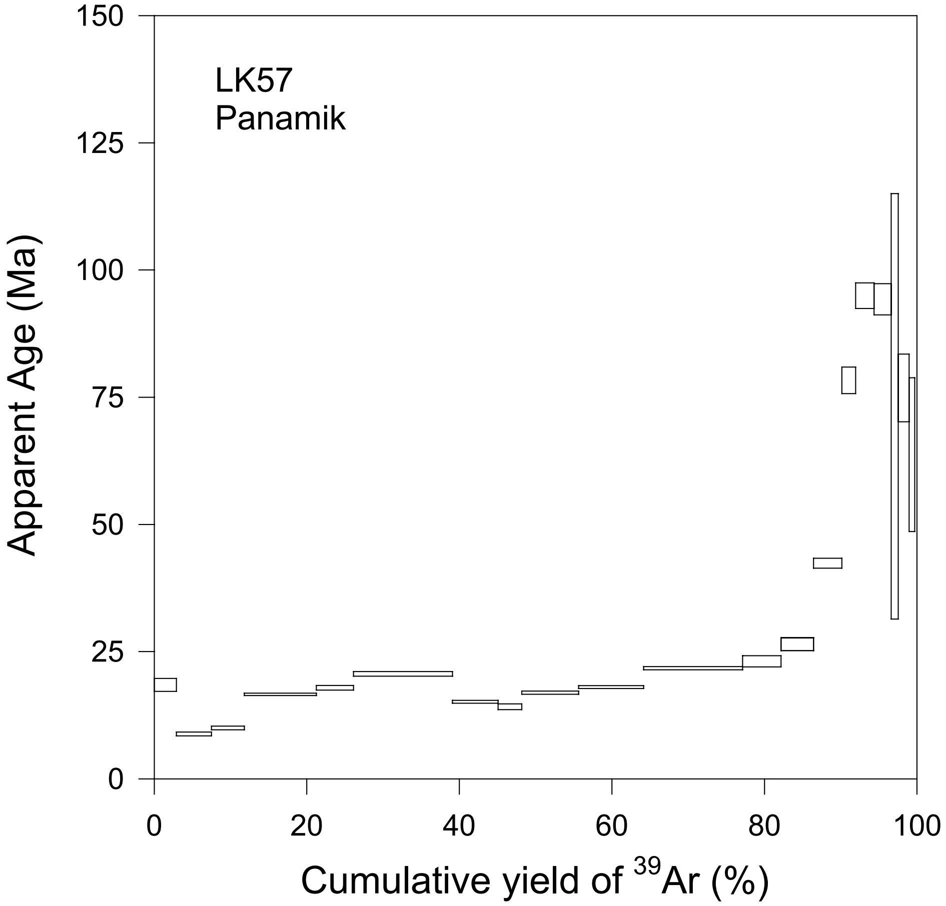

Fig. 4.10 *$^{40}Ar/^{39}Ar$ step heating results shown as apparent age spectrum for the sample LK57. The vertical side of the each box is 2σ error in apparent age without including error in J.*

Table 4.13 *Argon isotopic composition and apparent ages of sample LK67 (between Panamik and Tegar, Shyok Suture Zone) at different temperature steps. The errors in ages are without and with (bracketed) errors in **J**. The errors quoted are in 1σ.* ***J= .002294 ± .000014***

Temp. °C	$^{36}Ar/^{39}Ar$ ± 1σ	$^{40}Ar/^{39}Ar$ ± 1σ	Age(Ma) ± 1σ	^{39}Ar%	$^{40}Ar^*$%	$^{37}Ar/^{39}Ar$ ± 1σ	$^{40}Ar/^{36}Ar$ ± 1σ
400	0.1552	53.07	29.62	0.63	13.60	1.36	342.01
	0.0013	0.31	1.84(1.85)			0.13	3.36
450	0.02659	11.275	14.08	2.57	30.30	1.19	424.0
	0.00097	0.068	1.20(1.20)			0.14	15.6
500	0.013927	6.946	11.67	7.86	40.75	0.7930	498.71
	0.000049	0.041	0.15(0.17)			0.0080	3.11
550	0.011995	7.950	18.14	9.01	55.42	0.8132	662.78
	0.000042	0.047	0.17(0.20)			0.0072	4.14
600	0.01803	9.875	18.72	4.92	46.05	0.779	547.71
	0.00023	0.59	0.34(0.36)			0.012	7.48
650	0.014923	8.568	17.12	10.55	48.53	0.9233	574.15
	0.000082	0.55	0.20(0.23)			0.0018	4.40
700	0.014384	7.016	11.40	4.63	39.41	1.2004	487.73
	0.000050	0.044	0.16(0.18)			0.0024	3.22
750	0.010423	6.052	12.26	4.71	49.11	1.2964	580.63
	0.000046	0.039	0.15(0.17)			0.0048	4.21
800	0.007696	5.375	12.78	8.09	57.69	1.2018	698.42
	0.000027	0.033	0.12(0.14)			0.0037	4.51
850	0.009680	5.915	12.59	11.79	51.64	1.219	611.07
	0.000054	0.035	0.14(0.16)			0.018	4.67
900	0.010606	6.588	14.23	13.64	52.43	1.7445	621.14
	0.000044	0.039	0.15(0.17)			0.0059	4.15
950	0.014598	7.941	14.95	9.17	45.68	2.3755	544.0
	0.000051	0.048	0.18(0.20)			0.0057	3.49
1000	0.02134	10.71	18.15	4.53	41.15	3.801	502.10
	0.00036	0.11	0.46(0.47)			0.012	9.00
1050	0.0305	15.00	24.65	2.49	39.99	3.5	492.4
	0.0023	0.19	0.86(0.88)			13.6	36.3
1100	0.03408	21.17	45.36	1.36	52.43	6.624	621.19
	0.00014	0.30	1.17(1.20)			0.043	8.83
1150	0.04290	26.65	56.89	0.91	52.42	8.181	621.1
	0.00032	0.56	2.24(2.26)			0.016	13.7
1200	0.0350	23.95	55.44	0.76	56.80	8.454	684.0
	0.0010	0.76	3.25(3.26)			0.043	29.1
1250	0.0376	20.41	38.05	0.61	45.54	8.464	542.6
	0.0015	1.07	4.70(4.70)			0.017	36.0
1300	0.0458	26.73	53.81	1.03	49.39	9.140	583.9
	0.0010	0.80	3.41(3.43)			0.024	21.6
1350	0.0641	23.75	19.74	0.77	20.20	8.258	370.3
	0.0017	1.59	6.83(6.83)			0.017	26.7
TOTAL	0.016048	8.801	16.72	100.00	46.12	1.82	548.40
	0.000070	0.023	0.10(0.14)			0.34	2.73

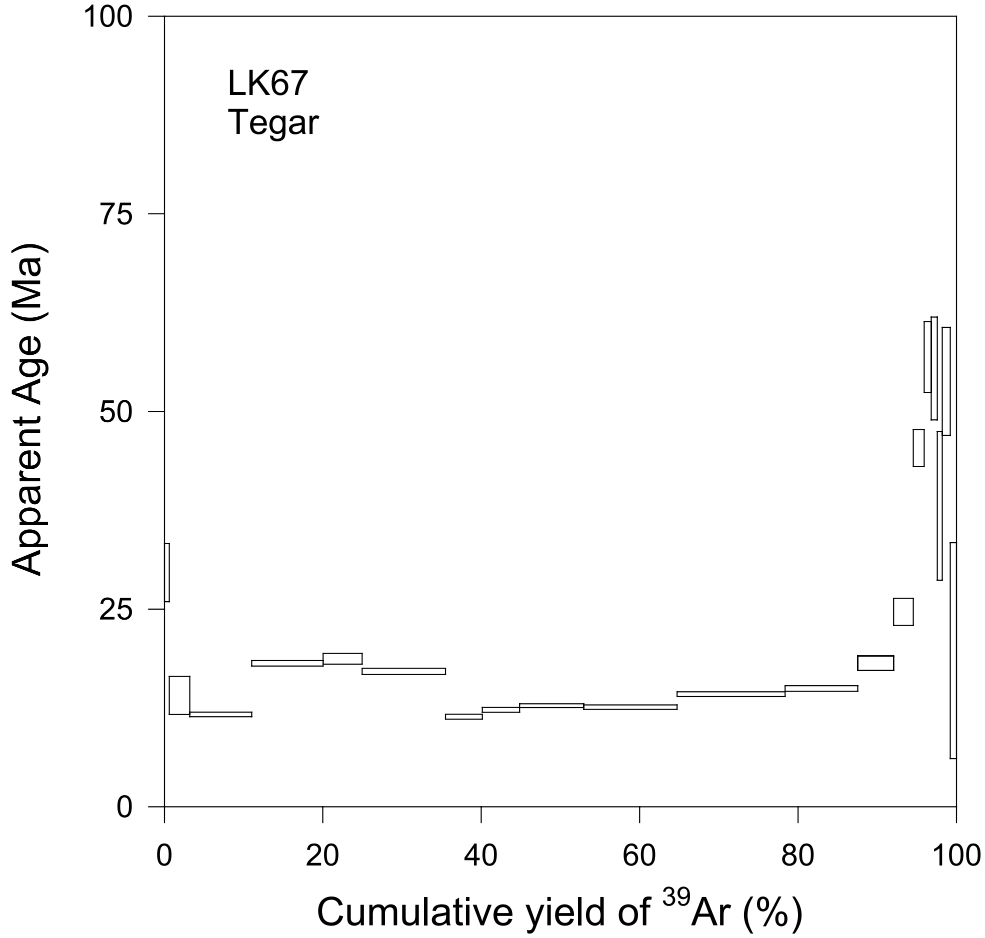

Fig. 4.11 *Ar/ Ar step heating results shown as apparent age spectrum for the sample LK67. The vertical side of the each box is 2σ error in apparent age without including error in J.*

Table 4.14 *Argon isotopic composition and apparent ages of sample LG188 (Tegar, Shyok Suture Zone) at different temperature steps. The errors in ages are without and with (bracketed) errors in **J**. The errors quoted are in 1σ.* ***J= .002447 ± .000013***

Temp. °C	$^{36}Ar/^{39}Ar$ ± 1σ	$^{40}Ar/^{39}Ar$ ± 1σ	Age(Ma) ± 1σ	^{39}Ar%	$^{40}Ar^*$%	$^{37}Ar/^{39}Ar$ ± 1σ	$^{40}Ar/^{36}Ar$ ± 1σ
500	.1232	37.40	4.39	.46	2.66	.4760	303.58
	.0016	.40	2.59(2.59)			.0046	4.93
550	.03847	13.05	7.43	.67	12.92	.3781	339.33
	.00088	.25	1.53(1.53)			.0035	9.92
600	.01990	7.796	8.43	2.17	24.57	.3815	391.75
	.00028	.084	.51(.51)			.0011	6.91
650	.02751	11.319	14.02	5.28	28.18	.47611	411.46
	.00015	.072	.33(.34)			.00095	3.26
700	.02383	10.397	14.74	4.82	32.26	.3407	436.24
	.00016	.068	.33(.34)			.0025	3.96
750	.01796	8.624	14.57	10.34	38.44	.26624	480.04
	.00015	.052	.27(.28)			.00053	4.77
800	.01062	6.749	15.86	6.36	53.49	.26385	635.29
	.00011	.046	.23(.24)			.00079	7.62
850	.009226	6.452	16.37	10.17	57.75	.42483	699.35
	.000064	.040	.17(.20)			.00085	6.26
900	.004340	5.128	16.89	22.00	74.99	.5656	1181.7
	.000038	.031	.13(.16)			.0021	12.2
950	.007587	6.403	18.27	11.16	64.98	1.7612	843.89
	.000059	.040	.17(.20)			.0035	8.09
1000	.006988	6.469	19.33	12.33	68.08	2.0900	925.7
	.000086	.040	.19(.21)			.0042	12.4
1150	.01645	11.048	27.09	5.63	55.99	4.3866	671.4
	.00023	.071	.40(.42)			.0088	10.1
1200	.01730	12.739	33.35	6.96	59.88	3.4714	736.49
	.00015	.079	.35(.39)			.0069	7.52
1300	.03600	19.32	37.90	1.28	44.93	3.5718	536.6
	.00087	.25	1.53(1.55)			.0075	14.6
1400	.0530	20.88	22.87	.37	24.98	3.174	393.9
	.0035	1.41	7.59(7.59)			.010	37.0
TOTAL	.012777	7.978	18.448	100.00	52.67	1.2669	624.35
	.000038	.017	.079(.125)			.0011	2.16

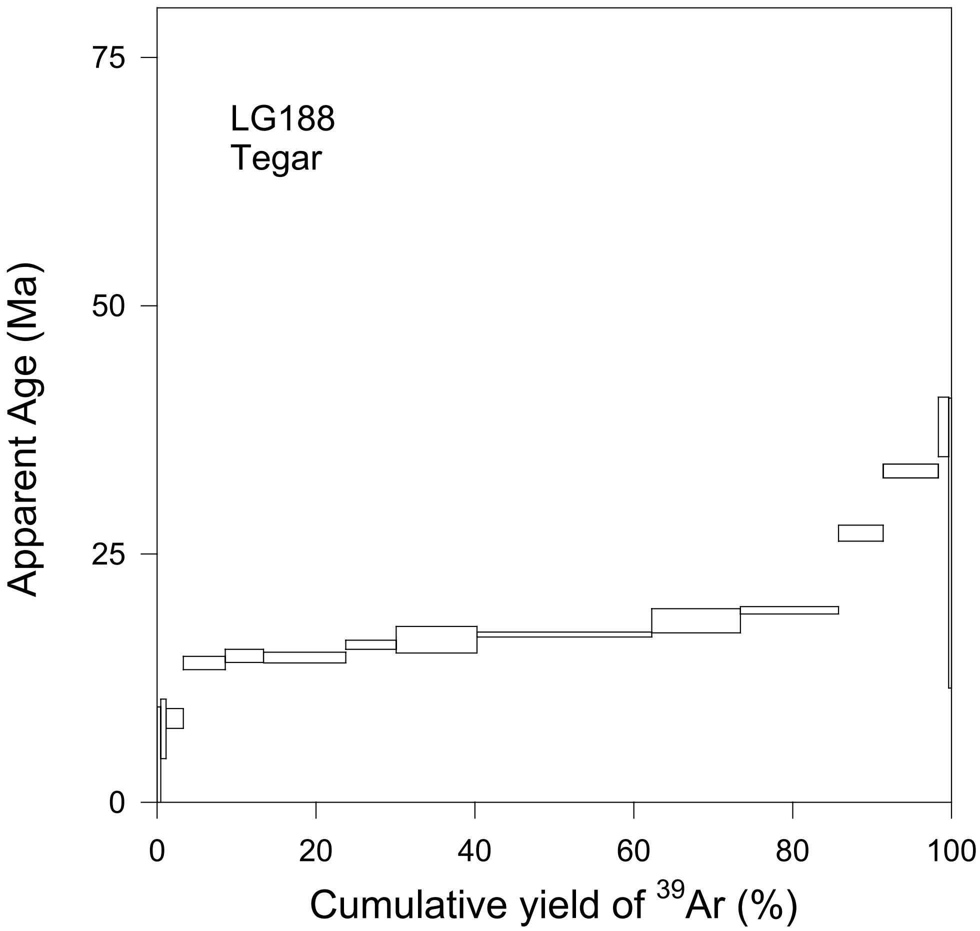

Fig. 4.12 *$^{40}Ar/^{39}Ar$ step heating results shown as apparent age spectrum for the sample LG188. The vertical side of the each box is 2σ error in apparent age without including error in J.*

Table 4.15** Argon isotopic composition and apparent ages of sample LK68 (between Panamik and Tegar, Shyok Suture Zone) at different temperature steps. The errors in ages are without and with (bracketed) errors in **J**. The errors quoted are in 1σ. **J= .002321 ± .000014

Temp. °C	$^{36}Ar/^{39}Ar$ ± 1σ	$^{40}Ar/^{39}Ar$ ± 1σ	Age(Ma) ± 1σ	^{39}Ar%	$^{40}Ar^*$%	$^{37}Ar/^{39}Ar$ ± 1σ	$^{40}Ar/^{36}Ar$ ± 1σ
400	0.0320	10.85	5.8	0.64	12.86	1.92	339.1
	0.0081	0.11	10.0(10.0)			0.23	86.3
450	0.005368	2.098	14.64	5.55	68.89	1.0284	949.70
	0.000028	0.032	0.12(0.15)			0.0021	7.32
500	0.003571	5.880	20.09	8.46	82.06	0.7565	1646.9
	0.000016	0.035	0.13(0.17)			0.0056	11.4
550	0.002562	7.001	25.95	12.07	89.19	0.7556	2733.1
	0.000021	0.049	0.15(0.21)			0.0070	26.1
600	0.00273	7.861	29.29	7.77	89.75	0.583	2881.7
	0.00017	0.047	0.26(0.31)			0.023	177.0
650	0.005398	9.459	32.63	21.74	83.14	0.6178	1752.3
	0.000019	0.055	0.20(0.27)			0.0026	10.8
700	0.004286	7.024	23.94	4.73	81.97	1.432	1638.8
	0.000030	0.056	0.17(0.22)			0.017	14.9
750	0.00440	6.861	23.13	4.12	81.05	1.6449	1559.4
	0.00017	0.046	0.27(0.30)			0.0033	60.6
800	0.004504	7.033	23.72	4.00	81.08	1.6177	1561.6
	0.000041	0.048	0.19(0.23)			0.0032	17.3
850	0.00476	7.969	27.30	5.84	82.46	1.7892	1684.5
	0.00016	0.050	0.27(0.31)			0.0041	57.1
900	0.003783	9.400	34.35	8.99	88.11	2.6632	2485.2
	0.000095	0.056	0.23(0.31)			0.0098	63.8
950	0.003744	10.939	40.70	8.11	89.89	3.0635	2921.7
	0.000046	0.066	0.24(0.34)			0.0061	39.0
1000	0.009287	13.552	44.69	4.16	79.75	4.917	1459.3
	0.000045	0.087	0.32(0.41)			0.032	10.9
1050	0.02277	28.84	90.28	1.28	76.67	10.885	1266.6
	0.00018	0.22	0.85(0.99)			0.022	13.7
1100	0.0183	46.76	165.26	0.52	88.41	12.978	2550.0
	0.0015	0.54	2.61(2.77)			0.091	207.8
1150	0.0223	60.95	214.38	0.44	89.21	14.74	2738.0
	0.0023	0.79	3.65(3.84)			0.35	279.7
1400	0.0135	58.07	213.30	1.58	93.14	17.40	4306.3
	0.0037	1.06	5.61(5.73)			0.12	1171.6
TOTAL	0.005066	9.817	34.50	100.00	84.75	1.9475	1937.6
	0.000082	0.025	0.14(0.24)			0.0040	31.5

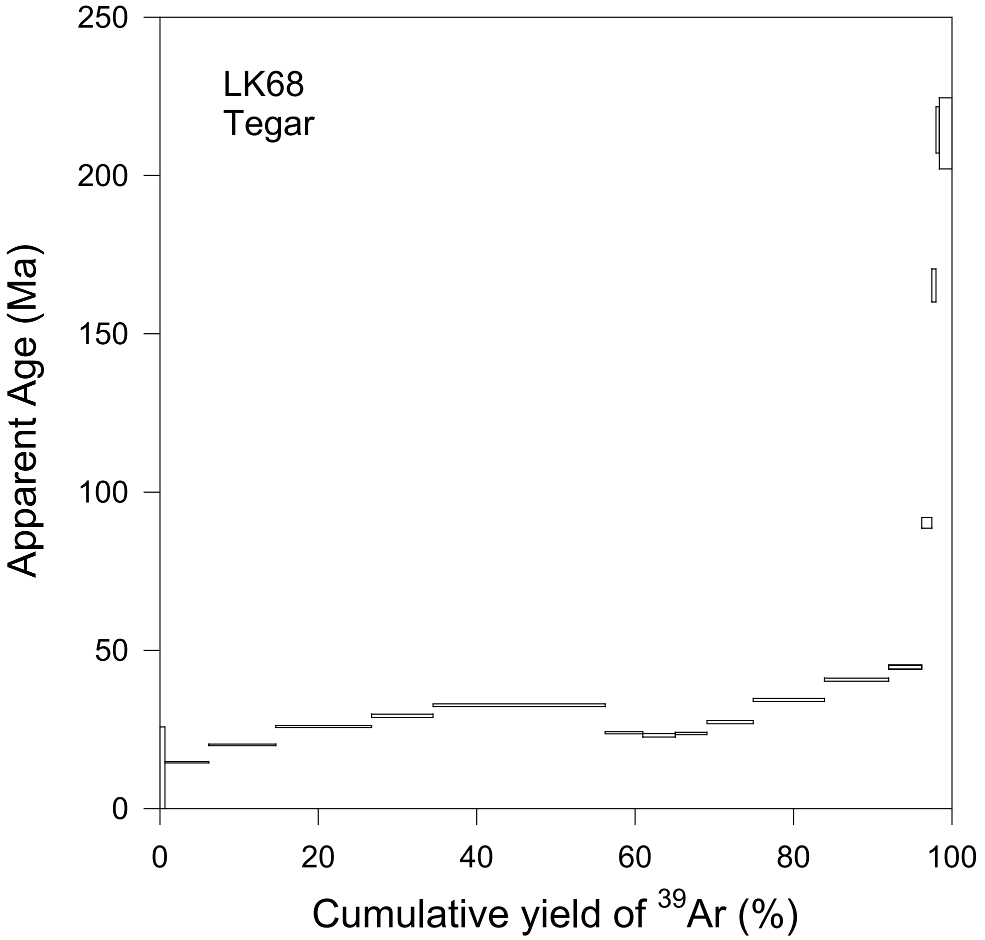

Fig. 4.13 *$^{40}Ar/^{39}Ar$ step heating results shown as apparent age spectrum for the sample LK68. The vertical side of the each box is 2σ error in apparent age without including error in J.*

Table 4.16 *Argon isotopic composition and apparent ages of sample LG197 (Tegar, Shyok Suture Zone) at different temperature steps. The errors in ages are without and with (bracketed) errors in **J**. The errors quoted are in 1σ. **J= .002362 ± .000013***

Temp. °C	$^{36}Ar/^{39}Ar$ ± 1σ	$^{40}Ar/^{39}Ar$ ± 1σ	Age(Ma) ± 1σ	$^{39}Ar\%$	$^{40}Ar^{*}\%$	$^{37}Ar/^{39}Ar$ ± 1σ	$^{40}Ar/^{36}Ar$ ± 1σ
500	.1373	112.26	282.10	.57	63.85	1.0813	817.4
	.0024	.89	3.96(4.21)			.0044	15.4
550	.0687	38.95	77.80	.85	47.91	1.068	567.2
	.0016	.48	2.68(2.71)			.031	14.8
600	.02948	21.23	52.56	3.45	58.96	1.3429	720.1
	.00040	.16	.78(.83)			.0096	11.1
650	.02178	14.26	33.04	5.68	54.87	2.0647	654.83
	.00026	.10	.50(.53)			.0041	8.86
700	.02216	15.56	37.99	6.21	57.92	2.1196	702.20
	.00023	.11	.49(.53)			.0060	8.48
750	.01112	12.157	37.40	12.15	72.96	1.7796	1092.8
	.00012	.076	.32(.38)			.0036	13.0
800	.00453	8.428	29.96	11.43	84.13	.9286	1862.3
	.00012	.058	.26(.31)			.0019	50.1
850	.004223	8.141	29.13	17.07	84.67	.6029	1928.0
	.000080	.052	.22(.27)			.0024	38.3
900	.003725	8.676	31.99	19.14	87.31	.994	2329.4
	.000072	.054	.22(.28)			.011	46.9
950	.01077	11.417	34.74	11.11	72.13	6.047	1060.3
	.00013	.073	.31(.37)			.012	13.9
1000	.01425	14.57	43.61	3.49	71.11	5.682	1022.8
	.00039	.13	.70(.74)			.011	29.2
1050	.02675	30.06	91.99	2.09	73.70	9.311	1123.6
	.00065	.24	1.20(1.30)			.019	28.6
1100	.04023	55.45	176.62	2.40	78.56	21.056	1378.1
	.00060	.36	1.42(1.69)			.042	22.2
1200	.06036	97.82	312.11	3.10	81.76	17.013	1620.5
	.00053	.58	1.90(2.47)			.034	16.4
1300	.0756	114.56	355.44	.91	80.50	15.202	1515.7
	.0027	.99	4.27(4.63)			.030	54.6
1400	.1310	115.08	299.1	.33	66.35	21.14	878.3
	.0092	3.55	15.8(15.9)			.14	66.8
TOTAL	.014526	17.181	54.09	100.00	75.02	3.2346	1182.74
	.000066	.036	.15(.33)			.0032	5.80

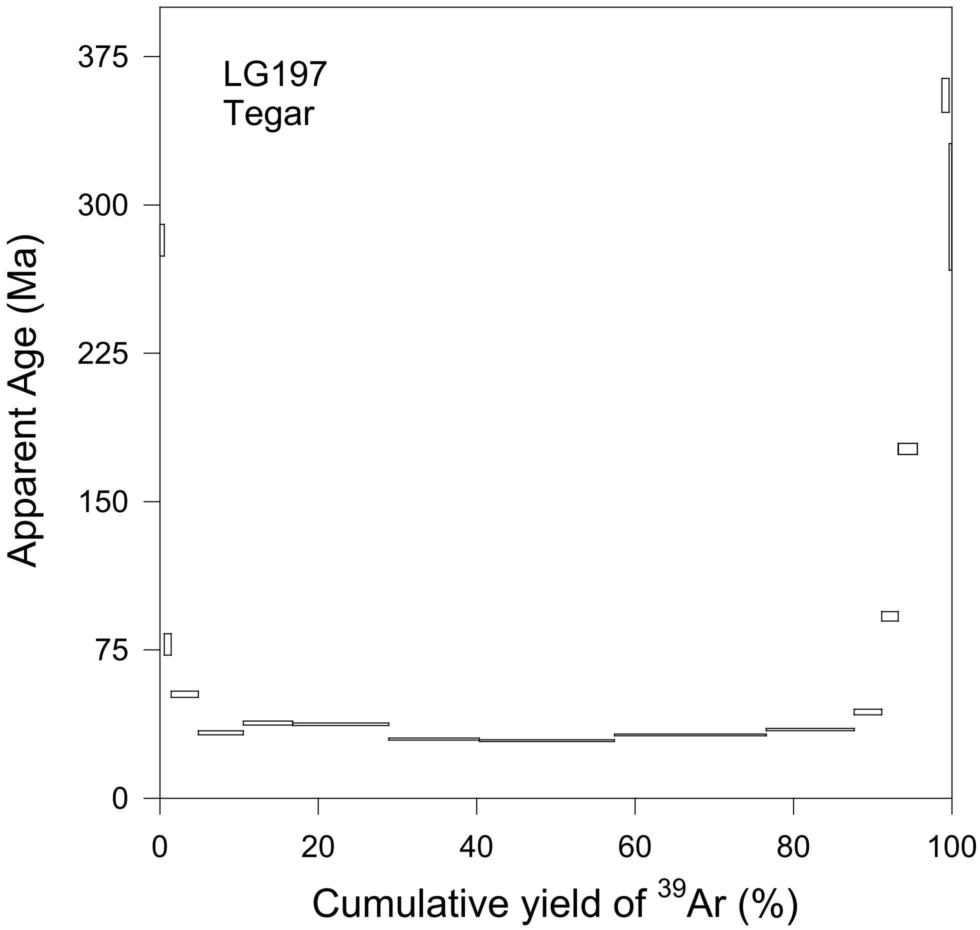

Fig. 4.14 *$^{40}Ar/^{39}Ar$ step heating results shown as apparent age spectrum for the sample LG197. The vertical side of the each box is 2σ error in apparent age without including error in J.*

Table 4.17** Argon isotopic composition and apparent ages of sample LG166 (Hunder, Shyok Suture Zone) at different temperature steps. The errors in ages are without and with (bracketed) errors in **J**. The errors quoted are in 1σ. **J= .002362 ± .000013

Temp. °C	$^{36}Ar/^{39}Ar$ ± 1σ	$^{40}Ar/^{39}Ar$	Age(Ma) ± 1σ	^{39}Ar%	$^{40}Ar^*$%	$^{37}Ar/^{39}Ar$ ± 1σ	$^{40}Ar/^{36}Ar$ ± 1σ
450	.099 .012	94.8 3.1	259. 17(17)	.03	69.08	2.121 .014	956. 116.
500	.0978 .0081	85.7 2.2	227. 12(12)	.05	66.27	2.259 .018	876. 76.
550	.2709 .0037	256.3 1.8	627.8 5(5.8)	.37	68.77	2.0351 .0052	946. 14.
600	.10180 .00041	83.62 .48	214.8 1.6(2.0)	1.72	64.03	1.4962 .0030	821.4 5.3
650	.05511 .00028	48.76 .33	133.28 .98(1.21)	4.49	66.60	1.2584 .0025	884.7 6.4
700	.02904 .00011	29.22 .17	85.84 .60(.76)	12.43	70.63	.8210 .0024	1006.2 6.2
750	.006691 .000035	14.047 .081	50.70 .30(.40)	25.20	85.92	.45894 .00092	2099. 15.
800	.003302 .000027	12.347 .072	47.81 .26(.37)	15.43	92.10	.38084 .00097	3740. 36.
850	.004273 .000041	14.747 .086	56.55 .31(.44)	10.82	91.44	.6155 .0021	3451. 38.
900	.005637 .000043	17.39 .10	65.78 .36(.51)	11.98	90.42	.6696 .0013	3085. 28.
950	.007964 .000048	21.40 .12	79.36 .44(.62)	9.38	89.00	.8260 .0017	2687. 21.
1000	.01469 .00011	36.17 .21	130.73 .73(1.01)	4.16	88.00	1.0674 .0021	2462. 22.
1050	.02687 .00016	62.38 .36	218.2 1.2(1.6)	2.77	87.27	1.1879 .0024	2321. 18.
1100	.06855 .00060	133.72 .79	428.2 2.4(3.2)	.67	84.85	2.367 .019	1951. 20.
1150	.1877 .0028	347.5 3.8	946.2 5.9(7.2)	.18	84.04	6.862 .094	1851. 30.
1200	.2264 .0054	405.0 3.1	1058.7 7.2(8.5)	.08	83.48	7.358 .047	1788. 44.
1300	.2928 .0082	543.2 5.5	1319.8 8.5(9.9)	.08	84.07	9.339 .043	1855. 53.
1400	.2763 .0055	457.6 3.5	1146.3 7.8(9.1)	.15	82.16	8.501 .065	1656. 35.
TOTAL	.015992 .000031	25.636 .047	86.95 .16(.49)	100.00	81.57	.72438 .00060	1603.0 3.9

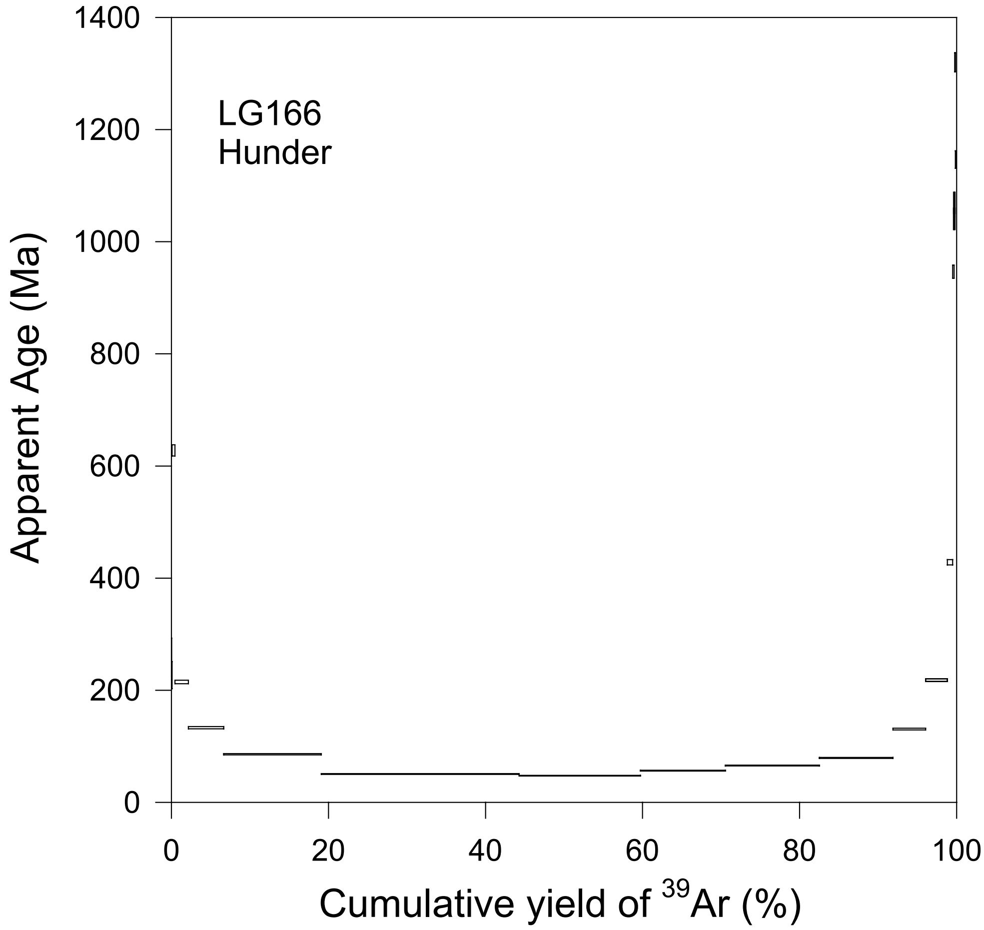

Fig. 4.15 *$^{40}Ar/^{39}Ar$ step heating results shown as apparent age spectrum for the sample LG166. The vertical side of the each box is 2σ error in apparent age without including error in J.*

Table 4.18** Argon isotopic composition and apparent ages of sample LK70 (between Panamik and Tegar, Shyok Suture Zone) at different temperature steps. The errors in ages are without and with (bracketed) errors in **J**. The errors quoted are in 1σ.* ***J= .002417 ± .000015

Temp. °C	$^{36}Ar/^{39}Ar$ ± 1σ	$^{40}Ar/^{39}Ar$ ± 1σ	Age(Ma) ± 1σ	^{39}Ar%	$^{40}Ar^*$%	$^{37}Ar/^{39}Ar$ ± 1σ	$^{40}Ar/^{36}Ar$ ± 1σ
400	0.16439 0.00057	57.14 0.33	36.95 1.29(1.31)	0.28	14.99	0.7256 0.0059	347.59 2.12
450	0.04923 0.00048	19.64 0.12	22.06 0.71(0.73)	1.67	25.93	0.1293 0.0013	398.95 4.35
500	0.01049 0.00017	7.39 0.15	18.62 0.50(0.51)	4.37	58.07	0.306 0.022	704.8 15.6
550	0.005009 0.000069	6.148 0.086	20.24 0.14(0.19)	7.68	75.93	0.1820 0.0023	1227.5 18.2
600	0.004249 0.000034	7.749 0.064	28.09 0.17(0.25)	13.70	83.80	0.0934 0.0075	1823.9 17.3
650	0.00588 0.00014	9.711 0.056	34.43 0.27(0.35)	25.82	82.12	0.0506 0.0056	1652.6 40.2
700	0.0020772 0.0000082	7.744 0.045	30.82 0.17(0.26)	11.91	92.07	0.102 0.023	3728.0 24.0
750	0.003263 0.000031	6.943 0.041	25.87 0.16(0.23)	5.68	86.11	0.1984 0.0085	2127.5 23.0
800	0.003369 0.000063	7.439 0.044	27.87 0.19(0.25)	4.80	86.62	0.5016 0.0034	2208.2 42.7
850	0.004010 0.000015	9.036 0.054	33.91 0.20(0.29)	5.44	86.89	0.655 0.013	2253.4 14.6
900	0.006617 0.000036	11.859 0.084	42.66 0.26(0.37)	5.91	83.51	1.675 0.013	17.92.2 13.3
950	0.004807 0.000065	12.890 0.076	49.32 0.29(0.43)	5.46	88.98	1.242 0.068	2681.4 38.9
1000	0.004951 0.000018	15.768 0.095	61.31 0.35(0.52)	4.74	90.72	0.516 0.015	3185.1 20.4
1050	0.02520 0.00043	27.41 0.21	85.01 0.97(1.10)	1.14	72.84	0.627 0.031	1088.0 20.0
1100	0.001113 0.000061	106.09 1.68	410.54 4.86(5.38)	0.37	99.69	1.80 0.16	95345.2 5353.2
1150	0.0767 0.0020	121.13 2.16	385.07 6.21(6.59)	0.35	81.30	17.98 1.47	1579.8 45.9
1200	0.1052 0.0052	61.33 3.00	127.2 13.5(13.5)	0.19	49.30	76.71 0.48	582.9 40.3
1250	0.1073 0.0053	65.91 2.36	143.3 11.4(11.4)	0.25	51.91	101.82 1.24	614.4 37.4
1300	0.0779 0.0060	102.52 2.86	316.9 12.2(12.4)	0.25	77.54	24.30 0.16	1315.4 108.2
TOTAL	0.007146 0.000046	10.827 0.029	37.60 0.11(0.26)	100.00	80.50	0.8670 0.0080	1515.1 10.2

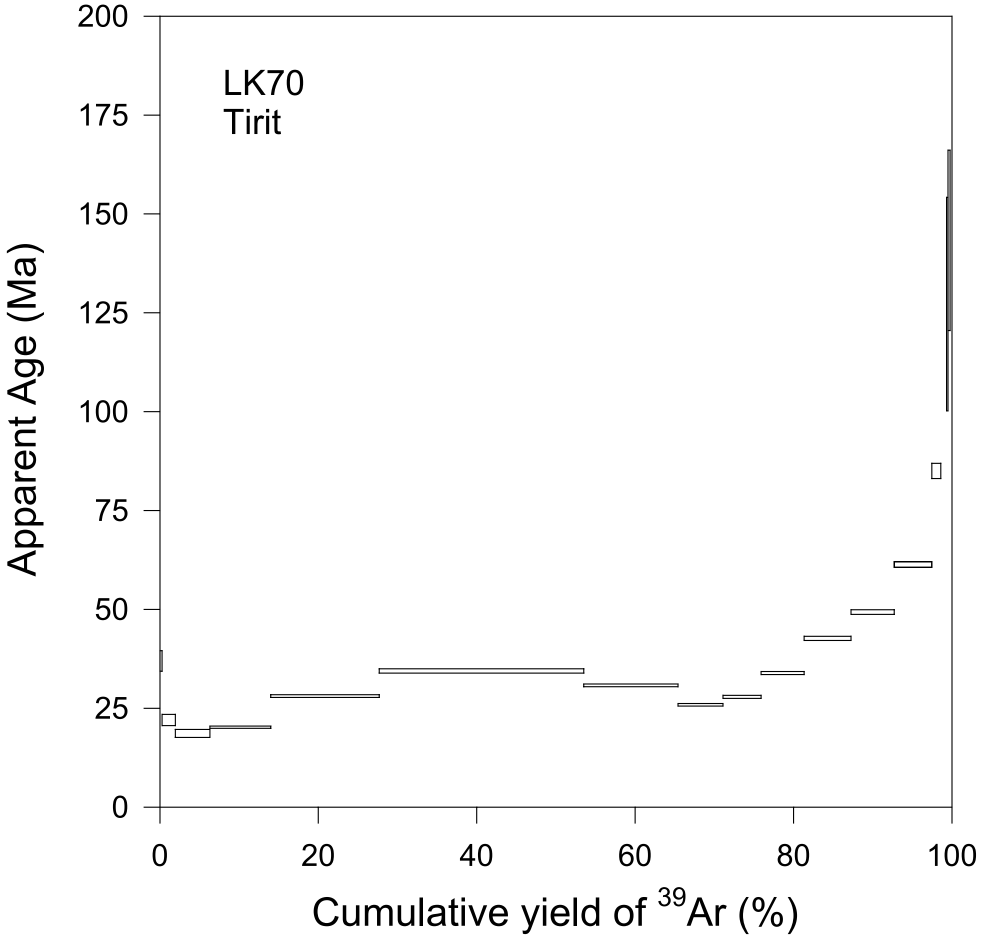

Fig. 4.16 *$^{40}Ar/^{39}Ar$ step heating results shown as apparent age spectrum for the sample LK70. The vertical side of the each box is 2σ error in apparent age without including error in J.*

Table 4.19** Argon isotopic composition and apparent ages of sample LK47 (Murgi, Karakoram Fault Zone) at different temperature steps. The errors in ages are without and with (bracketed) errors in **J**. The errors quoted are in 1σ. **J= .0022383 ± .0000132

Temp. °C	$^{36}Ar/^{39}Ar$ ± 1σ	$^{40}Ar/^{39}Ar$ ± 1σ	Age(Ma) ± 1σ	$^{39}Ar\%$	$^{40}Ar^*\%$	$^{37}Ar/^{39}Ar$ ± 1σ	$^{40}Ar/^{36}Ar$ ± 1σ
750	.004008	4.463	13.19	2.13	73.47	.654	1113.7
	.000034	.033	.13(.15)			.043	12.1
800	.00385	4.539	13.68	3.56	74.92	.408	1178.1
	.00012	.051	.23(.24)			.069	37.6
850	.003419	4.369	13.508	8.04	76.88	.2534	1277.89
	.000012	.026	.093(.122)			.0094	8.13
900	.0026922	4.179	13.610	13.98	80.96	.2493	1552.38
	.0000094	.025	.087(.118)			.0021	9.71
950	.002594	4.135	13.55	12.83	81.46	.125	1594.0
	.000045	.027	.10(.13)			.018	28.9
1000	.002072	4.015	13.685	12.13	84.75	.1204	1937.4
	.000015	.024	.086(.118)			.0095	17.3
1050	.0015376	3.895	13.839	16.13	88.34	.0892	2533.4
	.0000064	.024	.085(.118)			.0019	17.4
1100	.001078	3.723	13.69	9.67	91.44	.149	3453.5
	.000013	.029	.085(.14)			.020	49.5
1150	.00313	4.42	14.07	1.45	79.11	.895	1414.5
	.00016	.18	.75(.76)			.018	94.6
1200	.0193	20.71	59.56	.29	72.42	59.71	1071.3
	.0014	1.32	5.36(5.37)			3.85	104.9
1250	.0407	30.09	71.48	.10	60.01	29.89	738.9
	.0050	.56	6.06(6.07)			1.32	91.1
TOTAL	.003564	4.455	13.682	100.00	76.36	1.093	1249.91
	.000020	.011	.043(.091)			.019	7.56

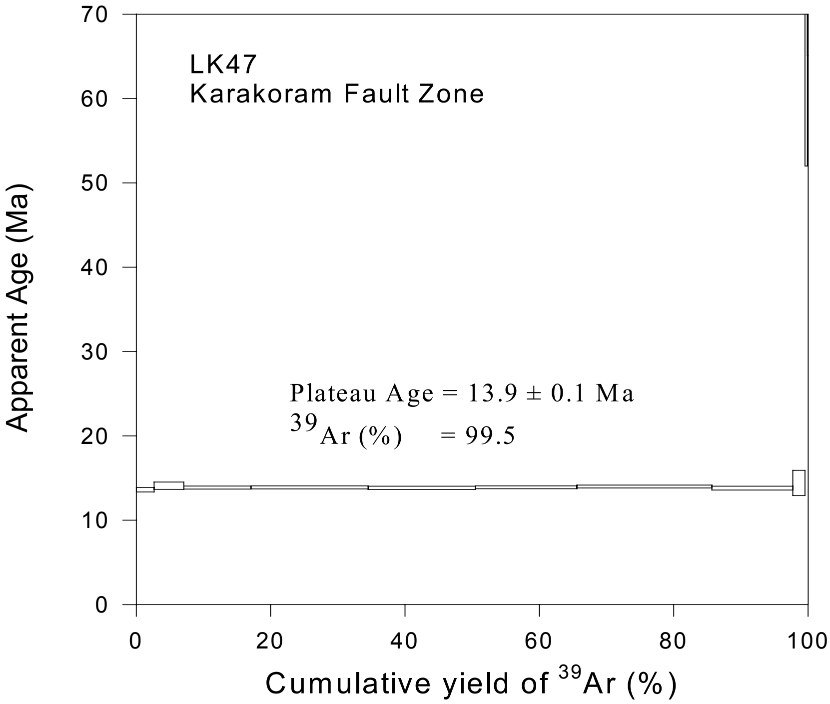

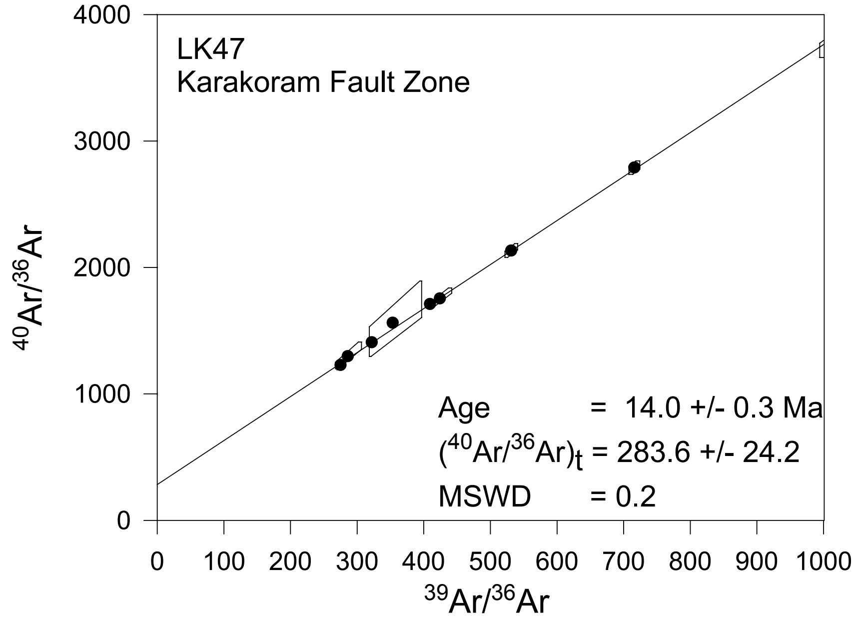

Fig. 4.17 *(Top) $^{40}Ar/^{39}Ar$ step heating results shown as apparent age spectrum for the sample LK47. The vertical side of the each box is 2σ error in apparent age without including error in J. Error in plateau-age includes error in J.*
(Bottom) $^{40}Ar/^{36}Ar$ vs. $^{39}Ar/^{36}Ar$ correlation diagram is also shown with isochron age, $^{40}Ar/^{36}Ar$ trapped ratio and MSWD value.

4.6.3. Khardung Volcanics

LK 86, an acidic volcanic sample, from the village Tirit is in direct contact with the Shyok volcanics (Figs 2.2 & 2.5). It yielded a complex age spectrum (Table 4.20 & Fig.4.18). For the first three consecutive steps and more than 40% of ^{39}Ar released the ages continuously rise from ~ 50 Ma to ~ 65 Ma. For the next three consecutive steps ages fall to ~ 30 Ma and then again continuously rise up to more than ~ 60 Ma. It appears to be the superimposition of the two cooling patterns similar to the Shyok Volcanics.

Rhyolite LK 88 from near the village Khardung, type locality of the Khardung, volcanics (Figs.2.2 & 2.5), yielded a plateau age of 52 .0 ± 0.4 Ma for the first five steps consisting of ~ 80 % of the cumulative ^{39}Ar released (Table 4.21 & Fig. 4.19). The remaining steps yielded continuously rising ages up to ~ 100 Ma. The isochron plotted for the five plateau steps yielded an age of 52.8 ± 0.9 Ma and the trapped ratio as 274.8 ± 38.5 Ma and MSWD of 1.5.

Another rhyolite LK 90 also taken from the vicinity of the village Khardung yielded a similar age spectrum. The plateau age for the first six consecutive steps consisting of 82 % of the gas released is 56.4 ± 0.4 Ma (Table 4.22 & Fig.4.20). The remaining steps yield continuously rising apparent ages up to ~ 120 Ma. The isochron age is 56.6 ± 0.9 Ma with the trapped ratio of 284.4 ± 28.5 and the MSWD 3.3.

Sample LG 601, an acidic volcanic sample, near the village Dungti (Fig.2.2) didn't yield a plateau. The age spectrum indicates thermal disturbances experienced by this sample subsequent to crystallization. Eight middle temperature steps yielded a mean age of 64.0 ± 1.2 Ma consisting of ~ 64% of ^{39}Ar released (Table 4.23 & Fig. 4.21). The correlation diagram of these eight steps yielded an age of 61.4 ± 2.4 Ma with trapped ratio as 303.2 ± 9.7 and MSWD 3.2. This age is interpreted to be the age of last major tectono-thermal event experienced by this sample.

LG 87, another acidic volcanic sample, near the village Chushul (Fig.2.2) yielded a plateau age of 57.0 ± 0.3 Ma for eleven consecutive steps consisting of more than 90 % of ^{39}Ar released (Table 4.24 & Fig. 4.22). Its isochron age is 57.5 ± 0.9 Ma with the trapped ratio as 288.8 ± 7.7 Ma and MSWD 2.7.

Table 4.20** Argon isotopic composition and apparent ages of sample LK86 (Between Khalsar and Khardung, Shyok Suture Zone) at different temperature steps. The errors in ages are without and with (bracketed) errors in **J**. The errors quoted are in 1σ. **J= .002573 ± .000016

Temp. °C	^{36}Ar/^{39}Ar ± 1σ	± 1σ	Age(Ma) ± 1σ	^{39}Ar%	^{40}Ar*%	^{37}Ar/^{39}Ar ± 1σ	^{40}Ar/^{36}Ar ± 1σ
400	0.00241	12.120	52.18	7.71	94.11	0.058	5019.9
	0.00012	0.070	0.32(0.46)			0.010	259.0
450	0.000739	13.878	62.31	15.03	98.43	0.103	18771.2
	0.000028	0.080	0.31(0.50)			0.015	708.9
500	0.000530	14.670	66.13	17.33	98.93	0.054	27680.2
	0.000018	0.085	0.33(0.53)			0.011	925.5
550	0.0005285	13.517	60.97	18.73	98.84	0.0580	25578.0
	0.0000038	0.078	0.30(0.49)			0.0034	222.9
600	0.0014177	9.954	43.72	8.37	95.79	0.09224	7020.9
	0.0000056	0.058	0.23(0.36)			0.00050	44.9
650	0.006294	8.644	31.22	5.75	78.48	0.1365	1373.46
	0.000023	0.050	0.20(0.28)			0.0031	8.63
700	0.002824	7.737	31.75	2.78	89.22	0.641	2740.0
	0.000058	0.046	0.20(0.28)			0.043	58.5
750	0.00447	7.982	30.65	1.64	83.44	0.815	1784.6
	0.00010	0.050	0.25(0.31)			0.026	41.9
800	0.004491	8.356	32.33	2.31	84.12	0.542	1860.6
	0.000052	0.051	0.21(0.30)			0.049	23.7
850	0.005194	8.870	33.73	1.49	82.70	0.921	1707.7
	0.000037	0.057	0.24(0.32)			0.0063	15.7
900	0.006023	9.236	34.28	2.37	80.73	0.3846	1533.6
	0.000071	0.056	0.24(0.33)			0.0028	19.9
950	0.00720	9.556	34.15	2.59	77.72	0.371	1326.4
	0.00022	0.058	0.37(0.43)			0.055	41.1
1000	0.00766	9.889	35.05	3.55	77.12	0.388	1291.4
	0.00011	0.058	0.28(0.35)			0.034	20.2
1050	0.005923	9.886	37.37	3.22	82.30	0.443	1669.2
	0.000022	0.059	0.24(0.33)			0.042	10.7
1100	0.00288	10.491	44.19	2.48	91.88	0.793	3640.9
	0.00022	0.065	0.39(0.48)			0.083	274.6
1150	0.00334	11.468	48.00	2.43	91.40	0.540	3435.3
	0.00034	0.085	0.57(0.65)			0.020	349.5
1200	0.00268	14.65	63.21	1.14	94.60	0.705	5472.7
	0.00085	0.20	1.42(1.47)			0.056	1729.1
TOTAL	0.002062	12.118	52.64	100.00	94.97	1.04	5875.8
	0.000045	0.027	0.12(0.35)			0.11	129.0

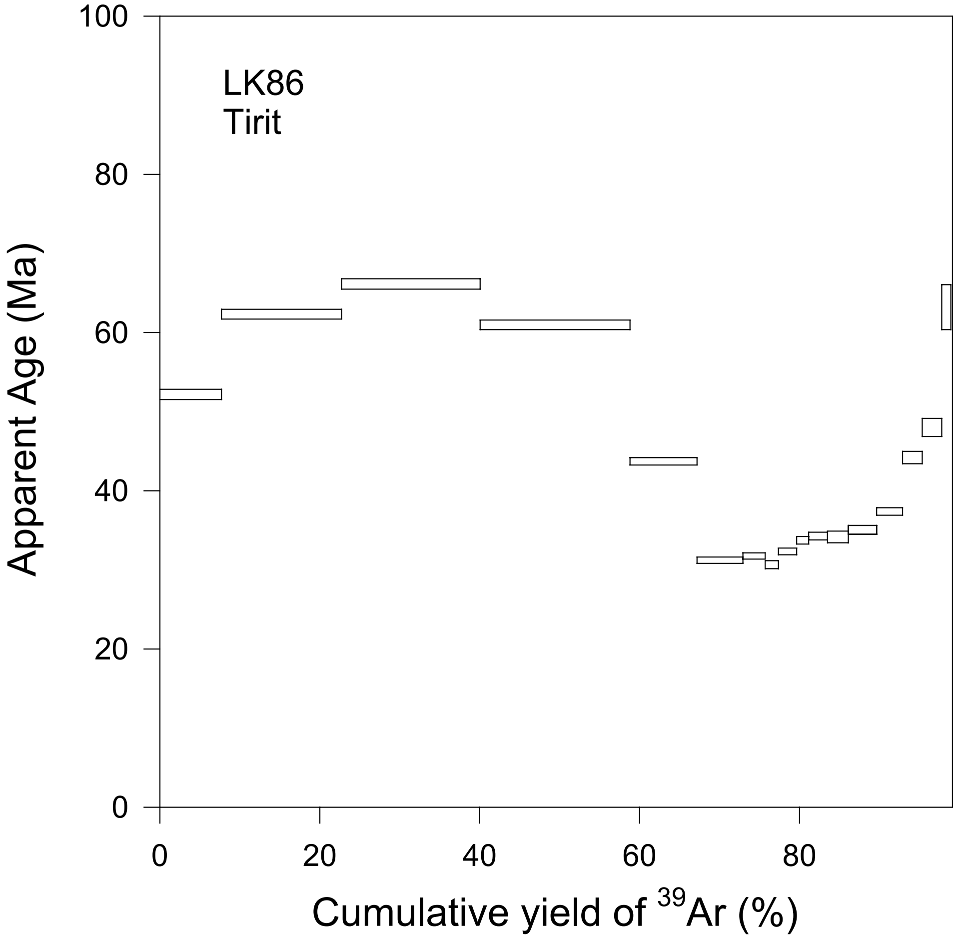

Fig. 4.18 *$^{40}Ar/^{39}Ar$ step heating results shown as apparent age spectrum for the sample LK86. The vertical side of the each box is 2σ error in apparent age without including error in J.*

Table 4.21** Argon isotopic composition and apparent ages of sample LK88(Khardung, Khardung Volcanics) at different temperature steps. The errors in ages are without and with (bracketed) errors in **J**. The errors quoted are in 1σ. **J= .002347 ± .000014

Temp. °C	$^{36}Ar/^{39}Ar$ ± 1σ	$^{40}Ar/^{39}Ar$ ± 1σ	Age(Ma) ± 1σ	$^{39}Ar\%$		$^{37}Ar/^{39}Ar$ ± 1σ	$^{40}Ar/^{36}Ar$ ± 1σ
400	0.006786	14.12	50.56	2.98	85.79	0.1566	2080.2
	0.000089	0.20	0.34(0.45)			0.0019	29.9
450	0.002643	13.04	51.16	7.66	94.01	0.0629	4932.7
	0.000045	0.12	0.28(0.41)			0.0022	87.8
500	0.0011938	13.100	53.18	25.48	97.31	0.00924	10973.4
	0.0000041	0.076	0.27(0.42)			0.00010	67.1
550	0.0011599	12.83	52.13	31.47	97.33	0.01423	11064.6
	0.0000084	0.16	0.63(0.70)			0.00012	153.4
600	0.006408	14.540	52.77	13.26	86.98	0.03555	2269.0
	0.000026	0.084	0.30(0.44)			0.00073	14.6
650	0.007283	14.190	50.26	4.19	84.83	0.0875	1948.5
	0.000029	0.089	0.33(0.44)			0.0021	13.3
700	0.016677	15.09	42.52	1.26	67.34	0.316	904.77
	0.000058	0.10	0.38(0.46)			0.028	6.32
750	0.02562	18.33	44.97	0.71	58.69	0.560	715.28
	0.00019	0.15	0.60(0.66)			0.042	7.52
800	0.02620	20.03	51.28	1.11	61.34	0.3241	764.40
	0.00016	0.13	0.53(0.61)			0.0042	6.54
850	0.02357	21.13	58.99	1.75	67.03	0.299	896.38
	0.00016	0.13	0.50(0.61)			0.042	7.78
900	0.024606	22.32	62.61	1.46	67.42	0.243	907.01
	0.000085	0.14	0.53(0.65)			0.030	6.11
950	0.03101	21.81	52.75	1.19	57.98	0.281	703.19
	0.00033	015	0.69(0.76)			0.014	8.75
1000	0.03794	28.76	72.81	1.25	61.01	0.304	757.97
	0.00030	0.20	0.80(0.91)			0.022	7.67
1050	0.03681	30.27	80.30	1.32	64.07	0.2853	822.39
	0.00017	0.22	0.77(0.91)			0.0094	6.42
1100	0.03674	32.98	91.32	1.27	67.08	0.214	897.62
	0.00015	0.30	1.10(1.22)			0.020	8.27
1150	0.03041	35.46	108.77	0.93	74.66	0.530	1166.3
	0.00098	0.62	2.68(2.76)			0.022	42.7
1200	0.0350	36.9	109.2	0.80	71.97	0.582	1054.3
	0.0097	10.0	10.9(10.9)			0.044	301.0
1250	0.0197	28.74	94.5	0.63	78.70	0.355	1455.5
	0.0037	2.27	10.1(10.1)			0.024	293.0
1300	0.0150	28.83	100.4	0.81	84.63	0.509	1922.0
	0.0045	2.19	10.2(10.2)			0.049	592.2
1350	0.026	37.66	122.7	0.46	79.66	0.834	1452.5
	0.017	0.58	19.5(19.5)			0.052	929.5
TOTAL	0.006407	15.207	55.51	100.00	87.55	0.0785	2373.4
	0.000094	0.075	0.27(0.43)			0.0013	36.1

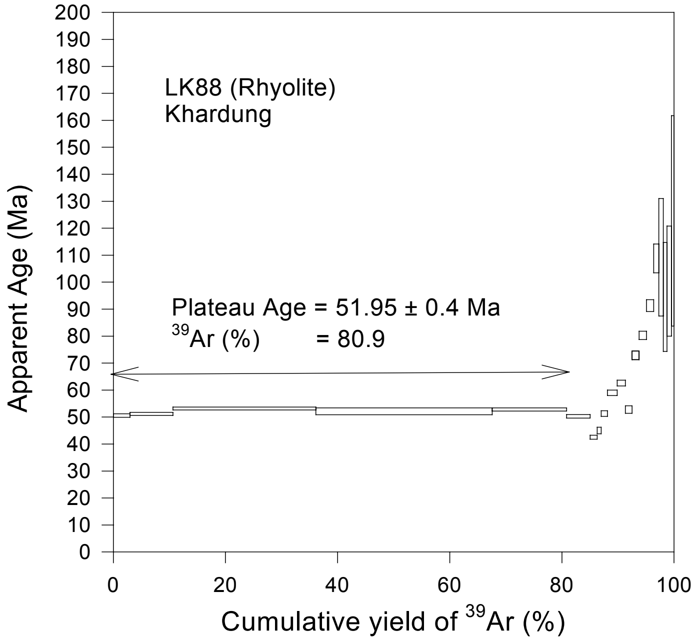

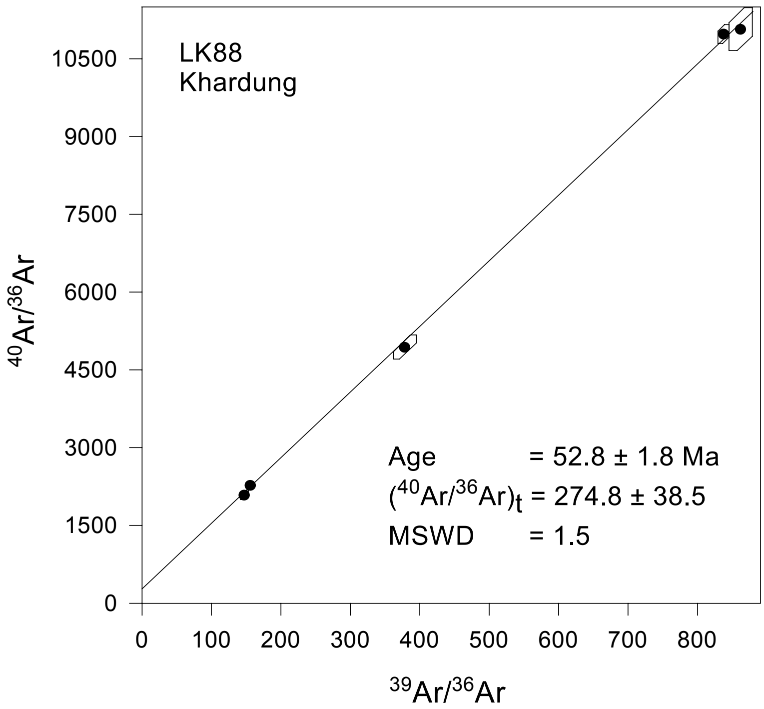

Fig. 4.19 *(Top) $^{40}Ar/^{39}Ar$ step heating results shown as apparent age spectrumfor the sample LK88. The vertical side of the each box is 2σ error in apparent age without including error in J. Error in plateau-age includes error in J.*

(Bottom) $^{40}Ar/^{36}Ar$ vs. $^{39}Ar/^{36}Ar$ correlation diagram is also shown with isochron age, $^{40}Ar/^{36}Ar$ trapped ratio and MSWD value.

Table 4.22** Argon isotopic composition and apparent ages of sample LK90 (Khardung, Khardung Volcanics) at different temperature steps. The errors in ages are without and with (bracketed) errors in **J**. The errors quoted are in 1σ. **J= .002458 ± .000016

Temp. °C	^{36}Ar/^{39}Ar	^{40}Ar/^{39}Ar ± 1σ	Age(Ma) ± 1σ	^{39}Ar%	^{40}Ar*%	^{37}Ar/^{39}Ar ± 1σ	^{40}Ar/^{36}Ar ± 1σ
400	0.00719 0.00020	15.571 0.094	58.66 0.42(0.56)	3.67	86.35	0.165 0.013	2165.2 61.0
450	0.001851 0.000019	13.334 0.090	55.83 0.29(0.45)	12.21	95.90	0.04547 0.00092	7204.8 83.2
500	0.001320 0.000015	13.280 0.077	56.27 0.29(0.46)	17.53	97.06	0.3310 0.00021	10060.1 123.8
550	0.00195 0.00011	13.34 0.13	55.71 0.53(0.64)	19.06	95.67	0.0273 0.0079	6832.0 376.6
600	0.0022784 0.0000079	13.862 0.089	57.56 0.34(0.50)	18.68	95.14	0.09095 0.00079	6084.3 40.8
650	0.008618 0.000075	14.98 0.11	54.32 0.44(0.55)	11.00	83.00	0.0401 0.0010	1738.6 18.9
700	0.00795 0.00029	13.53 0.13	48.91 0.65(0.72)	2.43	82.63	0.00090 0.00041	1701.7 63.8
750	0.00973 0.00024	13.37 0.12	45.94 0.54(0.61)	1.09	78.49	0.590 0.015	1373.8 35.2
800	0.02724 0.00044	19.96 0.16	52.05 0.82(0.88)	0.87	59.67	0.604 0.058	732.7 13.0
850	0.02715 0.00011	21.48 0.16	58.72 0.66(0.76)	0.88	62.66	0.500 0.062	791.29 6.43
900	0.02692 0.00012	22.59 0.17	63.76 0.64(0.75)	1.05	64.79	0.2866 0.0033	839.29 6.59
950	0.02308 0.00096	23.93 0.18	74.31 1.40(1.48)	1.24	71.49	2.83 0.12	1036.6 43.6
1000	0.03205 0.00030	27.27 0.20	77.24 0.87(0.99)	1.54	65.27	0.265 0.028	850.74 9.81
1050	0.03397 0.00012	30.18 0.25	87.17 1.00(1.13)	2.14	66.74	0.1433 0.0031	888.35 7.64
1100	0.02807 0.00024	32.43 0.32	103.96 1.10(1.27)	2.52	74.42	0.12198 0.00050	1155.3 13.5
1150	0.02232 0.00064	37.29 0.65	131.20 2.54(2.67)	1.61	82.31	0.1989 0.0015	1670.2 54.4
1200	0.0229 0.0016	38.50 1.41	135.43 6.09(6.15)	0.82	82.39	0.3866 0.0021	1677.6 132.2
1250	0.0297 0.0030	40.40 2.44	135.1 10.7(10.7)	0.62	78.31	0.535 0.023	1362.2 160.3
1300	0.0153 0.0044	36.90 2.98	138.2 13.4(13.4)	0.64	87.75	0.4940 0.0087	2412.8 720.9
1350	0.0305 0.0069	21.04 5.83	52.6 26.6(26.6)	0.41	57.15	0.7780 0.0016	689.7 245.9
TOTAL	0.006691 0.000055	16.046 0.054	61.33 0.23(0.45)	100.00	87.68	0.1243 0.0024	2398.3 21.1

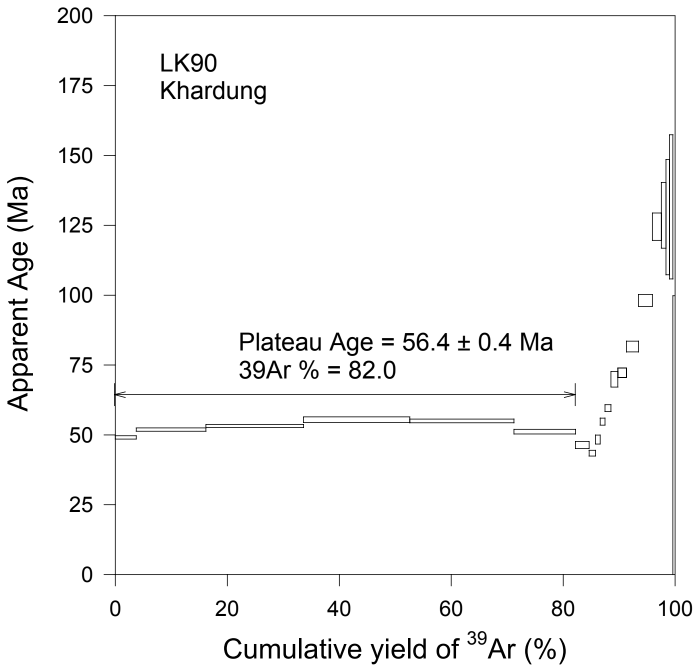

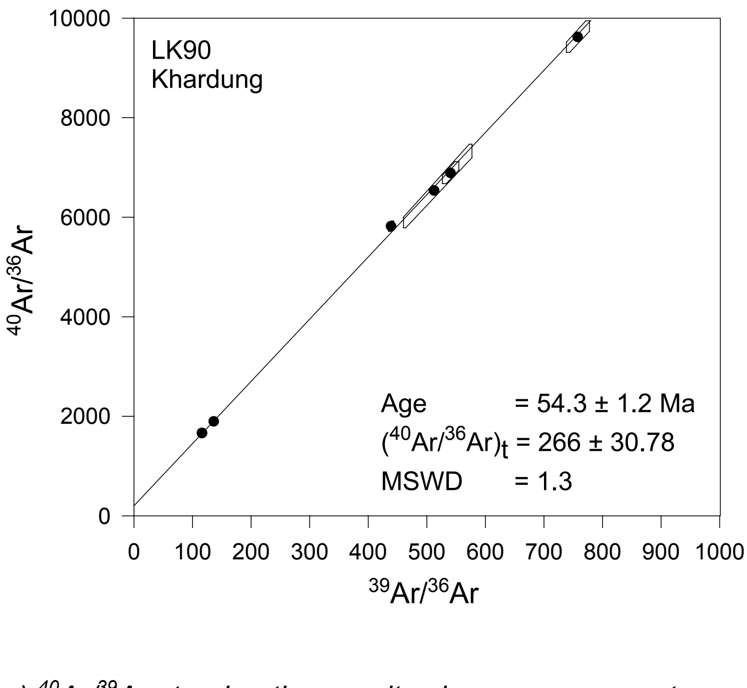

Fig. 4.20 *(Top) $^{40}Ar/^{39}Ar$ step heating results shown as apparent age spectrum for the sample LK90. The vertical side of the each box is 2σ error in apparent age without including error in J. Error in plateau-age includes error in J.*
(Bottom) $^{40}Ar/^{36}Ar$ vs. $^{39}Ar/^{36}Ar$ correlation diagram is also shown with isochron age, $^{40}Ar/^{36}Ar$ trapped ratio and MSWD value.

Table 4.23** Argon isotopic composition and apparent ages of sample LK601 (Dungti, Khardung Volcanics) at different temperature steps. The errors in ages are without and with (bracketed) errors in **J**. The errors quoted are in 1σ. **J= .002447 ± .000013

Temp. °C	$^{36}Ar/^{39}Ar$ ± 1σ	$^{40}Ar/^{39}Ar$	Age(Ma) ± 1σ	^{39}Ar%	$^{40}Ar^*$%	$^{37}Ar/^{39}Ar$ ± 1σ	$^{40}Ar/^{36}Ar$ ± 1σ
550	.1967	69.77	50.6	1.38	16.67	11.161	354.6
	.0067	2.19	11.6(11.6)			.030	15.7
600	.1034	37.82	31.82	5.05	19.23	12.52	365.86
	.0018	.41	2.74(2.75)			.20	7.24
650	.0653	28.90	41.86	7.39	33.20	12.892	442.36
	.0012	.27	1.91(1.92)			.049	9.25
700	.1066	44.42	56.08	9.37	29.06	12.607	416.54
	.0019	.31	2.68(2.70)			.025	7.96
750	.1414	59.36	75.95	5.63	29.61	12.868	419.83
	.0015	.44	2.54(2.57)			.026	5.41
800	.1255	55.31	78.71	4.45	32.96	14.898	440.80
	.0021	.48	3.26(3.28)			.030	8.36
850	.0537	34.22	79.20	4.93	53.62	13.517	637.2
	.0019	.38	2.83(2.86)			.031	23.6
900	.0413	26.22	60.77	8.07	53.41	15.960	634.2
	.0013	.22	1.84(1.87)			.032	20.4
950	.03310	26.99	74.39	15.66	63.76	23.07	815.4
	.00071	.21	1.20(1.26)			.16	18.4
1000	.03896	28.59	73.81	11.18	59.73	28.476	733.7
	.00097	.20	1.43(1.48)			.057	18.8
1050	.043	30.58	77.27	9.89	58.51	29.171	712.2
	.013	8.66	1.86(1.90)			.058	213.4
1100	.1143	64.39	130.26	3.00	47.54	57.76	563.3
	.0028	1.08	5.50(5.55)			.12	16.5
1200	.1763	115.34	259.48	7.93	54.83	83.91	54.21
	.0013	.93	3.59(3.81)			.17	6.77
1400	.5022	274.80	486.0	6.07	46.00	169.04	47.22
	.0059	2.80	10.7(11.0)			.34	8.18
TOTAL	.1039	56.97	112.30	100.00	46.09	34.584	48.1
	.0029	1.56	1.01(1.16)			.038	15.6

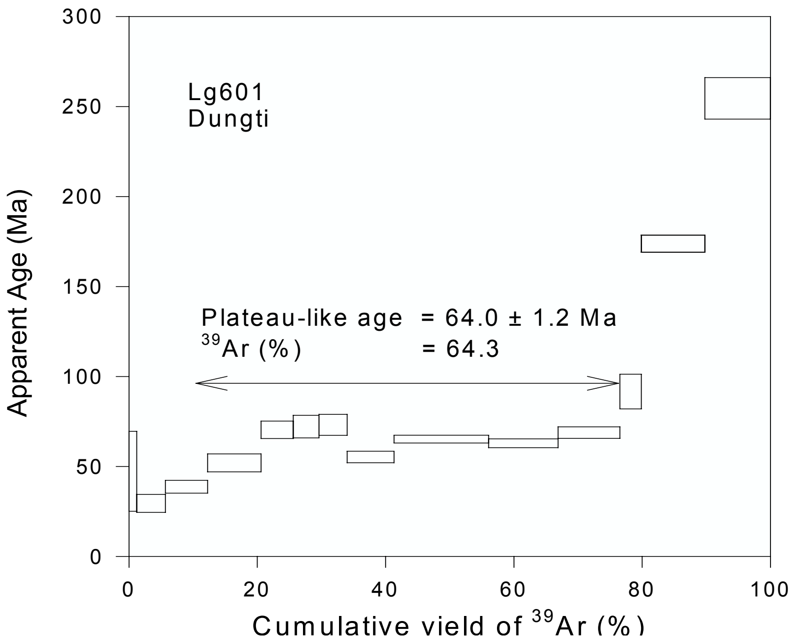

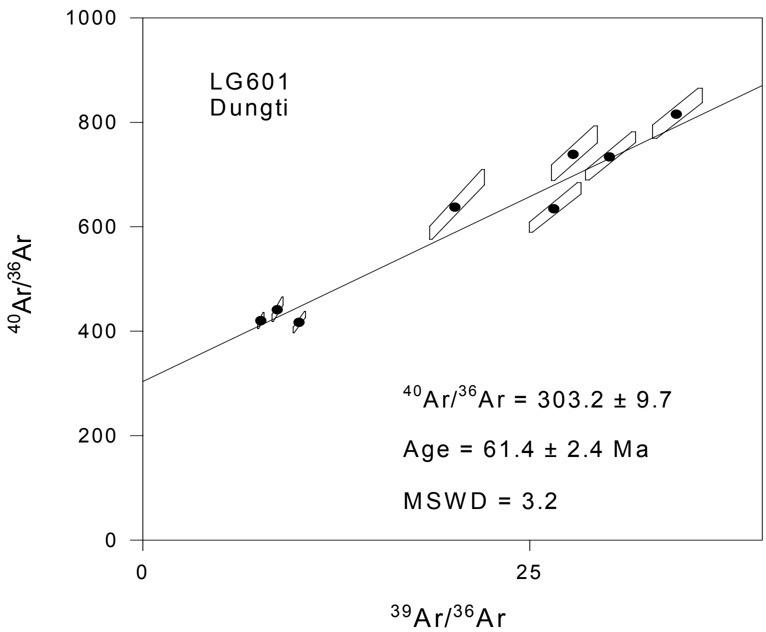

Fig. 4.21 *(Top) $^{40}Ar/^{39}Ar$ step heating results shown as apparent age spectrum for the sample LG601. The vertical side of the each box is 2σ error in apparent age without including error in J. Error in plateau-like age includes error in J.*
(Bottom) $^{40}Ar/^{36}Ar$ vs. $^{39}Ar/^{36}Ar$ correlation diagram is also shown with isochron age, $^{40}Ar/^{36}Ar$ trapped ratio and MSWD value.

Table 4.24** Argon isotopic composition and apparent ages of sample LG87 (Chushul, Khardung Volcanics) at different temperature steps. The errors in ages are without and with (bracketed) errors in **J**. The errors quoted are in 1σ. **J= .002447 ± .000013

Temp. °C	± 1σ	$^{40}Ar/^{39}Ar$ ± 1σ	Age(Ma) ± 1σ	^{39}Ar%	$^{40}Ar^{*}$%	$^{37}Ar/^{39}Ar$ ± 1σ	± 1σ
600	.09625	36.64	35.80	.49	22.36	1.802	380.62
	.00072	.24	1.28(1.29)			.019	3.66
650	.09314	37.34	42.79	1.38	26.28	1.6291	400.85
	.00040	.22	.91(.94)			.0091	2.68
700	.03929	24.69	56.80	.95	52.97	3.1107	628.29
	.00039	.16	.76(.81)			.0062	7.17
750	.03848	24.19	55.69	3.64	52.99	2.3444	628.61
	.00016	.14	.54(.62)			.0047	4.12
800	.02915	21.68	56.76	4.07	60.27	1.3788	743.84
	.00013	.13	.49(.57)			.0028	5.00
850	.02206	20.06	58.79	4.17	67.50	1.0341	909.35
	.00011	.12	.45(.54)			.0021	6.44
900	.019247	18.82	57.02	7.70	69.77	1.1790	977.55
	.000079	.11	.41(.51)			.0051	6.36
950	.011053	17.102	60.05	16.70	80.90	.5302	1547.27
	.000043	.099	.37(.48)			.0011	9.85
1000	.00996	16.327	58.12	13.55	81.98	.4061	1639.8
	.00014	.094	.39(.49)			.0074	24.1
1050	.01130	16.49	57.11	8.36	79.74	.433	1458.8
	.00017	.34	1.04(1.08)			.010	30.5
1100	.011213	16.215	56.05	9.18	79.57	.5408	1446.1
	.000054	.094	.36(.46)			.0011	10.1
1150	.010955	16.308	56.78	10.80	80.15	.49935	1488.6
	.000051	.095	.36(.46)			.00100	10.3
1200	.012813	16.385	54.75	12.52	76.89	.7964	1278.72
	.000055	.095	.36(.46)			.0016	8.48
1250	.01718	16.82	51.08	1.93	69.82	1.6396	979.0
	.00038	.12	.69(.74)			.0049	22.6
1300	.02971	18.41	42.00	2.74	52.31	2.1820	619.67
	.00025	.12	.57(.61)			.0044	6.44
1400	.01905	17.73	52.60	1.82	68.24	1.9703	930.5
	.00045	.16	.88(.92)			.0050	23.3
TOTAL	.016570	17.877	56.39	100.00	72.61	.8466	1078.91
	.000036	.043	.15(.33)			.0015	3.10

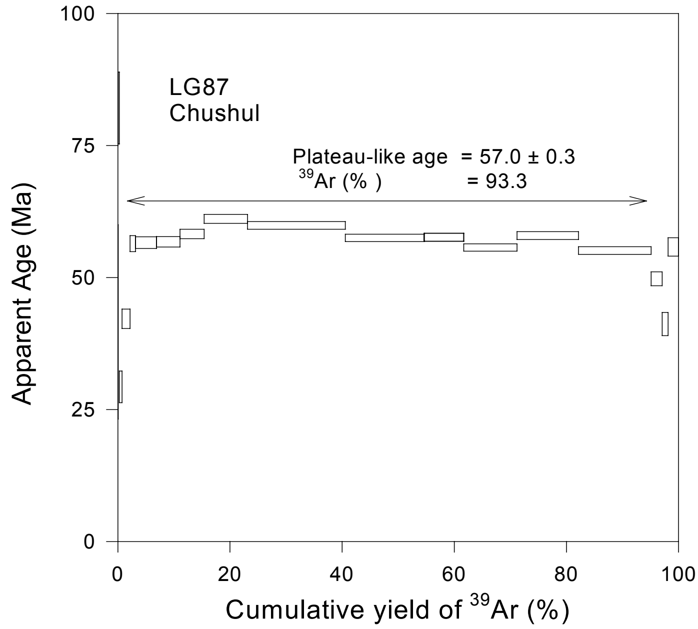

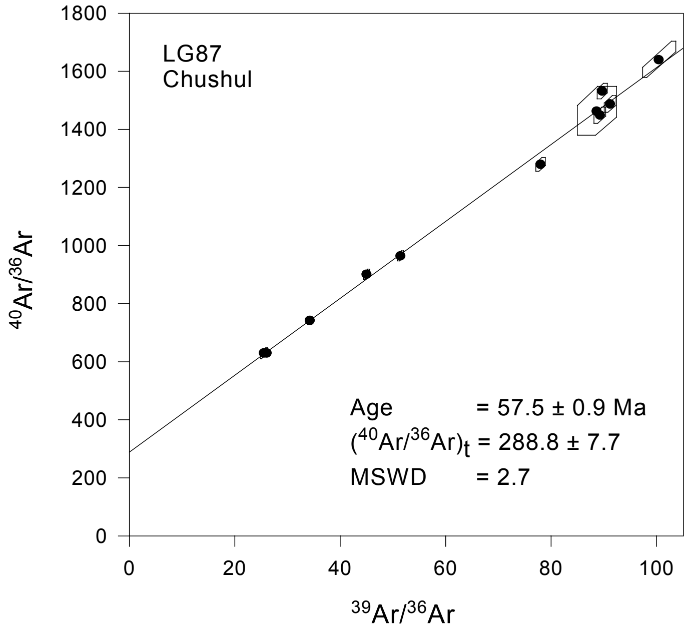

***Fig. 4.22** (Top)* *for the sample LG87. The vertical side of the each box is 2σ error in apparent age without including error in J. Error in plateau-like age includes error in J.*
(Bottom) $^{40}Ar/^{36}Ar$ vs. $^{39}Ar/^{36}Ar$ correlation diagram is also shown with isochron age, $^{40}Ar/^{36}Ar$ trapped ratio and MSWD value.

Chapter Five

Discussion

5.1 Perspective

Importance of studying the Trans Himalayan zone to understand the evolution of the spectacular mountain ranges of Himalaya and the vast Tibetan plateau has been realized ever since the early explorers dared to penetrate the Himalaya (Lydekker, 1883; Hayden, 1907; Auden, 1935; Wadia, 1937; Heim and Ganser, 1939).

Geological information gathered over the years from the different parts of the Himalaya-Tibet orogen system has helped in establishing the stratigraphical and structural relationships and developing a broad scenario of the development of the system. However, a complete understanding of the response of the continents to collision and the subsequent deformation leading to the uplift of a vast area requires not only information regarding the spatial relationships but also information on the time scales involved in the various events, as well as on the exhumation and uplift of the deep crustal rocks to a very high altitude at present. The use of radio-isotopes for obtaining the time information has vastly helped to this end. The temperature sensitive radio chronometers such as ^{40}Ar-^{39}Ar have turned out to be especially useful in this context. The key to understand the collision related process, as pointed out earlier, lies in the Trans Himalayan Zone which not only contains the suture between the two continents but also has witnessed the pre-,syn-, and post-collision magmatic and deformation activities.

The Ladakh region in India of N-W Trans-Himalaya, bounded by the Karakoram batholith in the north and the Zanskar and Tso Morari crystallines in the south has preserved almost the complete geological history from Paleozoic passive margin sediments to subduction related magmatism and post collision molasses (Fig.2.2). From south to north, Ladakh provides a complete section through shelf deposits, trench zone, fore-arc basin, calc-alkaline intrusive and back arc deposits (Virdi, 1987). In the following I discuss the results obtained (summarized in Table 5.1) from the four major units of the Ladakh, viz. Indus Suture Zone, Ladakh batholith, Shyok volcanics and Khardung volcanics of the Shyok Suture Zone in the Northern Ladakh, in the perspective of available information and unanswered problems of the Ladakh sector.

Table 5.1 *Summary of the results.*

Geological Unit	Sample and Location	Age Ma	Remark	Implication
INDUS SUTURE ZONE	LK182 Sumdo	38.3 ± 0.6	Highest temp. plateau-like	Reset or syn-collisional?
	LK176 Sumdo	46.75 ± 0.7	Mid temp. plateau	Resetting event
	LK209 Chiktan	128.2 ± 2.6	Plateau age*, Isochron and the Integrated age	Age of the formation
DRAS VOLCANICS	LG290 Dras	85.6 ± 0.6	Plateau like	Formation age
LADAKH BATHOLITH	LK198 Himia	36.04 ± 0.4	Cooling pattern	Slow exhumation
	LK198-Muscovite	29.82 ± 0.2	Plateau age*	High thermal regime
	LK24 Leh	46.25 ± 0.6	Mid temp. Plateau-like	Upper limit for the end of Subduction
	LK24-Biotite	44.63 ± 0.6	Plateau age*	High thermal regime
KARAKORAM FAULT ZONE	LK47 Murgi	13.9 ± 0.1	Plateau Age*	Age of Karakoram fault activation
SHYOK SUTURE ZONE	LG166 Hunder		Excess Argon Pattern	
	Lg197 Tegar	~ 30 Ma	Excess Argon Pattern	The maximum limit
	LG188 Tegar	Min age ~12 Ma, Max. age ~30 Ma	Cooling Pattern	Reset signatures

	LK48 Murgi	Min. age ~12 Ma, Max. age ~ 20 Ma	Cooling pattern	Reflecting a major tectonothermal event at ~20 Ma
	LK57 Panamik	Max. age ~20 Ma at intermediate Temperatures	Two cooling patterns, the higher temperatures giving very high age	Overprinting of a tectonothermal event at ~20 Ma
	LK67 Tegar	Max. age ~20 Ma at intermediate Temperatures	Two cooling patterns, the higher temperatures giving very high age	Overprinting of a tectonothermal event at ~20 Ma
	LK68 Tegar	Max. age ~30 Ma at intermediate Temperatures	Two cooling patterns, the higher temperatures giving very high age	Overprinting of a tectonothermal event at ~20 Ma
	LK70 Tirit	Max. age ~35 Ma at intermediate Temperatures	Two cooling patterns, the higher temperatures giving very high age	Overprinting of a tectonothermal event at ~20 Ma
KHARDUNG VOLCANICS	LK86 Tirit	Max. age ~60 Ma at intermediate steps.	Two cooling patterns	Overprinting of a tectonothermal event at ~ 60 Ma.
	LK88 Khardung	52.4 ± 0.4	Plateau age*	Age of the volcanism

	LK90 Khardung	56.4 ± 0.4	Plateau age*	Age of the volcanism
	LG87 Chushul	57.0 ± 0.3	Plateau age*	Age of the volcanism
	Dungti	64.0 ±1.2	Plateau age*	Age of the volcanism

- *Trapped $^{40}Ar/^{36}Ar$ ratio for the Plateau age is atmospheric within error.
- The MMHb-1 of 520.4 ± 1.7 Ma standard used for all the samples.
- The errors quoted are 2σ.

5.2 Indus Suture Zone

Indus Suture, with its characteristic ophiolitic mélanges marks the line of closure of the Tethys ocean. The deep sea Tethys sediments are grouped into the Lamayaru complex while the fore-arc sediments are grouped into Nindam formation (Sinha and Upadhyay, 1993). The well-preserved sections of continental passive margin sediments are exposed in the Spiti and Zanskar sections. The back arc sediments are found along the northern margin of Ladakh batholith.

5.2.1. The Ophiolitic mélange of Indus Suture Zone

The southern margin of the Ladakh batholith is separated from the Tethyan sequences by Indus Suture characterized by the ophiolitic mélange. Discontinuous ophiolitic mélanges can be traced throughout Ladakh from west to east. The Zildat mélange is believed to be the eastern continuation of western Shergol ophiolite and is overlain by Nidar ophiolites. It is exposed mainly in the Sumdo Nala (Fig.2.4). This ophiolitic mélange is characterized by pillow lavas, basalts, peridotites, serpentinites associated with chert and exotic limestone blocks. I have analyzed two samples (LK176 and LK182) from the Sumdo Nala section of this ophiolitic mélange and pillow lava (LK209) of the western Shergol ophiolitic mélange from Chiktan village (Fig.2.3), which lies between Bodhkharbu and Shergol.

Ophiolite obduction onto the continents has been a major phenomenon associated with a collisional orogeny. They mark the plate boundaries along which the collision of two continents takes place. The knowledge of the age of the obduction is very crucial to understand whether ophilolite emplacement marks the initiation of the collision (syn-collision) or it precedes the colloision. However the timing of obduction remains a matter of debate in the Ladakh -Zanskar region. Colchen et al. (1986) and Reuber (1986), suggested it to be of post-early Eocene age coinciding with the collision, while Searle (1986, 1988) and Searle et al. (1997) advocated it to be of Late Cretaceous i.e. Pre-collision age. This ambiguity results from the fact that the obduction timing is mainly deduced from the reconstructed stratigraphic sequences.

The effect of the ongoing collision on the trapped ophiolite with respect to their radioactive clocks has not yet been explored. Absolute dating of the rocks from the ophiolitic mélange in principle should give the age of the formation of the ocean floor. The variable absolute ages from the ophiolites have been interpreted to be showing the variable environments of formation, eventhough the consequent geochemical signatures have not been unambiguous (Thakur and Bhatt 1983). Alternatively, their variable absolute ages could be because of variable degree of resetting due to the collision-related deformation. I propose here that most of the ophiolites get reset during the continent-continent collision. This is reflected by the results of the two samples of the presumably upper parts of the ophiolite suite of Ladakh. While the basalts from Sumdo Nala of the Eastern Ladakh yielded complex age spectra, sample LK182 gave a cooling pattern with the maximum age of ~ 38 Ma (Fig. 4.2) and the sample LK 176 yielded a plateau at intermediate temperature steps giving an age of ~ 46 Ma (Fig.4.3). These samples, from the ophiolitic mélange of the Indus Suture, are reset by post-collision tectono-thermal activity. To retrieve the thermal history experienced by these two samples, their age spectra are modeled using the Multi Diffusion Domain model (Lovera et al. 1989).

5.2.2. Modeling the whole rock age spectra for basalts

Ar-Ar age spectrum obtained in a laboratory step heating experiment essentially follows the same laws of volume diffusion for the loss of Argon by which it has been retained during the cooling of the rock in nature. In principle, an age spectrum can be translated into the cooling history experienced by the sample. Lovera et al. (1989) proposed a method of retrieving this cooling history from the K-feldspars that have discrete non-interacting multi-diffusion domains (MDD). The MDD model proposed for the K-feldspar *can be extended for the whole rock if the different mineral phases are considered as different non-interacting diffusion domains*. These domains corresponding to different minerals in a whole rock sample will have different activation energies, however, Lovera et al. (1993) showed that the calculation of cooling histories is not very sensitive to the choice of single or multiple activation energy models. This model has not been used so far to derive the cooling histories from the whole rock samples. One of the reasons may be that many rocks may contain mineral phases which breakdown during the vacuum heating in the laboratory. For example biotite has been demonstrated to break down during the laboratory experiment (Harrison et al., 1985; Lo Ching-Hua et al., 2000). Therefore, I applied this MDD approach on the basalt samples and not to the granodiorite and granite samples of Ladakh batholith, which may have a significant amount of biotite. I used the FORTRAN programs given by Lovera (http://oro.ess.ucla.edu/argonlab/programs.html) to calculate the diffusion parameters and cooling history of these samples, with necessary modification.

The monotonic cooling model has been used to generate the age spectra for the two basalt samples, which exhibited cooling patterns. For the sample LK182 the model calculated age spectrum exactly matches with the experimentally derived age spectrum. The diffusion parameters and other model parameters used to calculate this age spectrum are given in the table 5.2.

Table 5.2. *Parameters used to model the cooling history of the two basalt samples*

Sample	Domain #	Volume fraction	Domain Size
LK182[a]	1	0.05908	0.00131
	2	0.15615	0.00170
	3	0.26910	0.00456
	4	0.16335	0.00578
	5	0.10135	0.01182
	6	0.13093	00.06231
	7	0.11352	0.20015
	8	0.00652	1.000
LK176[b]	1	0.08492	0.13277
	2	0.72296	0.32086
	3	0.19212	1.0000

a. activation energy E = 65.3 kcal/mol and $\log(D_0/r_0^2)$ =11.82 s^{-1} used to calculate the cooling histories for the sample LK182.
b. activation energy E = 28.3 kcal/mol and $\log(D_0/r_0^2)$ = 1.95 s^{-1} used to calculate the cooling histories for the sample LK176.

The activation energy and $\log(D_o/r_o^2)$ are calculated using the laboratory obtained data and correspond to the linear portion of the Arrhenius curve at initial low temperatures. Number of domains and their corresponding domain sizes and volumes are estimated using the $\log(r/r_o)$ plot as discussed in chapter 3 (Section 3.3). The various cooling histories corresponding to the age spectra are given in the figs.5.1 & 5.2 Sample LK176 has low ages at higher temperatures after yielding a plateau for the four middle temperature steps. This disturbed pattern at higher temperatures is not reflected in the model generated age spectrum. However, the experimentally obtained age spectrum matches with the model generated age spectrum for about the 80 % of total gas released. Hence the model gives a fairly good estimate of the cooling histories of these samples. Both the samples show a rapid cooling initially and slower subsequent cooling. A plausible interpretation for this kind of cooling history could be that both the samples have experienced a large tectonic event, with an associated temperature increase sufficient to reset the argon clock for these older suture ophiolitic basalts. The initial rapid cooling indicates a quick termination of that event. The subsequent slow cooling could be due to their exhumation by erosion if these samples were subjected to burial by that event. Such an event is most likely a large scale thrusting induced by the ongoing collision. The ages for this event registered by these two samples are ~38 Ma and ~46 Ma respectively, indicate that by that time they cooled sufficiently below the closure temperatures of their most retentive phase. This difference in age (~ 8 Ma) for this event probably reflects it's protracted nature, not unexpected for large-scale thrusts.

Another sample, LK 209 from western part of the Indus Suture ophiolite, however doesn't appear to have been affected by the post collision tectonothermal activity. The sample LK 209, Chiktan pillow lava is exposed north of the main Shergol ophiolitc mélange exposure. The plateau age of ~128 Ma yielded by this sample is indistinguishable from its integrated Ar-Ar age, indicating no post crystallization effects (Fig.4.1). The 128 Ma age of this pillow basalt therefore, provides an estimate of the time of formation of the part of the ocean which was subsequently trapped between the continents as ophiolites; however, the tectonic setting of formation of this ocean floor remains to be ascertained. This is the only age so far obtained from the ophiolites of Indus Suture which provides the timing of formation of the ocean floor.

5.3 The Ladakh batholith

The Ladakh batholith is generally calc-alkaline in nature ranging from gabbro to granodiorite to tonalite-granite, with granodiorite being the major constituent of the Trans-Himalayan batholith (Honegger et al., 1982; Sharma and Choubey, 1983).

Geochronological data from Ladakh batholith are rather scarce. Honegger et al. (1982) had given some Rb/Sr and U-Pb ages from western Ladakh, concluding that the main plutonic batholith intruded from ~ 100 Ma to 60 Ma though some much younger cooling ages were also obtained. The other geochronological studies from this area (Petterson and Windley, 1985; Weinberg and Dunlap, 2000) essentially give the pre-, to syn-collision crystallization ages related to the subduction along an Andean type margin. From Kohistan batholith of Pakistan, the western continuation of the Ladakh batholith, younger crystallization ages, as young as 29-25 Ma have been reported. (Treloar et al., 1989; George et al., 1993). The interrelationship of different magmatic units of this batholith is complex (Ahmad et al., 1998). A muscovite bearing leucogranite phase has been identified during the field work to be intruding into the main body of batholith at some places particularly in the Eastern Ladakh. This leucogranite phase may be similar to the Pari and Jagot granites of the Kohistan batholith. The best exposure of this leucogranites is found near the village Himia east of Leh (Figs.2.2 & 2.5). This Himia leucogranite and a biotite-granodiorite (LK24) from the base of *Shanti-stupa* near Leh have been analyzed for the present study.

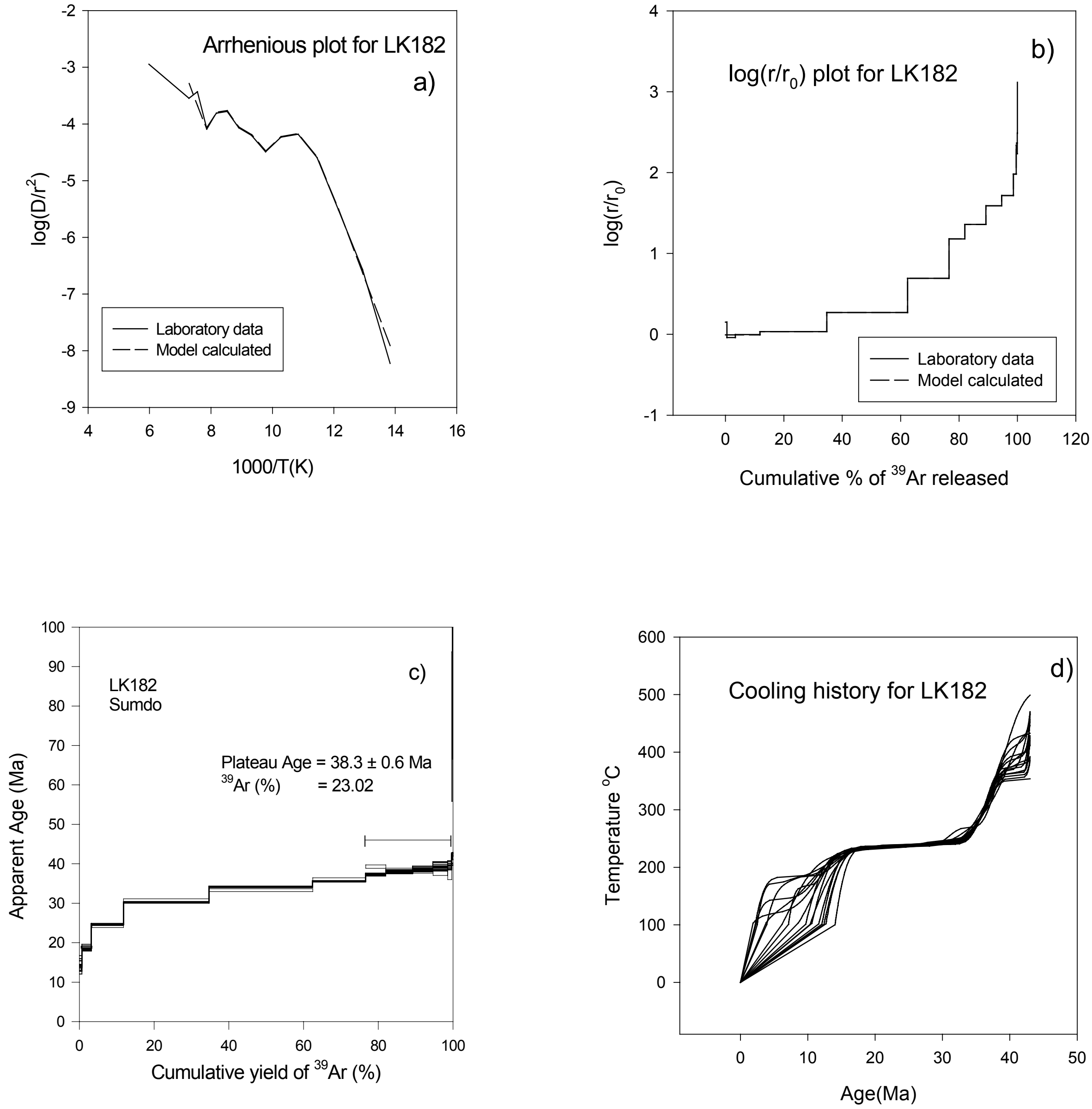

Fig.5.1 *(a) Arrhenius plot; linear portion at initial low temperatures corresponds to the activation energy and log (D_o/r_o^2) values used in the model (b) log(r/r_0) plot to estimate the diffusion parameters e.g. number of domains, volumes and sizes. (c) Laboratory obtained and modeled spectra corresponding to different cooling histories. (d) Cooling histories obtained by iteratively varying the initially assumed cooling history. The family of curves represents the total number of possible cooling paths to reproduce the laboratory obtained age spectrum.*

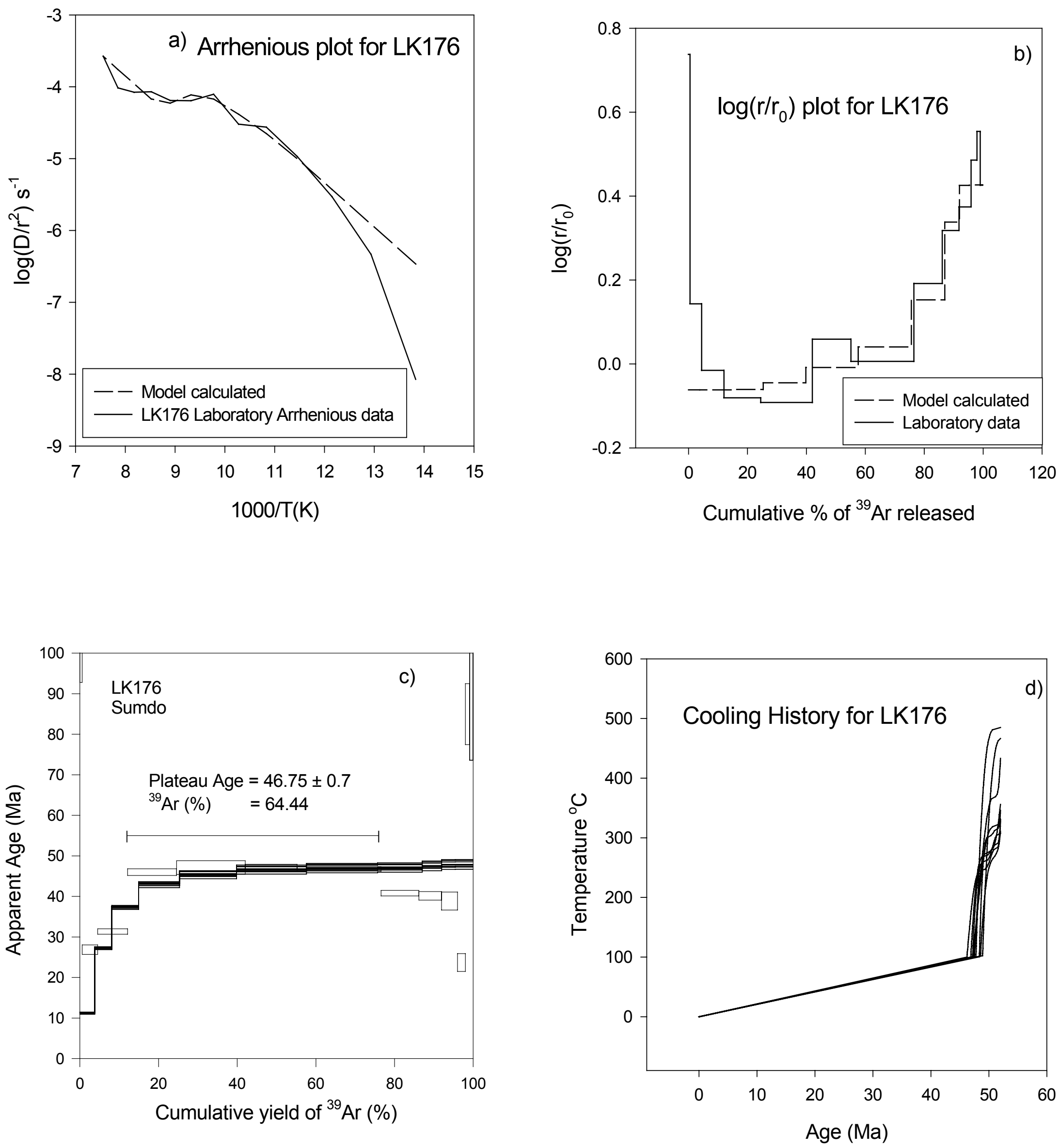

Fig.5.2 *(a) Arrhenius plot; linear portion at initial low temperatures corresponds to the activation energy and log (D_o/r_o^2) values used in the model (b) log(r/r_0) plot t_o estimate the diffusion parameters e.g. number of domains, volumes and sizes. (c) Laboratory obtained and modeled spectra corresponding to different cooling histories. (d) Cooling histories obtained by iteratively varying the initially assumed cooling history. The family of curves represents the total number of possible cooling paths to reproduce the laboratory obtained age spectrum.*

The results from these samples of the Ladakh batholith are discussed in the light of the results from Indus Suture Zone, already discussed in the previous section and the existing literature from different geographical locations. Leh granodiorite gives plateau-like age of ~ 46 Ma (Fig. 4.5) and Himia leucogranite gives a maximum plateau-like age of 36Ma (Fig. 4.7). These samples exhibit syn-, to post-collision tectonothermal effects. The muscovite from the Himia leucogranite yielded a plateau age of ~29 Ma (Fig.4.8). The whole rock and muscovite ages for the Himia leucogranite indicate that these samples have certainly experienced temperatures, higher than ~ 350^{o}C (closure temperature for muscovite), and probably represent the cooling after the post-collision crystallization. Such young post-collision cooling and crystallization ages are reported from the Kohistan batholith leucogranites. Searle et al. (1999) demonstrated that the leucogranites from the Kohistan batholith of Pakistan are similar to High Himalaya leucogranites.. These leucogranites are muscovite-garnet- tourmaline granite, which are clearly anatectic in origin. Most recent U-Pb ages obtained from these granites give crystallization time as 30.2 ± 0.3 Ma (Krol et al., 1996). Pari apatite and Jagot granites are reported to be 29 to 24 Ma (Treloar et al., 1989; George et al., 1993.) The present result from Himia granite from Ladakh batholith, shows that the post -collision magmatism was not only restricted to Kohistan but was widespread through out the Trans Himalayan batholith, as Gangdese batholith also contains such rocks. The N-Himalayan leucogranites, which cover an area of 4000 km^2, in the Eastern Himalayas also may be related to the crustal thickening induced melting caused by the post collision compressive tectonics as discussed by Le Fort (1986).

5.3.1. Post-collision magma generation: partial re-melting of batholith granitoids ?

The post- collision history of plate margins is dominated by the compressive tectonics, which leads to the crustal thickening. Dewey and Burk (1973), suggested that thickening of the crust can induce melting. Wyllie (1984) has demonstrated that a thickening of the crust at the active continental margin up to 50km will have 750^{o}C geotherm at its base. At that depth crustal melting can take place in the presence of fluids. The crustal thickening coupled with the large scale thrusting produces heat and causes the hydrous minerals to breakdown. The granitoids of Trans-Himalaya batholith have amphibole as a common phase. This amphibole can produce sufficient fluid to lower the solidus and generate the partial melt at the base of thickened crust. These partial melts then slowly intrude the earlier granitoids and cool slowly by conduction. This is reflected well in the whole rock age spectrum of anatectic Himia granite, which gives a slow cooling pattern from ~ 38 Ma to 18 Ma. The maximum age provides the lower bound on the crystallization time and indicates that it cooled through ~500^{o}C (closure temperature for hornblende) at ~38 Ma. The muscovite of the same rock yields a good plateau age as 29 Ma indicating that it was at least at 350^{o}C at that time. However, the amphibole granodiorites may need temperatures as high as 850^{o}C to 900^{o}C, to remelt. Hence, the exact heat source and mechanism for the post- collision magma generation remains to be established. For the generation of Higher Himalaya leucogranites- the thrusting along the MCT is supposed to cause sufficient heat from friction and burial for partial re-melting and emplacement of leucogranites in the Higher-Himalaya (Le Fort, 1986). The resetting signatures obtained from the ophiolites further indicate the wide spread post-collision thermal regime. De Sigoyer et al. (2000) record a strong heating of Tso Morari crystallines and attributed it to the crustal thickening. I propose that the tectonically induced heating soon after the collision at ~ 50 Ma slowly propagated away from the plate suture with deformation getting diffused into both the continental plates. The ages obtained from the two samples of basalts from the suture zone ophiolites indicate the protracted duration of the thermal event, which is also recorded by the Himia granite. There are evidences of deformation related strong heating and magma generation similar to the higher Himalayan leucogranites in the north of the suture zone too. In the north the U-Pb crystallization ages from Baltoro granites from Karakoram batholith are 21 ± 0.5 Ma (Parrish and Tirrul, 1989) and 25 .5 ± 0.8 Ma (Scharer et al., 1990). These granites are to the north of the Indus Suture, their anatectic origin and post-collision ages suggest that they might also have resulted from melting induced by crustal thickening. It therefore appears that the post-collision compressive tectonics have affected the pre existing rocks on both of the sides of the Suture.

5.4 Northern Ladakh (North of the Ladakh batholith)

North of the Ladakh batholith is characterized by the linear volcanic belts, and ophiolitic mélange, which separate it from the Karakoram batholith in the north (Figs. 2.2 & 2.5). The ophiolitic mélange of Nubra-Shyok valley and associated flyschoidal and Molassic sediments are believed to be representing the line of a subduction named as the Shyok Suture. This is the eastern extension of the Kohistan sector of Pakistan. Unlike the main suture between Indian and Asian plates, viz., the Indus Suture, the Shyok suture could not be traced all along the northern margin of the Trans Himalayan batholith. The Shyok suture ends in the Nubra-Shyok valley in the northern Ladakh.

Since the first reporting of the Shyok suture (Frank et al., 1977), several models have been proposed to explain the evolution of the island-arc terrain and its suturing with the Indian and Asian plates (Brookfield and Reynolds, 1981; Rai, 1983; Reynolds et al., 1983; Coward & Butler, 1985; Petterson & Windley, 1985; Sharma, 1987; Treloar et al., 1989; Searle et al., 1997). These models have usually been assumed to be valid for the whole Himalayan-Tibetan arc even though the Shyok suture could not be extended to east of the Ladakh sector. Shyok suture in Pakistan has been studied rather in detail with only a few studies carried out in the Ladakh sector of India. However, the debate on the age of the suture and whether it is older or younger than the Indus suture, as well as the mode of subduction/suturing has not yet been settled. Brookfield and Reynolds (1981), & Reynolds et al. (1983) suggested that the Shyok suture didn’t close until Miocene and the Indus suture closed earlier in the Late Cretaceous. Coward & Butler (1985), Petterson & Windley (1985), Treloar et al. (1989), and Searle et al. (1997) favored an early closure of the Shyok suture in Cretaceous. The mode of the subduction and closure also remained a matter of debate. Rai (1982) argued against any subduction along the Shyok suture. Rai (1983) reported upper Cretaceous to Eocene marine fossils from the flysch of the Shyok suture zone. This makes it almost synchronous with the Indus suture zone flysch.

Furthermore, the significance of the pyroclastic acidic Khardung volcanics of the northern Ladakh (Figs. 2.2 & 2.5) could not be realized fully as its age remains controversial. While it appears to be overlain by the Eocene Shyok Molasse (Rai, 1983) on the basis of K-Ar ages (Sharma & Gupta, 1978) they have been assigned to Oligocene (Thakur and Mishra, 1984). Raz and Honegger (1989) described these pyroclastic volcanics from near the Teah village north of Khalsi, which are exposed in a 16 km^2 area and form 500m thick dome. These rhyolites and rhyodacites follow the trachybasalts and trachyandesites interbedded with the basalt-andesitic flows.

5.4.1. The Shyok Suture Zone

Apart from the sporadic occurrences of the ophiolitic mélanges of serpentinites and ultra basics, intercalated with flysch, molasse and volcano-sedimentary sequences, a variety of volcanic rocks ranging from basalts to basaltic andesites to andesites are reported from the Nubra-Shyok valley and are grouped into the Shyok volcanics. Shyok volcanics are a very heterogeneous sequence comprising of basalts to andesites. The heterogeneity is maximum near the village Murgi, where an isolated outcrop of serpentinites of the Shyok ophiolite is present in the Shyok volcanics. The Shyok volcanics are in contact with flysch, metasediments and molasses at different places. At most of the places the volcanics are greenish gray, fine grained and massive in nature. The andesites are widely distributed and look tectonically transposed at many places.

A total of the 14 whole rock samples from northern Ladakh (Figs. 2.2 & 2.5) were analyzed by the step heating experiment. Four of these samples are of the Khardung volcanics, two from the type locality near the Khardung village and the two from its eastern most extension, near the Chushul and Dungti areas. The samples of the Shyok volcanics are collected mainly along the Nubra River, comprising the major geochemical varieties of this suit, including the mélange unit of Murgi.

The age spectra are disturbed, but show a consistent pattern. Two samples LG166 (Fig. 4.16) and LG 197(Fig. 4.15) from Hunder and near Tegar villages respectively yielded saddle-shaped age spectra characteristic of the excess argon. The minimum ages of ~50 Ma and 30 Ma could be the upper bound on the formation of these samples. Two samples LG 188 & LK48 from near Tegar & Murgi villages respectively yielded similar pattern of continuously rising ages, starting from ~13 Ma and going as high as ~ 20 to 30 Ma (Figs. 4.16 & 4.9).

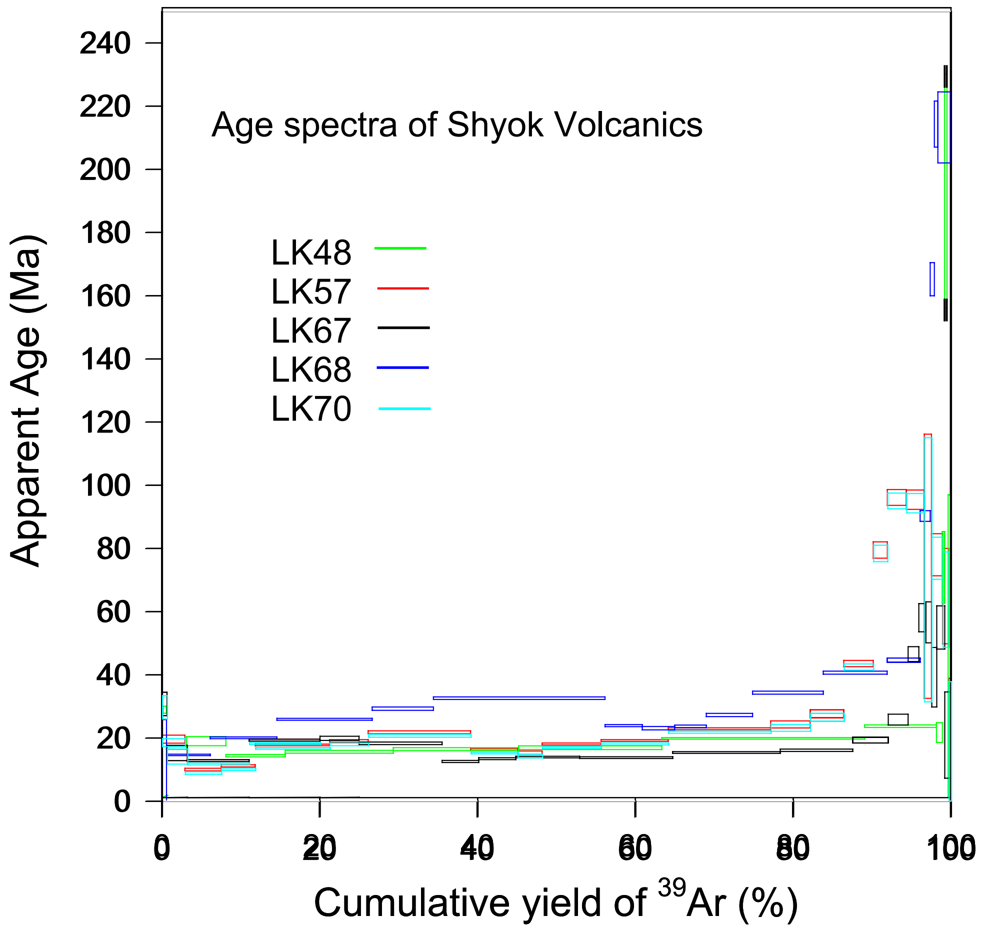

Fig.5.3 *Age spectra of Shyok Volcanics plotted together to show the consistency in their pattern*

Four samples LK57 from Panamik, LK67 and LK68 near Tegar and LK70 from near Tirit village's yield similar age spectra Figs. (4.10 to 12), which are characterized by the two distinct increasing-age patterns. The age spectra of these samples, when plotted together overlap and show two distinct patterns (Fig. 5.3) The first rising-age pattern from ~ 10 ma to 12 Ma, and going up to ~ 20 to 30 Ma for the first 40 to 50 % of the ^{39}Ar released. The second pattern also starts from the low age ~ 14 Ma and goes very high (> 70Ma)at the highest temperature..

The samples also show a systematic change with location: as the distance from the Khardung volcanics decreases (Fig.2.2), the ages in the first pattern become higher. The sample near Tirit, which is the nearest to Khardung volcanics of all the samples analyzed, yields as a high an age as ~40 Ma for the first 50% of the gas released.

The age spectra show the multi-tectonothermal events experienced by these samples**.** The high ages obtained for the higher temperature steps for the Shyok volcanics suggest that these may be pre-existing rocks. Rolland et al. (2000), suggest the age of the base of the Nubra-Shyok volcanics unit to be Middle Cretaceous ~108 to 92 Ma, on the basis of forminifera *Orbitolina* bearing limestone interbedded with the Shyok basalts and andesites of the Shyok volcanics. Rai (1983) also suggested that the Shyok volcanics are older than the overlying Saltoro flysch, which yielded upper Cretaceous to Eocene fossils such as *Cyclammina* sp. of upper Cretaceous & *Numulites* sp. of Eocene. These evidences indicate that the older Shyok volcanics are affected by the later tectono-thermal events. The remarkable consistency of their age spectra (Fig. 5.3) suggests that they reflect a large-scale tectonothermal event which had effects on a regional scale.

5.4.2. Khardung Volcanics

These basic Shyok volcanics are in contrast with the acidic & rhyolitic Khardung volcanics of the Nubra-Shyok. Khardung volcanics are pyroclastic in nature. They form a linear and irregular belt along the northern margin of the Ladakh batholith and appear to be directly overlying the batholith. These volcanics consist of rhyolite, rhyodacite, dacite, tuffs, ignimbrites and volcano-sedimentary sequences. Spheroidal to ovoidal lapilli are reported from the topmost tuffaceous bed of these rocks. These tuffaceous rocks are conformably overlain by the thick lahar unit consisting of unsorted boulders and pebbles derived from the acidic volcanics. The acidic volcanism is supposed to be continuous further east up to Chushul in eastern Ladakh. The presence of lapilli, tuffs and lahar indicate the near-surface explosive eruption of these rocks.

The signatures of the younger tectonothermal event reflected in the Shyok volcanics age-spectra is absent in the Khardung volcanics. Rhyolite samples LK 88 and LK90 from the vicinity of the village Khardung (Figs. 2.2 & 2.5) yielded good plateau ages of 52 .0 ± 0.4 and 56.4 ± 0.4 Ma respectively for more than 80 % of ^{39}Ar released and with atmospheric trapped ratios (Figs. 4.19 & 4.20). Sample LG 87 from the eastern extension of the Khardung volcanics near Chushul (Fig. 2.2) also yielded a plateau age of 57.0 ± 0.3 Ma more than 90% of ^{39}Ar released and with atmospheric ratio (Fig 4.22). Sample LG601, from the further east, near Dungti (Fig.2.2) didn't yield any plateau age, however a plateau-like age of 64.0 ± 1.2 Ma was obtained from the middle temperature steps (Fig. 4.21). All the four age spectra of the Khardung volcanics show higher apparent ages at higher temperature steps. These results indicate that explosive acidic volcanism continued at the southern margin of Asian plate at least between 64 to 52 Ma. This is consistent with the observation that these are overlain by the Eocene Shyok molasse (Rai 1983). These volcanics are not affected by the younger tectonothermal events which affected Shyok volcanics. The strikingly different results from the two adjacent volcanic belts indicate that these two belts formed in two different tectonics settings and evolved independently and were later juxtaposed by some large scale tectonic event, probably the activation of the Karakoram fault.

5.4.3. Simultaneous and independent evolution of the island and continental arc along the southern margin of the Asian plate

Recently Rolland et al. (2000), showed that the back-arc like geochemical signatures of the northern suture of Kohistan sector are not present in the Shyok Suture zone of the Ladakh sector. They further noted that the acidic volcanism of Khardung represents an Andean type margin like Tibet, while the Kohistan sector's northern suture represents the suturing of an island arc with the continent. Raz and Honegger (1989) provided field evidences for the presence of continental crust before the calc-alkaline magma intrusion in the northern Ladakh. They reported meta-sediments, shales, sandstones, quartzites, and marbles indicating of the continental crust. A 50 m thick layer of calc-silicates yielded *Megalodan* & *Lithiotis,* the characteristic fossils of Late Triassic to Early Jurassic, which are also reported from Kashmir (Fuchs 1982) and Karakoram (Gregan and Pant, 1983). Based on these observations it appears that the island arc setting of Kohistan sector and the northern suture doesn't extend to the east of Nubra-Shyok valley. This means that pre-collision geometry of the south Eurasian margin was such that only western side of it had small oceanic plate/crust, which facilitated the intra-oceanic subduction of the Tethys in the western side around ~ 85 Ma ago as revealed by Dras island arc sample LK290. Jurassic fossils and older ages of Khardung volcanics indicate Andean type subduction for most of the plate in the east at the same time (Fig. 5.4). In this scenario the Island arc and continental arc evolved simultaneously but in different tectonic settings. The present day Shyok Suture Zone and Kohistan- type island arc sector represent the small portion of oceanic plate at the western part of the southern margin of the Asian plate. The flyschoids and ophiolitic mélange of the Shyok Suture formed after the Indus Suture closed along the continental part of the Asian plate. Though, according to this model, the suturing along Shyok is younger than the Indus Suture, the time difference doesn't seem to be significant, given the very small volume of the oceanic part of the Asian plate.

Sample LK 47, taken from a sheared zone along the Karakoram Batholith, in tectonic contact with the Shyok ophiolitic mélange near village Murgi (Figs. 2.2 & 2.5), yielded a very good plateau age of 13.9 ± 0.1 Ma with atmospheric trapped ratio (Fig 4.18). I have interpreted this age to be the activation age of Karakoram Fault. This is supported by Searle et al. (1998) who suggested that the activation of the Karakoram fault is post-leucogranite generation in the Karakoram batholith, i.e. younger than 18-15 Ma.
This further substantiates the model proposed here for the evolution of the northern Ladakh as Karakoram fault activation appears to be responsible to bring the Shyok volcanics in juxtaposition with the Khardung volcanics. The age spectra of Shyok volcanics also indicate an event at 12-14 Ma. Furthermore the proposed model also explains the positioning of the Karakoram fault (Fig. 5.4), which appears to have been facilitated by the weak zone between the continent-oceanic transition at the southern margin of the Asian plate.

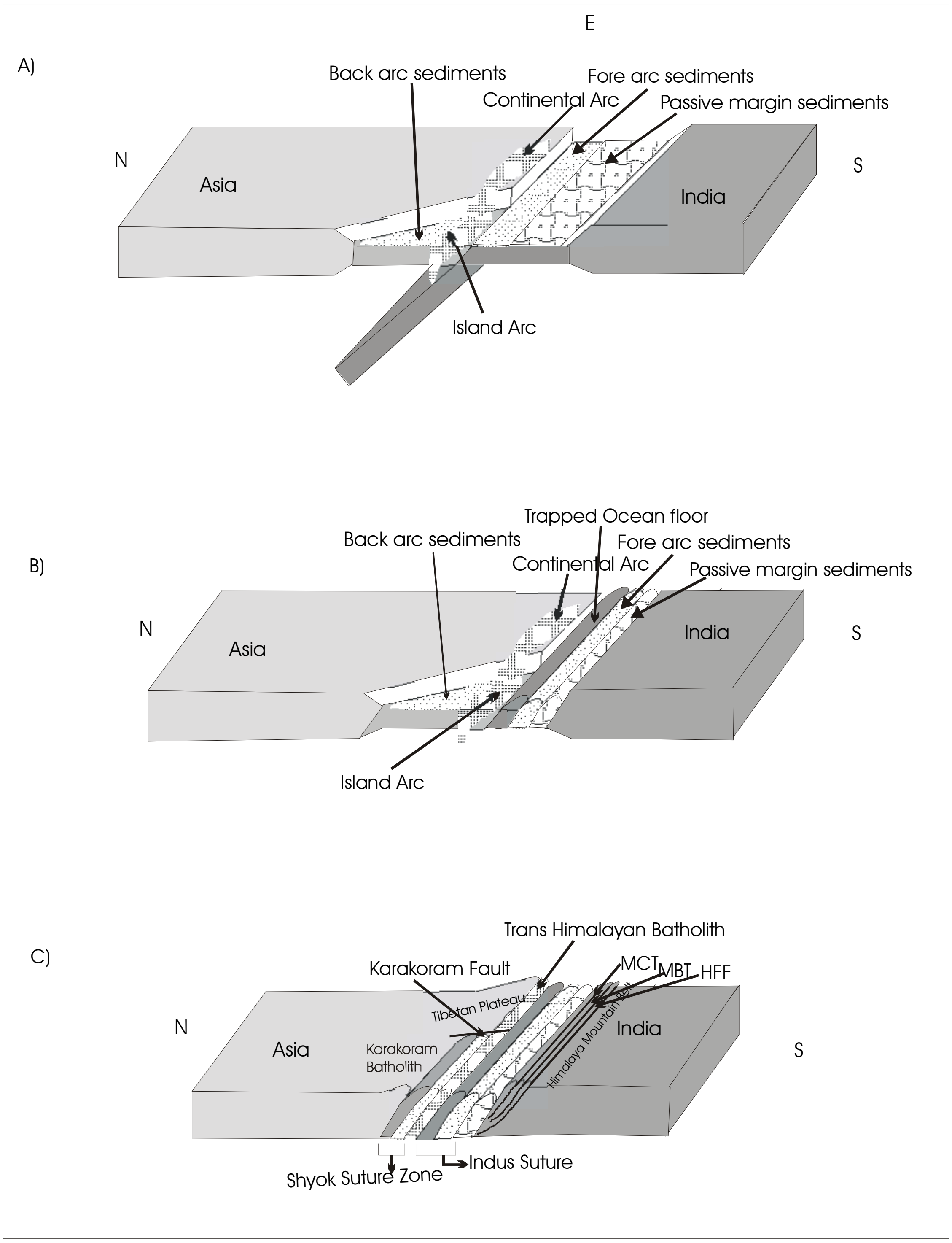

Fig. 5.4 *Cartoon diagram showing the evolution of the southern margin of the Asian plate. (A) Pre-collision boundary of the southern margin of Asian plate was partly oceanic at western end which subsequently gave rise to island arc magmatism and the back arc sedimentation while at the same time the continental margin of the plate was having the continental arc magmatism. (B). The Indus Suture closed as the Tethys ocean completely subducted , it compressed the small part of the*

oceanic crust along the Asian margin and caused the breakage along the continent-oceanic boundary. (C). The small part of the oceanic plate along the Asian continental plate formed the Shyok Suture Zone with the characteristic ophiolites and flyschoids. The boundary between the continent and ocean later acted as plane of weakness to facilitate the formation of Karakoram Fault.

For the most part the Trans Himalaya evolved in an Andean type setting, except for the small portion of intra-oceanic crust in the western side, giving rise to the Kohistan island arc.

5.5 Conclusion

The Ar-Ar data from the three main tectonomorphic subdivisions of the Trans-Himalaya in Ladakh region, viz., Ladakh batholith, the Indus suture zone ophiolites and the Shyok Suture Zone volcanics provide a thermochronological sequence for the evolution of the India-Asia collision zone. The age of the collision and tectonization along the northern and southern margins of Ladakh batholith is not significantly different. The end of the subduction-related magmatic activity is represented by the highly differentiated and explosive Khardung volcanics of northern Ladakh, is dated between ~52 to 64 Ma. Consequent to the India-Asia collision at ~52 Ma, deformation started at the plate boundaries producing sufficient crustal thickness for remelting of the Ladakh batholith in the presence of fluids at ~46 Ma. The high thermal regime at the suture lasted at least till ~35 Ma ago, as registered by the basalts of Indus suture ophiolites in Sumdo. The trapped ophiolites of suture are clearly affected by the post-collision tectono-thermal activity though its intensity and extent varied between different units of the ophiolite as well as different geographical locations. Basalts from the Sumdo indicate a minimum of ~17 Ma duration of the high thermal regime since the collision, while the ~128 Ma old pillow basalt from Chiktan, from the western part of the Indus Suture, remained unaffected by post-collision thermal events. The ages obtained from the Ladakh batholith and particularly that from the Himia leucogranite suggest that the relationship of this with the coeval leucogranites of Higher Himalaya and Karakoram, which are to the south and north of it, needs to be explored. I propose that the continuously propagating deformation into the continental plates away from the suture has emplaced the 25-20 Ma granites of Karakoram batholith in the north and ~20 Ma granites of Higher Himalaya along MCT south of the suture. This tectonothermal activity along the MCT in the

Higher Himalaya, south of the suture, and in the Karakoram batholith, north of the suture, is therefore the large-scale manifestation of the process, which started with collision at the plate boundaries in Trans-Himalaya. Such a scenario obviates the necessity of separate mechanisms to explain the formation of Trans-Himalaya, Higher Himalaya, and Karakoram leucogranites. The deformational style dominated by the N-S compression was later replaced by the eastward extrusion of the Tibetan plateau along the large-scale strike slip faults. The Karakoram fault is believed to mark the western boundary of the extruding Tibetan block. The ~ 14 Ma age obtained from the micaceous segregation from the Karakoram batholith along the right bank of the Nubra river in the northern Ladakh, is interpreted to be the age of the Karakoram fault activation. This younger large-scale event has disturbed and reheated the volcanics of the Shyok suture zone but the eastern continental arc remained unaffected indicating the separate and independent history and evolution of the two regions. The Karakoram strike slip fault could have juxtaposed these in the present position.

Chapter Six

Evolution of the India-Asia collision zone in space and time: a synthesis of thermochronological data

6.1 Introduction

India-Asia collision has resulted in contrasting styles of deformation in the two continents involved, as manifested by the Himalayan mountain chain on the Indian continent and the Tibetan plateau on the Asian continent. These spectacular results of the ongoing collision between the two continental plates have attracted the attention of many earth scientists and wealth of information has been generated over the years (Allegre et al, 1984; Yin and Harrison, 2000). Several review papers have attempted to synthesize the available information to build a general understanding of the evolution of the India Asia collision zone (Harrison et al, 1992; Le Fort, 1996; Searle, 1996; Hodges, 1999; Pande, 1999; Yin & Harrison; 2000). However, these reviews have been founded on the studies conducted in the Tibetan plateau (north of the Trans Himalaya) and that of Himalayan mountain chain (south of the Trans Himalaya). Little emphasis has been given to the Trans Himalayan Tethys zone which consists of the suture and the pre-, syn- and post-collision magmatic rocks, mainly due to absence of information about this zone except from a couple of isolated patches as of Kohistan sector in western part and Gangdese sector in central part, which are mainly studied for stratigraphy, structure and neotectonics (Garzanti and Van Haver, 1988; Beck et al., 1995; Rowley, 1996; Treloar et al., 1996; Bilham, et al., 1997; Aitchison et al., 2000; Clift et al., 2000.) .

Rowley (1996) has highlighted the importance of the suture zone in constraining the timing of initiation of the collision, which is the fundamental question to be answered, in any attempt to build a scenario of the evolution of the collision zone. The age of initiation of the collision has still remained debatable because of the problem of correlation of the highly jumbled up stratigraphy of the suture zone. The stratigraphic estimates of the age of initiation of the collision range from 56 Ma to 40 Ma (Beck et al, 1995; Rowley, 1996). The approach of paleomagnetism assumes that the sudden decrease in the northward velocity of the Indian plate is due to the initial contact between the two continents (Dewey et al., 1989). This has been doubted (Butler, 1995), because the lithospheric response to the collision is not well understood. The approach of dating the youngest rock of the Trans Himalayan batholith, to constrain the age of the collision, has also been challenged in the light of new younger dates obtained for the batholith (Yin & Harrison 2000). The problem of the age of initiation of the collision has implications for our understanding of crustal accommodation in the collision zone since the collision started (Patriat and Achache, 1984). It is obvious that crustal accommodation in Himalaya and Tibet led to high mountain chains and the uplifted plateau but the calculated amount of crust to be accommodated, using the northward drift of Indian plate since collision, exceeds the amount that existed in these region (Coward and Butler, 1985, Ratschbacher et al., 1994, Guillot et al 2000). Various theoretical models have been proposed to explain the mechanisms of crustal accommodation (Davis et al., 1983; England and Houseman, 1986; Dalhen and Barr, 1989, Houseman and England, 1996). However, it has been soon realized that process of crustal accommodation, leading to deformation and uplift, has been highly variable in time and space as revealed by chronological and thermochronological studies (Harrison et al. 1992; Krol, et al., 1996; Chung et al., 1998). Chronology of different tectonic events and cooling histories of the magmatic and metamorphic rocks, as determined using temperature sensitive radiogenic isotope systems, provide useful information on the exhumation rates and the tectonic control of the deformation. This ^{40}Ar-^{39}Ar study of Ladakh sector of Trans Himalaya provided some information regarding the thermal state of different units through time. I have already discussed these results regarding the chronology of different tectonic events and its implication for the regional tectonic evolution in chapter 5. Here, I focus on the temperature data from the present study, in light of available thermochronological data from the other regions of the India-Asia collision zone, to build up a broad scenario for the evolution of India-Asia collision zone through time. This synthesis also attempts to throw light on the problem of crustal accommodation in the collision zone since the collision, and attempts to highlight the importance of thermochronology to understand the process of crustal accommodation through time.

6.2 Review of Thermochronological data

6.2.1. Thermochronology of Indus Suture

The basalts (samples LK176 & LK182) of Indus Suture, from Ladakh, yielded rapid cooling rates between ~ 46 Ma to ~ 35 Ma, followed by a slower cooling (Figs. 5.1 & 5.2). The cooling rate around ~ 46 Ma was > 150°C/Ma and between 38 to 35 Ma it was around ~ 30°C/Ma (Table 6.1). This is interpreted to reflect the large scale thrusting along the plate boundaries, resetting the Ar clock of the older ophiolite basalts of the suture, soon after the collision as discussed in chapter 5.

6.2.2. Thermochronology of Trans Himalayan Batholith

K-feldspar thermochronology of the plutonic rocks of the Kohistan batholith, western continuation of Ladakh Batholith, has yielded a variety of cooling rates for the different time periods (Krol et al., 1996). In the western Kohistan, the cooling rates were of the order of 40°C/Ma between 44 to 41 Ma. At 41 Ma cooling rates increased dramatically to 80°C/Ma (Krol et al., 1996). In eastern Kohistan, muscovite crystallization age from the Indus confluence aplites was found to be ~ 30 Ma (Krol et al., 1996). This is consistent with the $^{40}Ar/^{39}Ar$ age of muscovite from the Himia leucogranite of Ladakh batholith and indicates a cooling through ~ 350°C at that time (Table 6.1). The whole rock age spectrum of this rock yielded a cooling pattern from 38 to 18 Ma (Fig. 4.7). This indicates that the thermal regime was sufficiently high at ~ 38 Ma to partially re-melt the pre-existing subduction related granodiorites of Ladakh Batholith and form the leucogranite with constituent muscovite being at 350°C at ~ 30 Ma. The $^{40}Ar/^{39}Ar$ dating along the normal faults of South Tibet Detachment (STD), in the Gangdese batholith, east of Ladakh, yielded a rapid cooling episode between 8 to 4 Ma (Harrison et al, 1992), indicating the formation of the STD at ~ 8 Ma. Since the STD is supposed to be gravitational collapse structure due probably to the relaxation of stress during the eastward movement along the Red River fault, the Tibetan plateau is believed to have attained its full elevation by that time (Harrison et al, 1992).

Table 6.1 *Summary of time and temperature information derived from the present study*

Tectonic setting	*Time (Ma)*	*Cooling rate / Temperature*	*Remark*
Indus Suture Zone (ISZ)	46	150^{o}C/Ma	Derived using the MDD model (Fig. 5.2) on the basalt (LK176) from ISZ ophiolite.
	38 to 31	30^{o}C/Ma	Derived using the MDD model (Fig. 5.1) on the basalt from ISZ ophiolite (LK182).
Ladakh batholith	46	550 ^{o}C	Closure temperature of the hornblende, a major phase of the sample, and the maximum apparent age (Fig.4.5) of the whole rock granodiorite sample LK24.
	36	More than 350 ^{o}C	Maximum closure temperature of muscovite, a major phase of the two-mica leucogranite(LK198) and the maximum apparent plateau-like age of the leucogranite (Fig. 4.7)
	30	350^{o}C	Closure temperature of the muscovite and the plateau age of the muscovite LK198M (Fig. 4.8)
	44	300^{o}C	Closure temperature of the biotite and the plateau age of the biotite LK44B. (Fig. 4.6)
Shyok Suture Zone (SSZ)	60-52	700^{o}C	Minimum temperature of eruption of Khardung volcanics (LK88,99 &LG 87, 601) and their plateau ages, interpreted as duration of emplacement/eruption , (Figs. 4.19 to 4.22)

	20	500°C	Minimum closure temperature of the highest retentive phase (pyroxene in these samples) of the shyok volcanics(LK 48,57,67 68, 70) , and their reset apparent age (Fig. 5.3).
		350°C	Closure temperature of the mica and plateau age (Fig. 4.18) of the micaceous segregate LK47 from the Karakoram fault zone.

6.2.3. Thermochronology of north of the Suture

$^{40}Ar/^{39}Ar$ analyses of K-feldspar samples from the northwest of Lhasa yielded age gradients between 55 and 40 Ma that are suggestive of slow cooling (~ 10°C per million year) during the initial phase of collision (Copeland et al., 1990). The corresponding low average unroofing rates (<0.3 mm/yr), indicate a slow thickening during the initial period of post-collision. Similar K-feldspar analyses of several other plutons north of the Lhasa did not reveal fast cooling rates. Uplift rate for the Quxu pluton near Lhasa, derived by plotting the ages with elevation, yielded a sharp change in the rate at ~ 20 Ma from 0.08 ± 0.02 mm/yr, to > 2 mm/yr (Zeitler, 1985). The same unroofing rates were derived by the K-feldspar thermochronology by Richter et al. (1991), for the Quxu pluton, reinforcing the conclusion that a sharp change in the unroofing rate has occurred in this region of Tibet at ~ 20 Ma. This is interpreted to be due to the rapid uplift, and hence greater crustal accommodation during this time period in the southern Tibet. The thermochronological studies in the far north of the suture, near central Kunlun, revealed the fast unroofing rates at ~ 20 Ma (Arnaud et al., 1991). In the western region the Karakoram batholith, north of the suture, yielded rapid cooling rates between 17 Ma to 5 Ma (Searle, 1996). These are related to the intrusion of Baltoro leucogranite above 750°C at 25 -21 Ma into the already hot country rock and cooled slowly for 4 Ma till ~ 17 Ma ago (Searle, 1996).

6.2.4. Thermochronology south of the Suture

In the south of the suture, the Main Central Thrust, separating the Higher Himalayas from the Lesser Himalaya, has been found to be active between ~ 25 Ma to 18 Ma from the crystallization ages of Higher Himalaya anatectic granites and the deformation along the hanging wall of MCT (Copeland et al., 1991; Harrison et al., 1998). $^{40}Ar/^{39}Ar$ dating of the individual detrital grains from the Bengal fan also confirms rapid denudation and erosion rates in the early Miocene (Copeland et al., 1990). Recently Najaman et al. (2001) showed detrital muscovites from the foreland basin of Pakistan to be between 40 to 36 Ma, indicating rapid uplift and erosion since then. Further younging of deformation towards south was supported by the fission track cooling ages from the Main Boundary Thrust (MBT) near Kohat region of northwest Pakistan, indicating a rapid cooling episode between ~ 10 to 8 Ma, related to the uplift of the MBT. The youngest thrust system in the southern most Himalaya, the Main Frontal Thrust (MFT) (Baker et al., 1988), separating the foreland sediments from the Himalaya, is shown to be active at 2.1 -1.6 Ma using magnetostratigraphy by Johnson et al. (1986) and Baker et al. (1988). The present day convergence is presumably accommodated in the east -west extension of the southern Tibet along the South Tibet Detachment (STD) zone (Armijo et al., 1986).

6.3 Propagation of deformation through time

The present day strain partitioning into various regions in the collision zone provides very important clues to understanding of the crustal accommodation. The development of GPS technology has helped in quantifying the present day relative plate motions. Out of the present day convergence rate of ~ 50 mm/yr, the total shortening rate in the Himalaya is estimated to be 18 ± 7 mm/yr (Lyon-Caen and Molnar 1985; Molnar 1988). This is consistent with the recent GPS measurements (Bilham et al., 1997), which give the convergence rates across Himalaya to be between 17.5 ± 2 mm/yr to 20.5 ± 2mm/yr. Most of the present day convergence is estimated to be partitioned in the east-west extension along the strike slip faults. The major among them are Karakoram - Jiale - Red River fault system in the south, accommodating ~ 20 to 32 mm/yr and Altyn Tagh in north, accommodating ~ 30 mm/yr (Avouac and Tapponier, 1993). The rest of the convergence is being partitioned across the Tien Shan, north of the Tarim Basin in China. However, these present day estimates as such can not be extrapolated back in time. Thermochronological data from different regions of the collision zone indicate that the mode and rate of crustal accommodation have been highly variable in space and time. The rapid cooling rates in suture zone in Ladakh and Kohistan starting soon after the collision (~50 Ma) and the cooling ages of ~ 30 Ma from these region clearly indicate that most of the collision-related deformation was accommodated along the plate boundaries then. Thermochronological data from Tibetan plateau and Karakoram batholith, (north of the suture) and from the higher Himalaya (south of the suture), cluster around ~ 20 Ma. This indeed has been a major period of deformation and most of the present day features of the collision zone probably initiated at this time, by brittle crustal-stacking according to the critical taper wedge model for Himalaya (Dalhen and Barr, 1989; Davis et al., 1983) and by viscous thickening according to the thin viscous sheet model for Tibet (England and Houseman, 1986; Houseman & England 1996). These data also indicate the propagation of deformation away from the suture into both the continents with time. The southward younging of the thrusts in Himalaya, in the form of MBT activation at ~ 10 Ma and MFT activation at ~ 2 Ma, and similarly the northward younging of the thickness in the Tibetan Plateau as predicted by the thin viscous sheet model and as seen in the thermochronological data, also substantiate the proposition that the deformation and crustal accommodation has propagated away from the suture with time and has now reached up to the Tarim basin as reflected in by the Tien Shan fault activity. The ~ 8 Ma date from the STD and those of the other strike slip faults, indicates that lateral extrusion of the South Asian block started late in the history to further accommodate the crust. The lateral extrusion has since become the major mode of crustal accommodation with time as reflected in the present day estimate of strain partitioning.

6.4 Late accommodation of crust within the NW Trans Himalaya: Deformation in Shyok Suture Zone

The sequence of deformation and mode of crustal accommodation discussed above brings out that on a larger spatial scale the deformation propagated away from the plate boundaries into the continents with time.

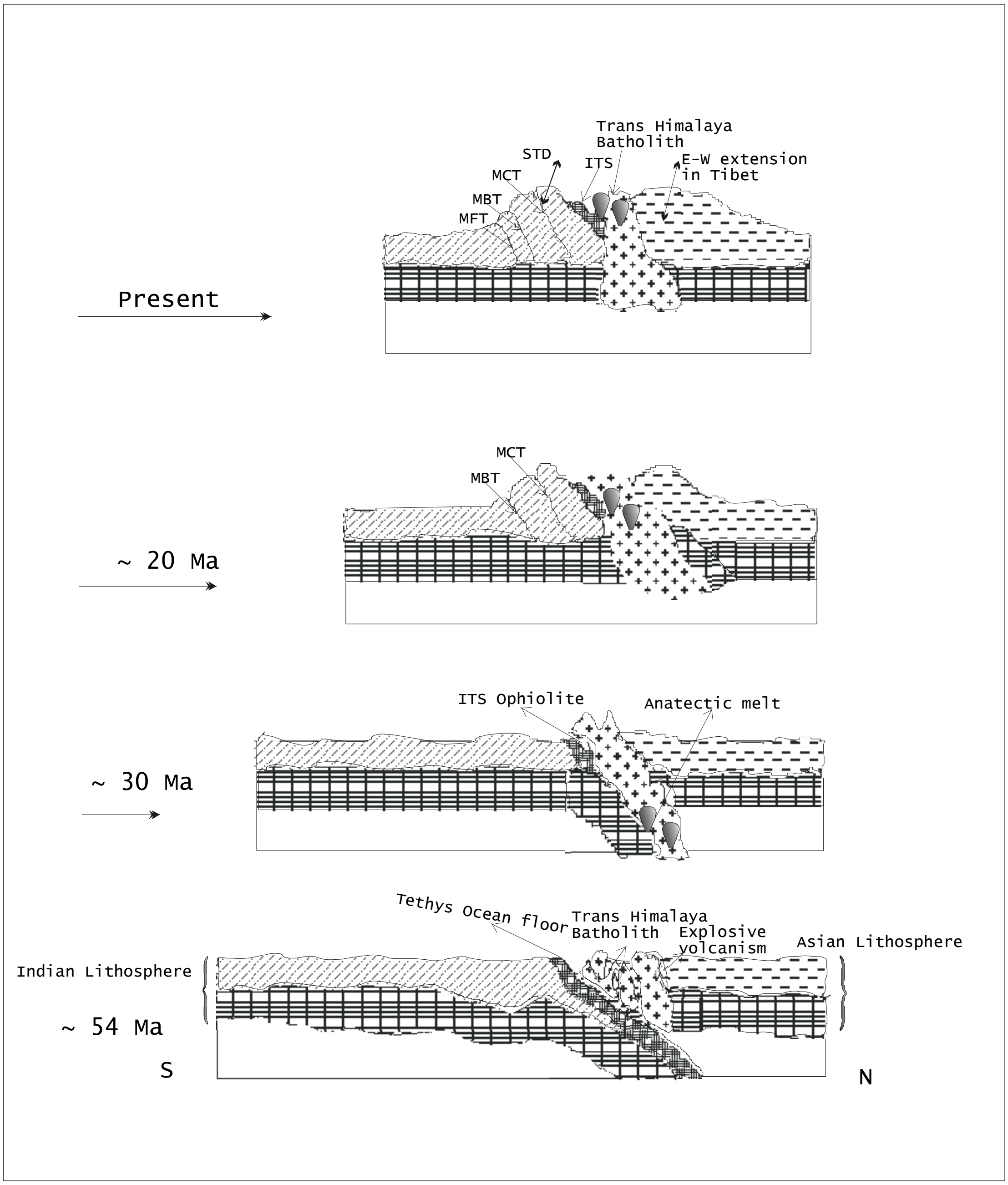

Fig. 6.1 *Cartoon diagram showing the evolution of India-Asia collision zone with time. Four main stages are shown here. Collision started at ~54 Ma ago and depicted here as showing the completion of suturing of the continents with trapped/obducted Tethys ocean and cessation of subduction related magmatism forming the Trans Himalayan batholith. Till ~ 30 Ma ago most of the deformation and crustal accommodation was restricted to plate boundary, resulting southward thrusting of the ophiolites and thickening of the Trans Himalayan batholith and southern margin of the Tibet. The thrusting at boundary and thickening of the crust generated partial anatectic melt at this time. In the next stage ~ 20 Ma ago, widespread deformation took place in the south as well as north of the plate boundary. Most of the crust accommodated in thrusting along the MCT(Main Central Thrust) in Himalayas and uplifting the Tibetan plateau in the north. (Fig. caption continued on next page)*

Later stage the deformation propagated farther away from the boundary and manifested in the form of MBT(Main Boundary Thrust), and MFT(Main Frontal Thrust)/HFF(Himalayan Frontal Fault) in the south and thickening of the northern margin of the Tibetan plateau. Accommodation of the crust is now taking place mostly in the strike slip movement of large faults in Tibetan region and E-W extension of Tibet

The synthesis of the available results indicates that most of the deformation and uplift of the Tibetan Plateau in north as well as that of Higher Himalaya along MCT took place around 20Ma. However, the results of the present study obtained from the Shyok Suture Zone of northern Ladakh indicate towards a strong tectono-thermal event around ~20 Ma in this region. These results, and other various geological and geochemical evidences as discussed in detail in chapter 5, further reveal that the regions east of Karakoram Fault was not much affected by this event, and the island arc in west of Karakoram fault and the continental arc in the east evolved independently and simultaneously. This points towards an internal adjustment of the NW Ladakh sector of the Trans Himalaya, which could have accommodated a significant portion of the crust, which when taken into consideration, can account for some of the amount exceeding the theoretical estimates of the crustal accommodation

Plateau age of ~14 Ma obtained by the fault zone sample from Karakoram batholith (LK47) is the age of fault activation. I propose here that internal adjustment of the crust in the Shyok Suture Zone was facilitated by this fault activation, which brought in juxtaposition the Kohistan-Shyok island arc with the Ladakh-Gangdese continental arc (Fig. 5.4). Recently Weinberg and Dunlop (2000) proposed on the basis of the cooling history of the shear zone samples, that shearing took place in NW Ladakh around ~22 Ma. They further stated that this dextral shearing took place within a zone of approximately 100 km-width including Ladakh batholith and a portion of Karakoram batholith and was responsible for the regional trend of the Ladakh batholith. This is in agreement with my results and interpretation of deformation in northern Ladakh.

6.5 Scope for further work

The response of continents to collision and consequent mountain building process is fundamental geological problem and deserves detailed study to fully understand the phenomenon to be able to apply it to older inactive orogens. Thermochronological studies provide complementary and much needed information about rate of exhumation/uplift and time sequence for the various tectono-thermal events. Though the data in this field is fast accumulating, the proper theoretical framework to understand and interpret it, is still lacking.

Collision is major process of continental crust building and making continents to supercontinents which affects the overall global climate and biosphere. However, very few isotopic studies using oxygen, strontium, neodymium, lead etc. have been carried out (Srimal et al., 1987) to understand the petrogenetic aspects of collision related magmatic processes. This leads to confusion over the younger post collision ages obtained from the various parts of the collision zone.

In my view any future work on these active collision belt should be on following lines:

1. K-feldspar thermochronology and mineral dating of different magmatic and metamorphic units of the Trans Himalayan zone to understand the complete cooling/exhumation history of this zone.
2. Development of theoretical and numerical simulations incorporating thermochronological data to understand the response of continental crust to collision and controls of deformation and crustal accommodation.
3. Petrogenetic studies of the magmatic rocks of the collision zone.
4. The petrogenetic and chronological correlation to bring out magma evolution in an orogenic belt .

References

Abbott, L.D., Silver, E.A., Anderson, R.S., Smith, R., Ingles, J.,C., Kling, S.,A., Haig, D., Small, E., Galewsky, J., and Sliter, W. (1997) Measurements of tectonic surface uplift rate in a young collisional mountain belt. *Nature* 385, 501-507.

Acharyya, S.K., and Sastry, M.V.A (1979) Stratigraphy of the eastern Himalaya. *Geol. Surv. Ind. Misc. Pub.* 41, 49-67.

Acharyya, S.K., (1997) Stratigraphy and tectonic history reconstruction of the Indo-Burman-Andaman mobile belt. *Ind. J. Geol.* 69, 211-234.

Ahmad, T., Thakur, V.C., Islam,R., Khanna, P.P. Mukherjee, P.K. (1998) Geochemistry and geodynamic implications of magmatic rocks from the Trans-Himalayan arc. *Geochem. J.* 32, 383-404.

Aitchison, J.C., Badengzhu, Davis, A.M., Liu, J., Luo, H., Malpas, J.G., McDermid, I.,R.,C., Wu, H., Ziabrev, S.V., Zhou, M. (2000) Remnanats of a Cretaceous intra-oceanic subduction system within the Yarlung-Zangbo suture (southern Tibet). *Earth Planet. Sci. Lett.* 183, 231-244.

Allegre, C.J., Courtillot, P., Tapponnier, P., and 32 others (1984) Structure and evolution of the Himalaya-Tibet orogenic belt. *Nature* 307, 17-22.

Alexander, Jr., E., C., Michelson, G.M., and Lanphere, M.A. (1978) MMHb-1: A new ^{40}Ar-^{39}Ar standard. In *Short papers of the Fourth International Conference on Geochronology, Cosmochronology, and Isotope geology,* ed. Zatman, R.E., *U.S. Geol. Surv. Open-File* report 78-701, 6-8.

Arita, K. (1983) Origin of the inverted metamorphism of the lower Himalayas, central Nepal. *Tectonophysics* 95, 43-60.

Armijo, R., Tapponier, P., Mercier, J.L., and Han, T., (1986) Quaternary extension in southern Tibet: field observations and tectonic implications. *J. Geophys. Res*. 91, 13803-138072.

Armijo, R.; Tapponier, P; and Han, T. (1989) Late Cenozoic right-lateral strike-slip faulting in southern Tibet. *J. Geophys. Res*. 94, 2787-838.

Arnaud, N. O., Ronghua, X., Yuquan, Z., (1991). *C. R. Acad. Sci. Paris* 312, 905.

Auden, J. B. (1935) Traverses in the Himalaya. *Geol. Surv. Ind. Rec.* 69, 123-167.

Avouac, J.P., and Tapponier, P.,(1993). Kinematic model of active deformation in Central Asia. *Geophys. Res. Lett.* 20, 895-898.

Baker, D., M., Lillie, R., J., Yeats, R., S., Johnson, G., D., Yousuf, M., and Zamin, A., S., H., (1988). Development of the Himalayan Frontal Zone, Salt Range, Pakistan. *Geology* 16, 3-7.

Baksi, A.K., Archibald, D.A., Farrar, E. (1996) Intercalibration of $^{40}Ar/^{39}Ar$ dating standards. *Chem. Geol*. 129, 307-324.

Beck, R.A., Burbank, D.W., Sercombe, W.J., Riley, G.W., Bery, J.R., Afzal,J., Khan, A.M., Jurgen, H., Cheema, A., Shafique, N.A., Lawrence, R.D., and Khan, M.A. (1995) Stratigraphic evidence for an early collision between northwest India and Asia. *Nature* 373, 55-58.

Bilham, R., Larson, K., Freymueller, J., and project ldylhim members. (1997). GPS measurements of present- day convergence across the Nepal Himalaya, *Nature* 386, 61-64.

Bird P. (1978) Initiation of intracontinental subduction in the Himalaya. *J. Geophys. Res.* 83, 4975-4987.

Bevington, P.R. (1969). Data reduction and error analysis for the physical sciences. *McGraw Hill Co., New York.*

Brereton, N.R. (1970). Corrections for interfering isotopes in the $^{40}Ar/^{39}Ar$ dating method. *Earth Planet. Sci. Lett.* 8, 427-433.

Brereton, N.R. (1972). A reappraisal of the $^{40}Ar/^{39}Ar$ stepwise degassing technique. *Geopphys. J. R. Astron. Soc.* 27, 449-478.

Brookfield, M.E., and Reynolds, P.H., (1981). Late Cretaceous emplacement of Indus Suture Zone, ophiolitic mélange and an Eocene-Oligocene magmatic arc on the Northern edge of the Indian plate. *Earth Planet. Sci. Lett*, 55, 157-162.

Brookfield, M.E., and Andrews-Speed, S.P., (1984) Sedimentology, petrography and tectonic significance of the shelf, flysch and molasses clastic deposits across the Indus Suture Zone, Ladakh, NW India. *Sed. Geol.* 40, 249-286.

Burbank, D.W., Beck, R.A., and Mulder, T., (1997) The Himalayan foreland basin. In *Tectonic evolution of Asia,* (eds. A Yin and T M Harrison) 149-188.

Butler, R. (1995) When did India hit Asia? *Nature* 373, 20.

Chung, S.L., Lo C-C, Lee, T-Y, Zang Y, Xie, Y, et al (1998) Diachronous uplift of the Tibetan plateau starting 40 Myr ago. *Nature* 394, 769-73.

Clift, P.D., Degnan, P.J., Hannigan, R., Blusztajn, J., (2000). Sedimentary and geochemical evolution of Drass foreac basin, Indus suture, Ladakh Himalaya, India. *GSA Bull.* 112, 450-466.

Colchen, M., Mascle, G. and Van Haver, T. (1986) Some aspects of collision tectonics in the Indus Suture Zone, Ladakh. In: *Collision Tectonics* (eds. Coward., M.P., Ries) Special Publication*, Geological Society of London* 19, 173-184.

Copeland, P., Harrison, T. M., and Le Fort, P. (1990) Age and cooling history of the Manasulu granite: Implications for Himalayan tectonics. *J Volc. Geotherm. Res.* 44, 33-50.

Copeland, P., Harrison, T. M., Hodges, K.V., Mareujol, P., Le Fort, P., and pecher, A. (1991) An early Pliocene thermal perturbation of the Main Central Thrust, central Nepal: Implications for Himalayan tectonics, *J. Geophys. Res.* 96, 8475-8500.

Coward, M., P., and Butler, R., H., (1985) Thrust tectonics and the deep structure of the Pakistan Himalaya. *Geology* 13, 417-420.

Dalhen, F.A., and Barr, T.D., (1989) Brittle frictional mountain building 1. Deformation and mechanical energy budget. *J.Geophys. Res.* 94, 3906 -3922.

Dalrymple, G.B. and Lanphere, M.A.(1974) ^{40}Ar-^{39}Ar age spectra of some undisturbed terrestrial samples. *Geochim.Cosmochim.Acta* 38, 715-738.

Dalrymple, G.B., Alexender, E.C., Jr., Lanphere, M.A., and Karker,G.P. (1981) Irradiation of Samples for ^{40}Ar/^{39}Ar dating using the Geophysical Survey TRIGA reactor, *U.S.Geol. Surv., Prof Paper.* 1176.

Dallmeyer, R.D. and Lecorche, J.P. (1990) ^{40}Ar/^{39}Ar polyorogenic mineral age record in the northern Mauritanide orogen, West Africa. *Tectonophysics* 177, 81-107.

Dalrymple, G.B., Izett, L., Snee, L., and Obradovich, J. (1993) ^{40}Ar/^{39}Ar age spectra and total fusion ages of tektites from Creceous-Tertiary rocks in the Beloc Formation, Haiti. *U.S.Geol. Surv. Bull.* 2065, 20.

Davis, D., Suppe, J., and Dahlen, F.A., (1983) Mechanics of fold and thrust belts and accretionary wedges. *J. Geophys. Res.* 88, 1153-1172.

De Sigoyer, J., Chavagnac, V., Villa, I.M., Luais, B., Guillot, S., Cosca, M., Mascle, G. (2000) Dating the Indian continental subduction and collisional thickening in the Northwest Himalaya: Multichronology of the Tso Morari eclogites, *Geology* 28, 487-490.

Dewey, J.F.,and Burk, K.C.A. (1973) Tibetan, Variscan and Precambrian basement reactivation: products of continental collision. *J.Geology* 81, 683-692.

Dewey. J.F., Cande, S., and Pitman, W.C. (1989) Tectonic evolution of the India/Eurasia collision zone. *Eclogae. Geol. Helve.* 82, 717-34.

Dodson, M.H. (1973) Closure temperature in cooling geochronological and petrological systems. *Contrib. Mineral. Petrol.* 40, 259-274.

England, P., C., and Houseman, G., A., (1986) Finite strain calculations of continental deformation. II: Application to the India-Asia plate collision. *J. Geophys. Res.* 91, 3664-36676.

Fleck, R.J., Sutter, J.F., and Elliot, D.H. (1977) Interpretation of discordant ^{40}Ar-^{39}Ar age-spectra of Mesozoic tholeiites from Antartica. *Geochim. Cosmochim. Acta* 41, 15-32.

Foland, K.A., Gilbert ,L.A., Serbing, C.A., and Chen, J.F. (1986) ^{40}Ar/^{39}Ar ages for plutons of Monteregian Hills, Quebec: Evidence for a single episode of Cretaceous magmatism. *Geol. Soc. Am. Bull.* 97, 966-974.

Frank, W., Ganser, A. and Trommsdroff. V., (1977) Geological observations in the Ladakh area (Himalayas), a preliminary report. *Schweiz Mineral. Petro. Mitt.* 57, 89-113.

Friedlander, G., Kennedy, J.W., Macias, E.S., and Miller, J.M. (1981) Nuclear and Radiochemistry 3rd ed., *Wiley, New York.*

Fuchs. G., (1979) On the geology of western Ladakh. *Jahrbuch der Geologischen Bundesanstalt Wien.* 122, 513-40.

Fuchs, G., (1982) The geology of the western Zanskar. Jahrbuch der Geologischen Bundesanstalt Wien 125, 1-50.

Gaetani, M., and Garzanti, E., (1991) Multicyclic history of the Northern Indian continental margin (Northwestern Himalaya). American association of Petroleum *Geologista Bulletin* 75, 1427-46.

Ganser, A. (1964) Geology of the Himalayas. *J. Willey*. London, U.K.

Garner, E.L., Murphy, T.J., Gramlich, J.W., Paulsen, P.J., and Barnes, I.L. (1975) Absolute isotopic abundance ratios and the atomic weight of a reference sample of potassium. *J.Res. Natl. Bureau Stand* 79A. 713-725.

Garzanti, E., and Van Haver, T., (1988) The Indus clastics: forearc basin sedimentation in the Ladakh Himalaya (India). *Sed. Geol.* 59, 237-49.

George, M.T., Harris, N. and Butler, R.W.H. (1993) The tectonoic implications of contrasting granite magmatism between the Kohistan island arc and the Nanga Parbat-Harmosh massif,Pakistan Himalaya. In: *Himalayan tectonics,*(eds.Treloar, P.J., Searle, M.P.) *Geological Society of London Special Publication* 74, 173-191.

Grasty, R.L. and Mitchell, J.G. (1966) Single sample potassium-argon ages using the omegatron. *Earth Planet. Sci. Lett.* 1, 121-122.

Gregan, J.T., and Pant, P.C. 1983 Geology and straitigraphy of eastern Karakoram, Ladakh. In *Geology of Indus Suture Zone of Ladakh,* (eds. V.C. Thakur and K.K.Sharma) Wadia Institute of Himalayan Geology, Dehardun, 99-106.

Guillot, S., Baratoux, D., Garzanti, E., Marquer, D., de Sigoyer, J.,(2000). India/Asia Convergence and Himalayan shortening. *Earth Sci. Frontiers. 15th HKT Abstract Volume*, 7 suppl., 417-418.

Harrison, T.M., Duncan, I., McDougall, I., (1985) Diffusion of ^{40}Ar in biotite: temperature, pressure and compositional effects. *Geochemica Cosmochemica Acta* 49, 2461-2468.

Harrison, T.M., Copeland, P., Kidd, W.S.F., and yin A., (1992) Raising Tibet. *Science* 255, 1663- 1670.

Harrison, T.M., Grove, M., Lovera, O.M., Catlos, E.J., (1998) A model for the origin of Himalayan anatexis and inverted metamorphism. *J. Geophys. Res.* 103, 27017-27032.

Hayden, H.H. (1907) The geology of the provenance of Tsang in Tibet. *Geol. Surv. Ind. Records* 36, 122-201.

Hebert, R., Beaudoin, G., Varfalvy, V., Huot, F., Wang, C.S., and Liu, Z.F. (2000) Yarlung Zangbo ophiolites, Southern Tibet revisited. *Earth Science Frontiers* 7 (Suppl.) 124-126.

Heim, A. and Ganser, A. (1939) Central Himalaya-Geological observations of Swiss expedition, 1936. *Societe Helvetique Science Naturelle memoire* 73, 1-245.

Hodges, K.V., Hubbard, M.S., and Silverberg, D.S., (1988) Metamorphic constraints on the thermal evolution of the central Himalayn orogen. *Royal Society of London Philosophical Ttransaction* A-326, 257-280.

Hodges, K.V., (1999) Tectonics of the Himalaya and southern Tibet from two perspectives. *GSA bull.* 112, 324-350.

Honegger. K. Dietrich,V.,Frank,W.,Ganser,A.,Thoni,M., and Trommsdrof,V. 1982, Magmatism and metamorphism in the Ladakh Himalayas (the Indus-Tsangpo suture zone). *Earth Planet. Sci. Lett.* 60, 253-292.

Houseman, G., and England, P.C., (1986) Finite strain calculation of continental deformation. 1. Method and general results for the convergent zones. *J., Geophys. Res.,* 91, 3651-63.

Houseman, G. and England, P. (1993) Crustal thickening versus lateral expulsion in the Indian-Asian continental collision. *J. Geophys. Res.* 98, 12233-12249.

Houseman, G., and England, P. (1996) A lithospheric thickening model for the Indo-Asian collision. In *The tectonic Evolution of Asia*, (eds A Yin, T.M. Harrison) 3-17.

Johnson, G.D., Raynolds, R.G., and Burbank, D.W., (1986) Late Cenozoic tectonics and Sedimentation in the north-western Himalayan foredeep. 1. Thrust ramping and associated deformation in the Potwar region. In *Foreland Basins,* ed. P.A. Allen and P. Homewood, *International Association for Sedimentology special publication* 8, 273-291.

Keleman, P., and Sonnenfeld, M.D., (1983) Stratigraphiy, structure, petrology, and local tectonics, central Ladakh, NW Himalaya. *Schweizer Mineralogische and Petrographische Mitteliungen* 63, 267-87.

Khan, M.A., Jan, M.Q., Windley, B.F., Tarney, J., and Thirlwall, M.F., (1989) The Chilas Mafic-Ultramafic Igneous complex: The root of Kohistan island arc in the Himalaya of northern Pakistan, in *Tectonics of the western Himalayas*, (eds. Melinconico, L., L., and Lillie, R.J.) *Geol. Soc. Am. Sp. Pap*. 232, 75-94.

Kong, X., and Bird, P. (1996) Neotectonics of Asia: thin shell, finite-element models with faults. In *The tectonics of Asia*, ed. (A Yin and T M Harrison) 18-35.

Krishnaswami, S., Trivedi, J. R., Sarin, M., Ramesh, R. and Sharma, K. (1992) Strontium isotopes and rubidium in the Ganga–Bramaputra river system: Weathering in the Himalaya, fluxes to the Bay of Bengal and contributions to the evolution of oceanic $^{87}Sr/^{86}Sr$. *Earth Planet. Sci. Lett.* 109**,** 243–253.

Krol, M.A., Zeitler ,P.K., and Copeland, P., (1996) Episodic unroofing of the Kohistan Batholith, Pakistan: Implications from K-feldspar thermochronology. *J. of Geophy. Res.* 101, 28,149-28,164.

Le Fort P. (1986) Metamorphism and magmatism during Himalayan Collision. In *Collision tectonics* (eds. Coward, M.,P., and Ries, A.C.) *Geological Society Special Publication* 19, 59-172

Le Fort, P. (1996) Evolution of the Himalaya. In *The Tectonic Evolution of Asia*, (eds. An Yin and T.M.Harrison) *Cambridge University Press*, New York. 95-106

Lee, J.K.W. (1995). Multipath diffusion in geochronology. *Contrib.Mineral.Petrol*. 120, 60-82.

Lo Ching-Hua. , Lee., J.K.W. Onstott T.C. (2000) Argon release mechanisms of biotite in vacuo and the role of short-circuit diffusion and recoil. *Chem. Geol.* 165, 135 -166.

Lombard, O. (1981) 8, rue de river CH-1204, Geneve, *Switzerland.*

Lovera, O.M., Grove,M., Harrison, T.M. (1989) The $^{40}Ar/^{39}Ar$ thermochronometry for slowly cooled samples having a distribution of diffusion domain sizes. *J. Geophy. Res.* 94, 17917-17,935.

Lovera, O.M., Richter, F.M., and Harrison, T.M. (1991) Diffusion domains determined by 39Ar Released during step heating. *J. Geophy. Res.* 96, 2057-2069.

Lovera, O.M., Heizler, M.T., and Harrison T.M., (1993) Argon diffusion domains in K-feldspar, II: Kinetic properties of MH-10, *Contrib. to Mineral. Petrol.* 113, 381-393.

Lydekker, R. (1883) The geology of the Kashmir and Chamba territories and the British district of Khagan. *Geol. Surv. Ind. Mem.* 22, 108-122.

Lyon-Caen, H., and Molnar, P.,(1985) Gravity anomalies, flexure of the Indian Plate, and the structure, support and evolution of the Himalaya and Ganga Basin. *Tectonics* 4, 513-538.

Mathur, N.S., and Pant, P.C. (1983) Early Eocene forminifera from Singhe La area, Zanskar region, Ladakh Himalaya. In *Geology of Indus Suture Zone of Ladakh*, (eds. V.C. Thakur and K.K.Sharma) Wadia Institute of Himalayan Geology, Dehardun. 151-156.

McCaferey, R., and Nalbek, J., (1998) Role of oblique convergence in the active deformation of the Himalayas and southern Tibet plateau. *Geology* 26, 691-94.

McDougall, I. And Harrison T.M.(1999) Geochronology and Thermochronology by $^{40}Ar/^{39}Ar$ method. *Oxford University Press.*

McIntyre, G.A., Brooks, C., Compston, W., and Turek, A. (1966) The statistical assessment of Rb-Sr isochron. *J. Geophys. Res.* 71, 5459-5468.

Merrihue, C., and Turner, G. (1966) Potassium-argon dating by activation with fast neutrons. *J. Geophys. Res*. 71, 2852-2857.

Misra, K.S.(1979) Himalayan transverse faults and folds and their parallelism with subsurface structures of north Indian plains-Discussion *Tectonophysics* 32, 353-386.

Mitchell, J.G. (1968) The argon-40/argon-39 method for potassium-argon age determination. *Geochim. Cosmochim. Acta* 32, 781-790.

Molnar, P., (1988) A review of geophysical constraints on the deep structure of the Tibetan Plateau, the Himalaya, and the Karakoram, and their tectonic implications. *Phil. Trans. R. Soc. Lond.,* A326, pp.33-88.

Molnar, P, and England, P., (1990) Late Cenozoic uplift of mountain ranges and global climate:chicken or egg? *Nature*, 346, 29-34.

Molnar, P., England, P., Martinod, J. (1993) Mantle dynamics, the uplift of the Tibetan plateau and the Indian monsoon. *Rev. Geophys.* 31, 357-96.

Najaman, Y., Pringle, M., Godin, L. and Oliver G. (2001) Dating the oldest continental sediments from the Himalayan foreland basin. *Nature* 410, 194-197.

Neir, A.O. (1950). A redetermination of the relative abundances of the isotopes of carbon, nitrogen, oxygen, argon and potassium. *Phys. Rev.* 77, 789-793.

Odin, G.S., and 35 others, (1982) Interlaboratory standards for dating purposes. In *Numerical dating in Stratigraphy,* Wiley, Chichester, 123-149.

Pande, K., (1999) Present status of K-Ar and ^{40}Ar-^{39}Ar data from the Himalaya. *Gond. Res. Group Mem.* 6, pp. 237-244.

Parrish, R.R., and Tirrul, R. (1989) U-Pb age of the Baltoro granite, northwest Himalaya, and implications for zircon inheritance and monazite U-Pb systematics. *Geology* 17, 1076-1079.

Patriat, P., and Achache, J., (1984) India-Eurasia collision chronology has implications for Crustal shortening and driving mechanism of plates. *Nature* 311, 615-621.

Petterson, M.G., and Windley, B.F. (1985) Rb-Sr dating of the Kohistan arc-batholith in the Trans-Himalaya of north Pakistan, and tectonic implications. *Earth and Planetary Science Letters* 74, 45-57.

Petterson, M.G. and Windley, B.F., (1991) Changing source regions of magmas and crustal growth in the Trans Himalayas: evidence from the chalt volcanics and Kohistan batholith, Kohistan, N. Pakistan. *Earth Planet. Sci. Lett.* 102. 326-341.

Pudsey, C.J. (1986) The northern suture, Pakistan: margin of a Cretaceous island arc, *Geol. Mag.* 123, 405-23

Rai, H., (1982) Geological evidence against the Shyok Palaeo-suture, Ladakh Himalaya, *Nature* 297, 142-145.

Rai, H., (1983) Geology of the Nubra valley and its significance on the evolution of the Ladakh Himalaya. In *Geology of Indus Suture Zone of Ladakh,* (eds. V.C. Thakur nd K.K.Sharma) Wadia Institute of Himalayan Geology, Dehardun, 79-91.

Ratschbacher, L., Frisch, W., Lui, G., and Chen, C., (1994) Distributed deformation in Southern and western Tibet during and after the India-Asia collision, *J.Geophys., Res.*.99, 19, 817-19945.

Ravi Shankar, Kumar, G. and Saxena, S.P., 1989. Stratigraphy and sedimentation in Himalaya: A reappraisal. *In Geology and Tectonics of the Himalaya* (Eds. Ravi Shankar et al.) *Geol. Surv. Ind. Spl. Pub. No.* 26, 1-60.

Raz, U., and Honneger, K. (1989) Magmatic and tectonic evolution of the Ladakh Block from field studies. *Tectonophysics* 161, 107-118.

Renne, P.R., Swisher, C.C., Deino, A.L., Karner, D.B., Owens T.L., and DePaolo D.J.(1998) Intercalibration of standards, absolute ages and understanding in ^{40}Ar-^{39}Ar dating. *Chem. Geol.* 145, 117-152.

Renne, P.R. (2000) K-Ar and ^{40}Ar-^{39}Ar dating. Quaternary Geochronology: Methods and Applications, *AGU reference shelf* 4, 77-98.

Reuber, I., (1986) Geometry of accretion and oceanic thrusting of the Spongtang ophiolite, Ladakh Himalaya. *Nature* 321, 592-596.

Reynolds, P.H., Brookfield, M.E., Halifex, G., McNutt., R.H., (1983) The age and nature of Mesozoic-Tertiary magmatism across the Indus Suture Zone, in Kashmir and Ladakh (NW India and Pakistan). *Geol. Rundschau* 72, 981-1004.

Richter, F.M., Lovera, O.M., Harrison, T.M., and Copeland, P., (1991) Tibetan tectonics From $^{40}Ar/^{39}Ar$ analysis of a single K-feldspar sample. *Earth and Planet. Sci. lett* 105, 266-278.

Richter, F.M.; Rowley, D.B. and DePaolo, D.J. (1992) Sr isotope evolution of seawater: the role of tectonics. *Earth Planet. Sci. Lett.* 109, 11-23.

Roddick, J.C., Cliff, R.A., and Rex, D.C. (1980) The evolution of excess argon in alpine biotite-A $^{40}Ar/^{39}Ar$ analysis. *Earth. Planet. Sci. Lett.* 48, 185- 208.

Rolland, Y., Pecher, A., and Picard., C, (2000). Middle Cretaceous back-arc formation and arc evolution along the Asian margin: Shyok Suture Zone in northern Ladakh (NW Himalaya). *Tectonophysics* 325, 145-173.

Rowley, D.B., (1996) Age of initiation of collision between India and Asia: A review of stratigraphic data. *Earth Planet. Sci. Lett.* 145, 1-13.

Ruddiman, W. F. and Kutzbach, J. E., (1991) Plateau uplift and climate change. *Sci. Am.* 264**,** 42–50.

Samson, S.D. and Alexander Jr, E.C., (1987) Calibration of the interlaboratory ^{40}Ar-^{39}Ar dating standard, MMHb-1. *Chemical Geology* 66, 576-591.

Scharer,U., Copeland, P., Harrison, T.M., Searle, M.P., (1990) Age cooling history and origin of post-collisional leucogranites in the Karakoram batholith: A multi-system isotope study, N. Pakistan, *J. Geol.* 98, 233-251.

Searle, M.P. (1986) Structural evolution and sequence of thrusting in the High Himalyan, Tibetan-Tethys and Indus Suture zones of Zanskar and Ladakh, western Himalaya, *J. Struct. Geol.* 8, 923-36.

Searle, M.P., Windley, B.F., Coward, M.P., Cooper, D.J.W., Rex, A.J., Rex, D.,Tingdong, L., Xuchang, X., Jan, M.Q., Thakur V., and Kumar, S. (1987) The closing of Tethys and the tectonics of the Himalayas. *Bull. Geol. Soc. Am.* 98, 335-67.

Searle, M.P.,(1988) Reply: Structural evolution and sequence of thrusting in the High Himalyan, Tibetan-Tethys and Indus Suture zones of Zanskar and Ladakh, western Himalaya, *J. of Struct. Geol.* 8, 923-36.

Searle, M.P. (1996) Cooling history, erosion, exhumation, kinematics of the Himalaya-Karakoram-Tibet orogenic belt. In *The Tectonic Evolution of Asia*, (eds. A. Yin and T.M. Harrison) *Cambridge Univ. Press, New York,* 110-137.

Searle, M., Corfield, R.I., Stephenson, B., McCarron, J.(1997) Structure of the North Indian continental margin in the Ladakh-Zanskar Himalayas: Implications for the timing of obduction of the Spongtang ophiolite, India-Asia collision and deformation events in the Himalaya. *Geol. Mag.* 134, 297-316.

Searle, M.P., Weinberg, R.F., and Dunlap, W.J. (1998) Transpressional tectonics along the Karakoram Fault Zone, northern Ladakh. In *Continental transpression and* *transtensional tectonics*, eds. R.E. Holdsworth and R.A. Strachan, Geol. Soc. Lond. Spec. Pub. 135, 107-326.

Searle, M.P., Khan, M.A., Fraser, J.E., Gough, S.J., Jan M.Q., (1999) The tectonic evolution of the Kohistan-Karakoram collision belt along the Karakoram Highway transect, north Pakistan. *Tectonics* 18, 929-949.

Sharma, K.K., and Gupta, K.R., (1978) Some observations on the geology of Indus and Shyok valleys between Leh and Panamik, District Ladakh, Jammu and Kashmir, India. *Recent researches in geology* 7, 133-143.

Sharma, K.K., and Choubey, V., M. (1983) Petrology, geochemistry and geochronology of the southern margin of the Ladakh batholith between Upshi and Chumathang. In: *Geology of the Indus Suture Zone of Ladakh* (eds. Thakur, V.,C., Sharma, K.K. *)* 41-60.

Sharma, K.K. (1987) Crustal growth and two-stage India-Eurasia collision in Ladakh.*Tectonophysics* 134, 17-28.

Sharma, K.K. (1990) Petrology, Geochemistry and Geochronology of the Ladakh Batholith and its role in the evolution of Ladakh magmatic arc. In: Geology and Geodynamic Evolution of the Himalayan Collision Zone (Ed. Sharma,K.K.), *Physics and Chemistry of the Earth* 17(2), 173-193.

Sharma, K.K.(1991) Petrochemistry and Tectonic environment of Dras, Shyok, Khardung and Chushul volcanics of Indus Suture Zone, ladakh: A comparative study. *Jour. Geol. Soc. Ind.* 133-148.

Sinha, A.K., and Upadhyay, R. (1993) Mesozoic Neo-Tethyan pre-orogenic deep marine sediments along Indus-Yarlung Suture, Himalaya, *Terra Nova* 5(2), 461-473.

Srimal, N. (1987), Basu, A.R., Kyser, T.K. (1987) Tectonic inferences from oxygen isotopes in volcano-plutonic complexes of the India-Asia collision zone, NW India. *Tectonics* 6, 261-273.

Snee, L.W., Sutter, J.F., and Kelly, W.C. (1988) Thermochronology of economic mineral mineral deposits: Dating the stages of mineralization at Panaqueira, Portugal, by high-presision ^{40}Ar-^{39}Ar age spectrum techniques on muscovite. *Econ. Geol.* 83, 335-354.

Steiger, R.H. and Jager, E. (1977) Subcommision on geochronology: Convention on the use of Decay constants in geo- and cosmochronology. *Earth Planet. Sci. Lett*. 36, 359-362.

Stoener, R.W., Schaeffer, O.A., and Katcoff, S. (1965). Half-lives of argon-37, argon-39, and argon-42, *Science* 148, 1325-1328.

Tahirkheli, R.A.K. and Jan, M.Q. (1979) Geology of Kohistan, Karakoram Highway, northern Pakistan. *Univ. Pesh. Geol. Bull. Spec. Issue* 11, 1-30.

Tapponier, P., Peltzer, G., and Armijo, R. (1975) On the mechanics of the collision between India and Asia. In *Collision Tectonics, Geol. Soc. Spec. Pub.* 19, 115-157.

Tapponier, P., Peltzer, G., Le Dain, A.Y., Armijo, R., and Cobbold, P., (1982). Propagating extrusion tectonics in Asia: new insights from simple experiments with plasticine. *Geology* 10, 611- 616.

Tapponier, P., Peltzer, G., abd Armijo, R., (1986) On the mechanics of the collision between India and Asia. In *collision Tetonics* (eds. M.P. Coward and A.C. Ries.) *Geological Society of London Special Bulletin* 19, 115-1157.

Thakur, V.C., (1981) Regional framework and geodynamic evolution of the Indus-Tsangpo suture zone in the Ladakh Himalaya. T*rans. Roy. Soc. Edin: Earth Sci.,* 72, 89-97.

Thakur, V.C., and Bagati, T.N. (1983). Indus Formation: an arc- trench gap sediments. In *Geology of Indus Suture Zone of Ladakh*, (eds. V.C. Thakur and K.K.Sharma) Wadia Institute of Himalayan Geology, Dehardun, 9-19.

Thakur, V.C., and Bhatt M.I (1983) Interpretation of Tectonic Environment of Nidar Ophiolite:A Geochemical approach. In: *Geology of Indus Suture Zone of Ladakh* (eds. Sharma,K.K., Thakur, V.C) 21-31.

Thakur, V.C., and Misra, D.K., (1983) Ophiolitic mélanges in the Indus suture zone: lithological descriptions and structural features. In *Geology of Indus Suture Zone of Ladakh*, (eds. V.C. Thakur and K.K.Sharma), Wadia Institute of Himalayan Geology, Dehardun.79-91.

Thakur, V.C. and Misra, D.K. (1984) Tectonic framework of the Indus and Shyok suture zones in eastern Ladakh (N-W Himalaya). *Tectonophysics* 101, 207-220.

Treloar, P.J., Rex., D.C., Guise, P.G., Coward, M.P., Searle, M.P., Windley, B.F., Petterson, M.G., Jan, M.Q., Luff, I.W., (1989) K/Ar and Ar/Ar geochronology of the Himalayan Collision in NW Pakistan: constraints on the timing of suturing, deformation, metamorphism and uplift. *Tectonics* 8, 881-909.

Treloar, P.J., Petterson, M.G., Jan, Q.M., Sullivian M.A., (1996) A re-evaluation of the Straitigraphy and evoltution of the Kohistan arc sequence, Pakistan Himalaya: Implication for magmatic and tectonic arc building processes. *J. Geol. Soc. London* 153, 681-693.

Trivedi, J.R., Gopalan, K., and Valdiya, K.S. (1984) Rb-Sr ages of granitic rocks within the lesser Himalayan nappes, Kumaun Himalaya. *Jou. Geol. Soc. Ind.* 35, 641-654.

Turner, G., Miller, J.A., and Gastry, R.L. (1966) The thermal history of the Bruderheim meteorite. *Earth Planet. Sci. Lett.* 12, 19-35.

Turner, G. (1971a). Argon 40-argon 39 dating: The optimization of irradiation parameters. *Earth Planet. Sci. Lett.* 10, 227-234.

Turner, G, (1971b) ^{40}Ar/^{39}Ar ages from the lunar maria. *Eart. Planet. Sci. Lett.* 14, 169-175.

Upadhyay, R., Sinha, A.K., Chandra, R., and Rai, H. (1999) Tectonic and magmatic evolution of the eastern Karakoram, India. *Geodyn. Acta* 12, 341- 58.

Valdiya, K.S. (1976) Himalayan transverse faults and folds and their parallelism with subsurface structures of north Indian plains. *Tectonophysics* 32, 353-386

Valdiya, K.S. (1984) Aspects of Tectonics: Focus on southcentral Asia. *Tata McGrawHill, New Delhi*.

Valdiya, K.S. (1998) *The Dynamic Himalaya.* University Press, Hyderabad, India.

Venkatesan, T.R., Pande, K. and Gopalan, K. (1986) ^{40}Ar-^{39}Ar dating of Deccan basalts. *Jour. Geol. Soc. India* 27, 102-109.

Venkatesan, T.R., Pande, K., Gopalan, K., (1993) Did Deccan volcanism pre-date the Cretacious/Tertiary transition? *Earth and Planet. Sci. Lett.* 119, 181-189.

Venkatesan, T.R., Pande, K., Sharma, K.K., and Chawla, H.S. (1994). Ar-Ar chronology of the Ladakh collision zone, north west Himalaya. (Abst.) *Int. Con. Geochronology, Cosmochronology and Isotope Geology,* Berkeley, 338.

Virdi,N.S.(1987) Northern margin of the Indian Plate-some litho-tectonic constraints. *Tectonophysics* 134, 29-38.

Wadia, D.N., (1937) The Cretaceous volcanic series of Astor-Deosai, Kashmir and its intrusives. *Geol. Surv. Ind. Records* 72, 151-161

Weinberg, R.F. and Dunlap, W.J., (2000) Growth and Deformation of the Ladakh Batholith, Northwest Himalayas: Implications for timing of continental collision and origin of calc-alkaline batholith. *J. Geol.* 108, 303-320.

Wendt, I. and Carl, C. (1991) The statistical distribution of the mean square weighted deviation. *Chem. Geol.* 86, (275-285)

Wijbrans, J.R. (1985) Geochronology of metamorphic terrains by ^{40}Ar-^{39}Ar age spectrum method. *Ph.D. diss. Australian National Univ.* Canberra.

Wittlinger, G., Tapponier, P., Poupinet, G., Mei, J., Danian, S., Herquel, G., Masson, F. (1998). Tomographic evidence for localized shear along the Altyn Tagh fault. *Science* 288, 74-76.

Wyllie,P.J., (1984) Constraints imposed by experimental petrology on possible and impossible magma sources and products. *Philosophical Transactions of Royal Society of London.* A310, 439-456.

Yin, A., Harrison, T.M., (2000) Geologic evolution of the Himalyan-Tibetan orogen. *Annu. Rev. Earth Planet. Sci*, 28, 211-80.

York, D. (1966) Least-squares fitting of a straight line. *Can. J. Phys.* 44, 1079-1086.

York, D. (1969) Least squares fitting of straight line with correlated errors. *Earth Planet.Sci.Lett.* 5, 320-324.

York, D., Hall, C.M., Yanase, Y., Hanes, J.A., and Kenyon, W.J. (1981) ^{40}Ar-^{39}Ar dating of terrestrial minerals with a continuous laser. *Geophys. Res. Lett.* 8, 1136-1138.

Zeitler, P.K., (1985) Cooling history of NW Himalaya, Pakistan. *Tectonics* 4, 127-51.